Development of an electrochemical biosensor for Nevirapine, based on a zinc oxide-nanoclay human serum albumin composite

by

Randall Smith

BTech: Chemistry (Cape Peninsula University of Technology)

Dissertation submitted in fulfilment of the requirements for the degree

Master of Applied Science in Chemistry

Cape Peninsula University of Technology

Supervisor: Prof MC Matoetoe

Bellville

December 2022

DECLARATION

I, **Randall Kenneth Smith** (202037886), declare that the contents of this thesis represent my unaided work and that this thesis has not previously been submitted for academic examination towards any qualification. Furthermore, it represents my own opinions and not necessarily those of the Cape Peninsula University of Technology.

Signed.....Date.....30/10/2022.....

ABSTRACT

The optical and electrochemical features of ZnO synthesized samples with various precursor salts (zinc nitrate, acetate, and chloride) yielded acceptable surface nature and diagnostic functional groups. Significant trends related to precursors showed aggregation of nanoparticles, size distribution, stability, and conductivity. The crystallinity of ZnO crystals showed preferred growth planes while electrochemical parameters indicated reversibility of the electrochemical behaviour of ZnO. Under the specific electrolyte conditions, the rate of electron transfer translated to current density, and electrical resistance and revealed that the nitrate precursor produced the preferred ZnO product. Preparing different ratios of nanoclay (PGV and 1.44P) to ZnO composites, provided information about the best performing composite based on optical and electrochemical qualities. HR TEM images and SAED patterns showed laminated clay layers and crystallinity in pristine 1.44P, including partial agglomeration and spherical particles in ZnO as well as exfoliation and amorphous nature of the 1.44P ZnO composite. FTIR and XRD confirmed the chemical identity of PGV and 1.44P ZnO composites while cyclic voltammetry suggested that 0.5g 1.44P ZnO has the best electron transfer. The use of this composite with HSA-modified glassy carbon electrode as a platform for electrooxidation of NVP resulted in a single peak at 0.63V as previously reported. The supporting electrolyte, 1x (0.1M) PBS and optimization of the differential pulse voltammetry methodology led to selectivity over a wide concentration range which was 2 to 38μM. A low LOD of 0.39μM and LOQ at 1.30μM indicates sensitivity and hence superiority of the modified electrode. Reproducibility of the modified glassy carbon electrode fabrication protocol resulted in RSD figures of 1.17% while the precision was 1.35% for single concentration measurements. The repeatability of the modified electrode for consecutive measurements was RSD of 0.99% whereas the percentage of accuracy to evaluate stability was 98.65%. The 0,5g 1.44P ZnO HSA biosensor was furthermore used in samples of spiked urine and pharmaceutical tablet producing RSD values of 4.47% and 2.64% respectively for determinations of the analyte.

Keywords: ZnO nanoparticles, chemical synthesis, precursors, characterization, properties

ACKNOWLEDGEMENTS

Extremely grateful for the opportunity to be enrolled as a student at CPUT again

Thankful to my supervisor Prof Matoetoe for the leadership and her guidance through the duration of the course and for some massive support especially during the challenging period of the pandemic including lockdown. To Dr. Silwana as well, the advice offered is appreciated in the journey of electroanalytical chemistry, and not to forget all the teaching staff in the chemistry department made it feel like home after returning to the academic environment after working in the field a few years.

Need to say thanks to electrochemical sensor masters students, Sapokazi Timakwe and Sizwe Ngcobo, who took away the lonely days, and also doctoral candidate, Calleb Otieno Duya, for encouragement on doubtful days. It was a pleasure also to have worked with some WIL students and fourth-year level students in nanotechnology.

To the technical staff, chemistry, and chemical engineering, your assistance has made a great difference when preparing nanoparticles and the characterization.

Wish to honor the CPUT Ubuntu postgraduate forum and the center for postgraduate studies (CPGS) for orientation and funding to make my postgraduate journey pleasant.

Want to dedicate the research to my father, Paul Smith (the late), and to my mother, Mina Smith, including my former employer, who played a big part in shaping my future.

Analytical laboratory services from iThemba labs and the University of the Western Cape as well as equipment from Metrohm made a huge difference in this study therefore extremely happy for the involvement of the people from these organizations.

DEDICATION

Want to remember my wider family as well for their belief and trust including patience.

The creator and master of the universe who grants wisdom as well as insight.

To youth in the western cape area who desire to enter university and create a future for themselves

The fellow scientists and chemists performing work in emerging disciplines not to give up and grow weary but to have the courage to go on.

PREFACE

Main objective and overview

The thesis prioritizes explaining the construction of a nanoclay zinc oxide (ZnO) human serum albumin (HSA) composite-based sensor for the electrochemical detection of Nevirapine (NVP). This objective was achieved through performing the synthesis of ZnO nanoparticles (NPs) from three different zinc salt precursors (nitrate, acetate, and chloride) and the functionalization of two nanoclays (nanomer PGV and nanomer 1.44P) with these synthesized ZnO NPs including characterization all nanoparticles and nanocomposites with spectrometry, microscopy and electrochemistry; fabrication of the sensor platform for NVP through glassy carbon electrode modification with nanocomposites and HSA; optimization of NVP detection parameters like electrolyte, fabrication procedure, and electrochemical detection mode; method validation by using optimum conditions to determine analytical criteria like electrode stability, reproducibility and repeatability; application to spiked urine and pharmaceutical tablet samples.

- **Chapter one** gives the background to Nevirapine, a literature review on the environmental fate of active pharmaceutical ingredients in drugs and shortcomings of traditional laboratory methods presents the suitability of electrochemistry techniques for Nevirapine and introduces point-of-care testing for effective drug monitoring and past electrochemical methods for Nevirapine. The purpose of a nanoclay ZnO modified electrode surface with human serum albumin, the problem statement, and research objectives of this study.
- **Chapter two** forms the literature review for the study; gives the background and classification of antiretrovirals and provides an overview of Nevirapine and its associated analytical laboratory methods. The electrochemical detection for HIV drug monitoring and electroanalytical techniques have already been developed for Nevirapine. The potential of modifying electrode surfaces with nanoclay zinc oxide-based composites and human serum albumin.

- **Chapter three** covers the hydrothermal and solvothermal, sol-gel, wet chemistry precipitation, and polyol processes for ZnO synthesis. The synthesis method used in this study and sample preparation for characterization of the synthesized zinc oxide nanoparticles. The results and discussion of characterization using SEM, UV/visible, FTIR, XRD spectroscopy, Zetasizer, and electrochemistry (cyclic voltammetry, differential pule voltammetry, and electrical impedance studies). This chapter also includes cyclic voltammograms of synthesized ZnO film modified glassy carbon electrodes at different scan rates, Ip vs v including $v^{1/2}$ plots, and using the Randles-Sevcik equation to determine diffusion coefficient. Details of applying the Laviron method to the experimental data are also stipulated to all together determine the associated ZnO electrochemical kinetic parameters characteristic of electron transfer due to the modifier film. Electrochemical impedance studies were used as a measure of electrical resistance experience due to platform modification
- **Chapter four** is about the modification mechanisms of nanoclay and synthesis of nanoclay ZnO composites with PGV and 1.44P. Results and discussion of characterization with HR TEM, FTIR, XRD as well as electrochemistry. The crucial electrochemical parameters were determined for the synthesized nanoclay ZnO composites as well as the ideal nanocomposite selected for the construction of the analytical platform for analyte detection.
- **Chapter five** concentrates on the fabrication of the biosensor for Nevirapine and optimization of the suitable electrochemical method to apply the platform to real samples
- **Chapter six** is the main conclusions of the research.

RESEARCH OUTPUTS

Seminar presentations

1. *Electrochemical silver nanoclay composite biosensor with human serum albumin for Nevirapine* literature review (flash talk). 5th International Symposium on Electrochemistry, Electrochemistry at nanostructured interfaces. Bellville, South Africa, 11 to 14 August 2019
2. *Impact of zinc salt precursors on the shape, optical, dispersity features and electrochemical properties of ZnO nanoparticles* (virtual oral). Cape Peninsula University of Technology postgraduate students conference, The road to innovative solutions for real problems. Bellville, South Africa, 30 November 2021
3. *Language proficiency in chemistry education* (poster). 26th IUPAC International conference on chemistry education, Curriculum, and assessment reform initiatives. Cape Town, South Africa, 18 to 22 July 2022

TABLE OF CONTENT

LIST OF FIGURES

LIST OF TABLES

LIST OF SCHEMES

LIST OF EQUATIONS

SUPPORTING INFORMATION

CHAPTER ONE: Background

1.1 Summary

This chapter gives background information on the Nevirapine while the literature review presents the issues it creates in the environment; the correlation between the persistence of the drug and the lack of complete adherence is made, especially in the case of the treatment of infected individuals. The development of electrochemical techniques and their relevance in point-of-care testing environments is considered including existing methods for NVP. The popularity of a nanoclay-based electrode modifier is introduced and how in a composite with zinc oxide and human serum albumin, useful electrochemical features will be delivered. The problem statement addresses the concern to quantify the analyte correctly while the research objectives outline the tasks to achieve the aim.

1.2 Background

Nevirapine (NVP), 11 -cyclopropyl-4 -methyl- 5,11-dihydro- 6H -dipyrido [3,2- b20, 30- e] [1,4] diazepin-6 -one, is knows a common non-nucleoside reverse transcriptase inhibitor (NNRTI) retrovirus drug.[1] In figure 1.1 is a depiction of its molecular structure as well as a three-dimensional (3D) view of the molecule. NVP forms part of four classes of drugs used in treating the human immune deficiency virus (HIV), a virus that leads to acquired immune deficiency syndrome (Aids).[1] Nevirapine stops the activities of DNA polymerase, which is an enzyme that synthesizes DNA molecules of the virus, by inhibiting HIV-1 multiplication. DNA molecules of the virus. This enzyme is essential for DNA replication and NVP works by attaching directly onto the catalytic site of this reverse transcriptase enzyme so that the RNA genome carried in the virus, isn't converted into double-stranded DNA.[2] Nevirapine can guard the immune system by reducing the spread of the virus since when the virus disperses, the human body's resistance is reduced, and hence other Aids-related conditions are prevalent.[3]

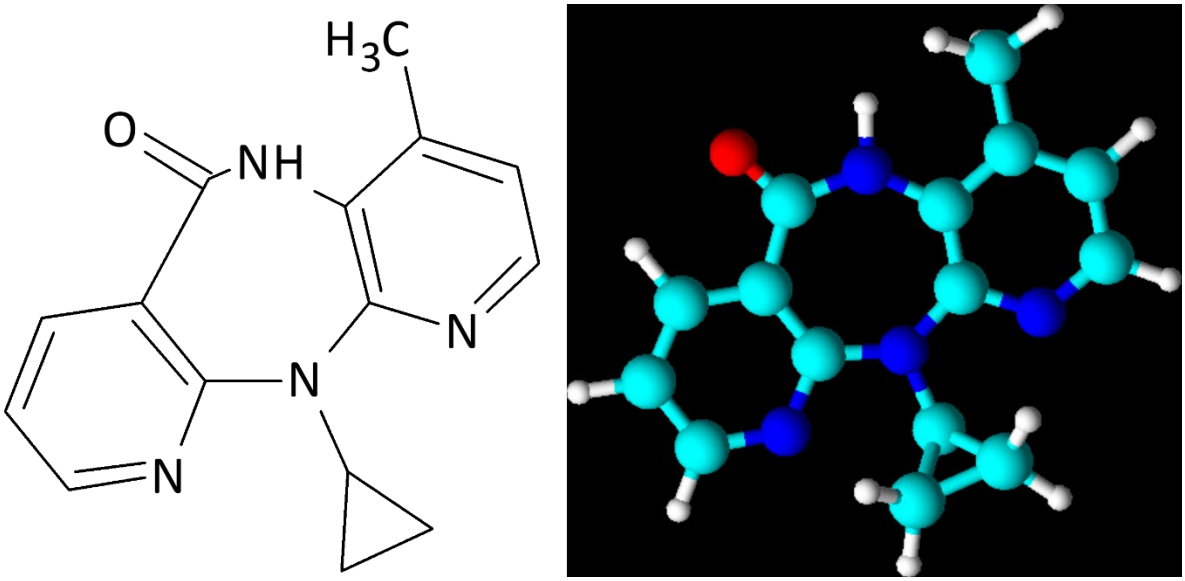

Figure 1.1: The molecular structure and three-dimensional projection of Nevirapine

Patients using NVP persistently can experience severe skin rash and even liver dysfunction.[4] However, the key to effective control of HIV is adherence to the treatment as well as the use of quality drugs. Presently, liver function monitoring and adherence are ensured through invasive monthly blood tests. As a means of improving the effectiveness of the drug, monitoring the levels of Nevirapine is crucial, especially in the case of mother-to-child HIV transmission prevention strategies, and can provide vital information about the prevention of antiretroviral drug resistance in resource-limited areas.[5] Furthermore can the information be used in taking consequent decisions during drug-drug interaction studies in HIV-infected individuals.[6]

1.3 Literature review

Pharmaceuticals have been reported as emerging water pollutants globally.[7, 8] There is an increase in chronic drug consumption due to deteriorating health because of new diseases and a lifestyle that exacerbates the problem. The presence of Nevirapine in water bodies has been reported to affect the growth of larvae and juveniles of the Mozambique tilapia (*Oreochromismossambicus*).[9] Secondly, there are challenges associated with wastewater treatment, especially with promising contaminants such as pharmaceuticals i.e., Nevirapine, due to its resistance to degradation.[10] Nevirapine's toxicity is said to affect largely the microbial populations, which is valuable

in effluent treatment at wastewater plants.[11] The Jukskei River in South Africa, has been identified as the largest contributor of emerging contaminants detected in the Hartbeespoort Dam. From this dam, the concentrations trend of these pharmaceutical drugs is reported as the following: efavirenz > Nevirapine > carbamazepine > methocarbamol > bromacil > venlafaxine.[12] From this information, HIV drug concentrations are the highest among emerging pollutants. This may pose a problem in the treatment of HIV, due to the possibility of drug resistance soon. Many analytical laboratory techniques have been employed for the effective quantification of Nevirapine. The most common techniques used are chromatography methods, which include high-performance liquid chromatography (reversed & normal phase), thin layer chromatography, coupled with detectors such as mass spectrometry.[13, 14] These chromatographic techniques are expensive, require specialized skill, involve lengthy protocol, and involve time-consuming sample preparation that includes the use of high volumes of organic chemical reagents. Organic chemicals are not environmentally friendly hence, a technique with their limited usage is more preferred. It has also been discovered that in certain instances, low sensitivity and selectivity of the analyte, make these techniques unsuitable for routine testing.[15, 16, 17]

1.4 Electrochemical techniques

Recently developed electrochemical methods have been adopted to counteract the problems of regular usage of chromatography techniques. There are reliable sensing technologies that are low-cost and simple to design. Organic compounds like drugs are easily detectable at electrode surfaces and the modification of these surfaces has resulted in an opportunity for a variety of analytes to be measured.[18, 19] The removal of Nevirapine from the body through urine is about 2.7% [20] and has a 48-hour shelf life in the plasma. Therefore, adherence of the drug to the patient's body can be monitored using improved recognition of the molecules utilizing point of care testing which can greatly save time and improve the current adherence monitoring systems.[21] The growth of biosensors and the simplicity of clinical laboratory analyzers are becoming the norm because clinical laboratory testing needs to be decentralized.[22] High-tech improvements make it possible for whole blood biosensors, substrate-specific and ion-selective electrodes to be fully operational; in an emergency hospital. [23] Through these techniques as little as 2 drops of blood can be used to perform many laboratory

measurements rapidly. There are reports of usage of these medical settings from newborn child intensive care to dialysis centers and patient aircraft transport units.[24] Crucial monitoring of glucose levels, occult stool, hemoglobin, and ovulation including urine pregnancy testing, are grouped as near-patient screening since it offers sooner decision-making regarding medical conditions as well as lowers additional costs related to hospitalization. By executing point-of-care testing, the patient's health is prioritized compared to complications suffered if a larger laboratory arrangement has not succeeded to play a significant role.[25] Electrochemical methods are ideal for POC testing and they present an opportunity for a high oxidative analyte like Nevirapine (figure 1.2). Thus, this reaction can be employed in its detection by a sensor. An effective sensor electrode for NVP needs to have good electrical conductivity and possible biocompatibility with enzymes or any proteins which can be used to amplify as well as improve selectivity and transfer electrons to the target (analyte) molecule. [16, 17]

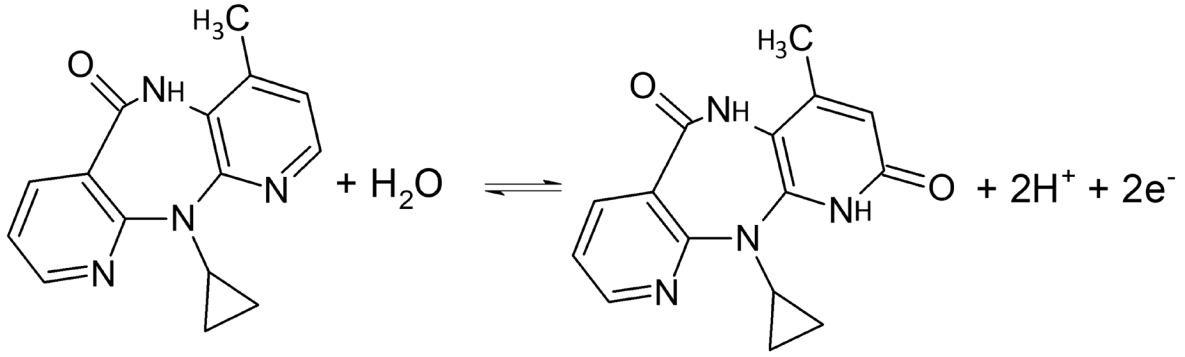

Figure 1.2: A proposed electrochemical mechanism for Nevirapine

Research involving the modification of a bare glassy carbon electrode with components like carboxylated multiwalled carbon nanotubes and silver nanoparticles (AgNPs) coated with 11-mercaptoundecanoyl hydrazine carbothioamide has been used with good linearity for the concentration of Nevirapine. At constant potential and in NaOH media[3], this amperometric electrochemical technique revealed that AgNPs have the best catalytic properties towards the analyte, NVP, in addition to the synergistic effect of the decoration of AgNPs with organic and inorganic molecules. The unfortunate drawback of this electrode modification is that NVP could not be oxidized under acidic media. There are other reports on the application of a modified

graphite electrode by a multiwalled carbon nanotubes/poly(methylene blue)/Au (gold) nanoparticles composite for the determination of Nevirapine in blood serum and pharmaceutical samples.[26] The studies show good linearity, indicating that the carbon nanotubes provide a π combinative arrangement with a very hydrophobic surface that causes substantial attraction to organic compounds through π to π electronic connections whereas methylene blue possesses reversible electron transfer features. The challenge though with this biosensor was the adsorption of unreacted monomer that led to clogging of the electrode surface which resulted in premature electrode fouling. An electroactive two-dimensional (2D) Pd@rGO decorated with MoS_2 quantum dots tailored electrode, has also been reported to display a relative rise in oxidation peak current proportional to the increase of NVP concentration.[27] 2D graphene oxide provides a good matrix but despite this, MoS_2 has structural defects like point defects that may play a negative role during biomedical assays.

1.5 Nanoclay electrode modifier

Nanoclay and its composite materials have attractive adsorption and ion-exchange capabilities because of their high surface area, porosity, and low electrical conductivity.[28] Montmorillonite (MMT) nanoclay belongs to smectite group of clays, has inorganic layered nanostructure, and is studied for use in pharmaceutical nano conversion since it overcomes several limitations of micro composites suggested for drug delivery. Many substances such as organic species and heavy metals have a strong affinity to nanoclay surfaces.[29] The effective performance of nanoclays in carbon paste electrodes has been shown through many electrochemical applications.[30] MMT is recommended for the detection of Nevirapine due to its outstanding drug delivery ability already widely reported. The nanoclay's conductivity is usually improved by functionalizing the nanoclay with conductive metals.[31] Zinc oxide nanoparticles (ZnO) have favorable properties and are exceptional for their broad energy bandgap and high exciton binding energy.[32, 33] Broad research has been done already for ZnO synthesis, characterization, and application in sensing devices.[34] ZnO has a high surface volume ratio so it will provide a large specific surface for analyte detection.[35] The combination of ZnO with nanoclay minerals has been done and resulted in unique hybrid materials with novel platform features. ZnO is biocompatible, absorbs several compounds due to its high isoelectric point, and has

been employed in photocatalytic studies.[36] ZnO was demonstrated to serve as a brilliant signal intensifier substrate for a wide range of molecules including serum albumins. Serum albumins have exceptional drug binding capacities and there are some reports on their reactivity to Nevirapine.[37] Therefore nanocomposites which include nanoclays in addition to ZnO, are ideal for sensors (chemical and biological).

1.6 Problem statement

The public health system allows for people affected by Aids to have ease of access to their treatment including treatment is low cost, requires little expertise to administer, and basic laboratory protocol to monitor dosages. Non-invasive techniques and portability of measuring devices are more attractive in practice for drug monitoring. Consistency in drug monitoring approaches is essential to streamline treatment options for patients as well as realistic turnaround times of such point-of-care technologies so that the correct amounts of active pharmaceutical ingredients are consumed. Electrochemical platforms based on nanoparticles can determine chemical and biological agents and offers the solution to an issue of specificity during determinations in biomedical and environmental samples. Modifying electrode surfaces with nanoparticles is novel and is significant to the HIV drug focused on in this study, Nevirapine, which is one of the most prescribed HIV drugs, is cheap, has a long-term tolerance, and is reliable in treatment, but due to drug-to-drug interactions in combined therapy, unexpected high or low NVP levels takes place. Nevirapine can be tested in human serum, urine, and saliva and is the point source to inspect effective adherence, but concerns associated with previous electrochemical sensors were poor analyte responses at low pH conditions instead of a wider pH range, unwanted modifier material adsorption at the electrode measuring surface and structural defects of surface modifier which results in reduced optimal analyte detection. Therefore, selective point-of-care diagnostic tools which oxidize analyte molecules are extremely necessary for active pharmaceutical ingredient monitoring in samples. The composition, individually and collectively, of electrode modifier composites, is vital in understanding their contributions to electrochemical behavior since it leads to characteristic signals apart from the analyte response. Therefore, electrode modifier film quality depends on the structural, electrical properties, and functionalization possibilities of individual modifiers. To overcome such concerns, an electrochemical

sensor using a zinc oxide nanoclay composite with human serum albumin (HSA) is proposed for the detection of NVP.

1.7 Objectives

The main objective of this study is to fabricate a zinc oxide nanoclay human serum albumin composite-based sensor for the electrochemical detection of Nevirapine. This objective will be achieved through the following tasks that form part of the sub-objectives:

1. Synthesis of ZnO, and the functionalization of nanoclay with ZnO will include using three different zinc salt precursors and two nanoclays
2. Characterization of the synthesized nanoparticles (ZnO and ZnO nanoclay composites) with spectrometry and electrochemistry
3. Fabrication of the sensor for Nevirapine through glassy carbon electrode modification of the nanoparticles and human serum albumin
4. Optimization of the detection of NVP through electrolyte, fabrication procedure, and detection mode.
5. Method validation: using optimum conditions to determine analytical parameters, determine electrode stability, repeatability
6. Application to spiked biological sample and pharmaceutical tablet.

1.8 References

1. Nagappa Laxman Teradal, Shankar Narayan Prashanth, Jaldappagari Seetharamappa. Electrochemical studies of Nevirapine, an anti-HIV drug, and its assay in tablets and biological samples. J. Electrochem. Sci. Eng. 2(2) (2012) 67-75
2. Purnima Hamrapurkar, Mitesh Phale, Priti Patil, Nitul Shah. Determination of Nevirapine in Human Plasma by High-Performance Liquid Chromatography with Ultraviolet Detection. International Journal of Pharm Tech Research. Vol.2, No.2, pp 1316-1324, April-June 2010
3. Elahe Ahmadi, Mohamad Reza Eyvani, Vahid Riahifar, Hossein Momeneh, Changiz Karami. Amperometric determination of Nevirapine by GCE modified with c-MWCNTs and synthesized 11-mercaptoundecanoyl hydrazine

carbothioamide coated silver nanoparticles. Microchemical Journal 146 (2019) 1218-1226

4. Reshmi Samuel, Marc Noguera Julian, Roger Paredes, Raveen Parboosing, Pravi Moodley, Lavanya Singh, Anneta Naidoo, and Michelle Gordon. HIV-1 Drug Resistance by Ultra-Deep Sequencing Following Short Course Zidovudine, Single-Dose Nevirapine, and Single-Dose Tenofovir with Emtricitabine for Prevention of Mother-to-Child Transmission. J Acquir. Immune Defic. Syndr. Volume 73, Number 4, December 1, 2016
5. Chinmoy Ghosh, Shashank Gaur, Ajay Singh, Chandrakanta P. Shinde, and Bhaswat S. Chakraborty. Estimation of Nevirapine from Human Plasma by LC-ESI-MS/MS; a pharmacokinetic application. J Bioequiv Availab. Volume 3(1): 020-025 (2011)
6. Margreke J.E. Brill. Elin M. Svensson, Mishal Pandie, Gary Maartens, Mats O. Karlsson. Confirming model-predicted pharmacokinetic interactions between bedaquiline and lopinavir/ritonavir or Nevirapine in patients with HIV and drug-resistant tuberculosis. International Journal of Antimicrobial Agents 49 (2017) 212–217
7. Paul E. Stackelberg, Edward T. Furlong, Michael T. Meyer, Steven D. Zaugg, Alden K. Henderson, Dori B. Reissman, Persistence of pharmaceutical compounds and other organic wastewater contaminants in a conventional drinking-water-treatment plant. Science of the Total Environment 329 (2004) 99-113
8. Timothy Paul Wood, Cornelia S.J. Duvenage, Egmont Rohwer. The occurrence of anti-retroviral compounds used for HIV treatment in South African surface water. Environmental Pollution 199 (2015) 235-243
9. U. Marie Clementine Nibamureke, Irene E.J. Barnhoorn, Gesina M. Wagenaar. Assessing the potential effects of Nevirapine in South African surface water on fish growth: A chronic exposure of Oreochromismossambicus. Volume 115 Number 3/4, March, April 2019
10. C. Schoeman, M. Dlamini, O.J. Okonkwo. The impact of a Wastewater Treatment Works in Southern Gauteng, South Africa on efavirenz and Nevirapine discharges into the aquatic environment. Emerging Contaminants 3 (2017) 95-106

11. Lawrence Obidike and Jean Mulopo. Effect of High Concentration of Nevirapine on the Growth of e. Coli in Wastewater Treatment. Proceedings of the World Congress on Engineering and Computer Science 2018 Vol II
12. Cornelius Rimayi, David Odusanya Jana, M. Weiss, Jacob de Boer, and Luke Chimuka. Contaminants of emerging concern in the Hartbeespoort Dam catchment and the uMngeni River estuary 2016 pollution incident, South Africa. Science of The Total Environment. Volume 627, 15 June 2018. 1008-1017
13. Srinivasa Reddy, Licto Thomas, K. S. Santoshkumar, Nirmala Nayak, Arindam Mukhopadhyay, and Saral Thangam. An LC-MS/MS method with column coupling technique for simultaneous estimation of lamivudine, zidovudine, and Nevirapine in human plasma. Journal of Analytical Science and Technology (2016) 7:17
14. Magda Caban, Jolanta Kumirska, Anna Bialk-Bielinska and Piotr Stepnowski. Analytical Techniques for Determining Pharmaceutical Residues in Drinking Water-State of Art and Future Prospects. Current Analytical Chemistry, 2016, Vol. 12, No. 2
15. Saeed Shahrokhian, Razieh Kohansal, Masoumeh Ghalkhani, and Mohammad K. Amini. Electrodeposition of Copper Oxide Nanoparticles on Pre-casted Carbon Nanoparticles Film for Electrochemical Investigation of anti-HIV Drug Nevirapine. Electroanalysis 2015, 27, 1989-1997
16. Daniel Apath, Mambo Moyo and Munyaradzi Shumba. TiO_2 Nanoparticles Decorated Graphene Nanoribbons for Voltammetric Determination of an Anti-HIV Drug Nevirapine. Hindawi Journal of Chemistry. Volume 2020, Article ID 3932715
17. Ana M. Esteva, Elias Blanco, Juan J. Pina, Abel I Balbin, Carmen Quintana, Pedro Hernandez. Determination of Nevirapine in the presence of cucurbit(7) uril with a gold electrode. J. Electrochem. Sci. Eng. 4(1) (2014) 37-44
18. Mamun Ur Rashid, Khairul Hassan Bhuiyan and M. Emran Quayum. Synthesis of Silver Nano Particles (Ag-NPs) and their uses for Quantitative Analysis of Vitamin C Tablets. Dhaka Univ. J. Pharm. Sci. 12(1): 29-33, 2013 (June)
19. Camila Alves de Lima, Edson Roberto Santana, Jamille Valéria Piovesan, Almir Spinelli. Silver nanoparticles-modified electrode for the determination of nitro compound-containing pesticides. Anal Bioanal Chem (2016) 408:2595-2606

20. C Swanepoel, H Bouwman, R Pieters & C Bezuidenhout Presence, concentrations, and potential implications of HIV-antiretrovirals in selected water resources in South Africa. Research Unit for Environmental Sciences and Management North-West University, Potchefstroom. WRC Report No 2144/1/14
21. Meri Kankaanpaa, Marika Holma-Eriksson, Sami Kapanen, Merja Heitto, Sari Bergstrom, Leila Muukkonen and Veli-Pekka Harjola. Comparison of the use of comprehensive point-of-care test panel to conventional laboratory process in emergency Department. BMC Emergency Medicine (2018) 18:43
22. Julie L.V. Shawa. Practical challenges related to point of care testing. Practical Laboratory Medicine 4 (2016)22–29
23. Josko Osredkar. Point-of-care-testing in laboratory medicine. Ljubljana University Medical Centre. Clinical Institute of Clinical Chemistry and biochemistry
24. Gregory J. Fermann and Joe Suyama. Point of care testing in the emergency department. The Journal of Emergency Medicine, Vol. 22, No. 4, pp. 393-404, 2002
25. Keith E. Kocher, William J. Meurer, Jeffrey S. Desmond, and Brahmajee K. Nallamothu. Effect of Testing and Treatment on Emergency Department Length of Stay Using a National Database. Academic emergency medicine. 2012; 19:525-534
26. Mohammad Bagher Gholivand, Elahe Ahmadi, Mozhdeh Haseli. A novel voltammetric sensor for Nevirapine, based on modified graphite electrode by MWCNs/poly (methylene blue) /gold nanoparticle. Analytical Biochemistry 527 (2017) 4-12
27. Preeti Tiwari, Narsingh R. Nirala, and Rajiv Prakash. Determination of the Anti-HIV Drug Nevirapine Using Electroactive 2D Material Pd@rGO Decorated with MoS_2 Quantum Dots. Chemistry Select 2018, 3, 5341 – 5347
28. Marina Massaro, Carmelo Giuseppe Colletti, Giuseppe Lazzara and Serena Riela. The Use of Some Clay Minerals as Natural Resources for Drug Carrier Applications. J. Funct. Biomater. 2018, 9, 58

29. Sarvaiya Jayrajsinh, Gauri Shankar, Yadvendra K. Agrawal, Lateef Bakre. Montmorillonite nanoclay as a multifaceted drug-delivery carrier: A Review. Journal of Drug Delivery Science and Technology 39 (2017) 200-209
30. Nagaraj P. Shettia, Deepti S. Nayaka, Shweta J. Malodea, Raviraj M. Kulkarnib. Nanomolar detection of acyclovir, an antiviral drug at nanoclay modified carbon paste electrode. Sensing and Bio-Sensing Research 14 (2017) 39-46
31. Ma. Manna Farrel B. Pinto, Danica Louise S. Bonga, Mary Fatima T. Tayad, and Mary Donnabelle L. Balela. Synthesis and Characterization of Silver Nanoparticles Anchored on Montmorillonite via Chemical Reduction. International Journal of Scientific and Engineering Research Volume 7, Issue 7, July 2016
32. Berna Dalkıran, Ceren Kaçar, Pınar Esra Erden, Esma Kılıç. Electrochemical xanthine biosensor based on zinc oxide nanoparticles-multiwalled carbon nanotubes–1,4-benzoquinone composite. JOTCSA. 2018; 5(1): 317-332
33. Maroua Mrad, Bilel Chouchene and Tahar Ben Chaabane. Effects of Zinc Precursor, Basicity and Temperature on the Aqueous Synthesis of ZnO Nanocrystals. S. Afr. J. Chem., 2018, 71, 103–110
34. Yao Wang, Dan Li, Junfeng Kang, Shiye Guan, Daoxin Wu. An Electrochemical Sensor Based on MB/Ag-ZnO/Graphene Modified Glassy Carbon Electrode for Determination of L-Tryptophan in Biofluid Samples. Int. J. Electrochem. Sci., 14 (2019) 5448-5461
35. Jaesik Yoon, Eunji Lee, Doohee Lee, Tae-Sik Oh, Young Soo Yoon and Dong-Joo Kim. Highly Sensitive Ag/ZnO Nanorods Composite Electrode for Non-Enzymatic Urea Detection. Journal of The Electrochemical Society, 164 (12) B558-B560 (2017)
36. Suchithra Padmajan Sasikala, T. A. Nibila, Kunnathuparambil Babu Babitha, Abdul Azeez Peer Mohamed and Ananthakumar Solaiappan. Competitive photo-degradation performance of ZnO modified bentonite clay in water containing both organic and inorganic contaminants. Sustainable Environment Research (2019) 29:1
37. A. Kluczewska, K. Michalik, Z. Drzazga, M. Kaszuba. About the Interaction of Human Serum Albumin with Nevirapine and Azidothymidine. Polish J. of Environ. Stud. Vol. 15 No. 4A (2006), 59-61

CHAPTER TWO: Literature review

2.1 Summary

This chapter discusses antiretrovirals, their classification of them, extensive background about the analyte of the study, analysis techniques for it, how electrochemical detection plays a role in HIV drug monitoring, and current methods for Nevirapine. What follows then are the roles of zinc oxide and nanoclay (bentonite and organoclay) in electrochemical sensors thereafter information on how electrochemical signals are improved by human serum albumin.

2.2 Antiretrovirals

The purpose of antiretrovirals is for the therapeutic administration of infections that are responsible for retroviruses like the human immune deficiency virus (HIV). Acquired immune deficiency syndrome (Aids) is the consequent occurrence due to the HIV illness.[1] Studies have shown that the AIDS virus has been found in high abundance in blood and semen.[2] Since HIV gradually attacks the immune system, the human body becomes prone to illnesses therefore opportunistic infections are possible. The virus replicates itself in the CD4 cell until it depletes them. Two types of HIV namely HIV type 1 and HIV type 2, are most likely to be diagnosed amongst humans where type 1 is the prevalent kind globally. Type 2 is specifically occurring in Western Africa including some cases noticed in India and Europe.[3] Only after 1996 more antiretroviral treatment drug options for HIV 1 were developed before clinical management of the disease was made up predominantly of prophylaxis opposing typical pathogens.

The establishment of inhibitors for reverse transcriptase and protease, which are two of the vital enzymes of HIV 1 as well as the introduction of drug routines, promote the complete effectiveness and reliability of HIV treatment.[4] Understanding in-depth the differences between viral and cellular enzymes has led to a strategy of launching specific drugs that are relevant to the virus and has reduced toxicity towards the host cell.[5]

2.3 Classification of HIV drugs

The goals of efficient HIV drug treatment choices or approaches are strongly linked to offering maximum as well as sturdy suppression of viral load, recovery and preserve immune operation by reducing HIV linked infection including non-infectious sickness, extended life anticipation of a person and hence the quality of life, prevention of onward spreading of HIV and limit the negative effects of treatment.[6] Effective expansion of medicines aimed at anti-HIV type 1 activity contributed to the onset of first-generation nucleoside HIV reverse transcriptase (NRTIs) inhibitors. What proceeded was a widening of such a grouping to other classes like non-nucleoside RT inhibitors (NNRTIs), protease (RT) inhibitors as well as entry inhibitors to the extent of about twenty drugs got licensed for HIV type 1 clinical treatment. This constituted of 11 RT, inhibitors, 8 PR inhibitors, and 1 fusion inhibitor; in situations where RT and PR inhibitor categories are dispensed together for highly active antiretroviral therapy (HAART), a prolonged life expectancy involving infected patients results in type 1 changing from having been fatal to more of chronic disease.[7] Scheme 2.1 is a compilation of the various kinds of HIV drugs and their respective transformation[8,9,10] in the human body.

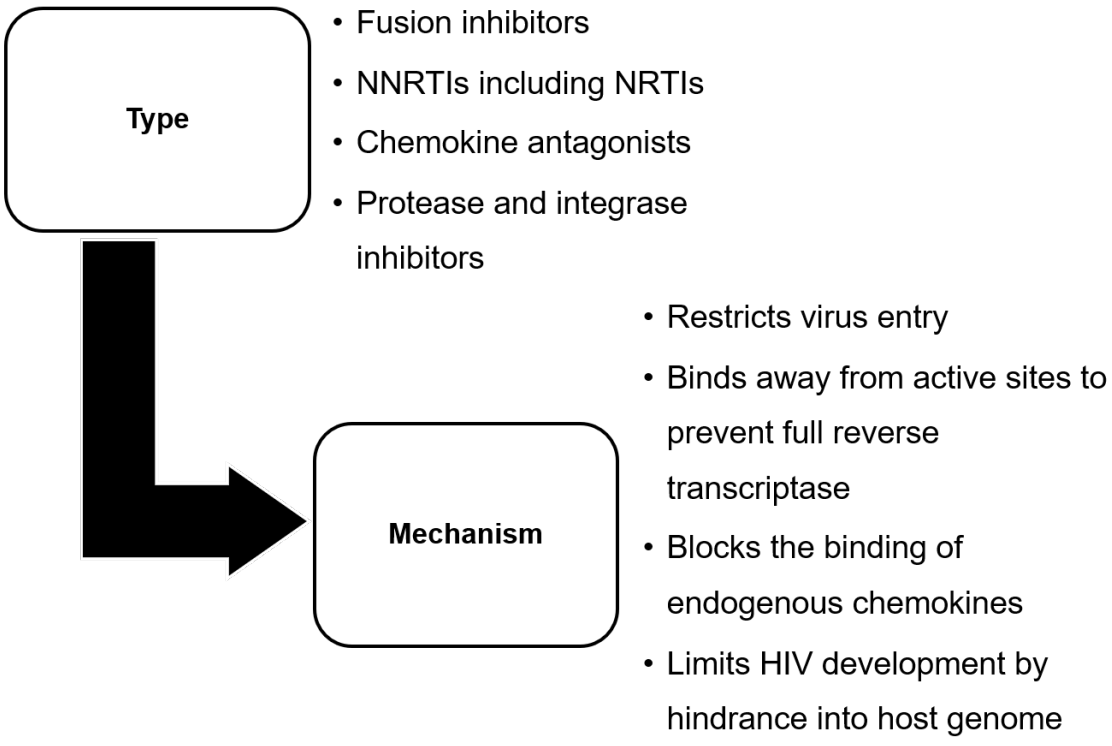

Scheme 2.1. The different types of antiretrovirals for HIV

The characteristic features of HIV, sort of antiretrovirals, and patient health conditions are contributing to problems affecting antiretroviral treatment. Such factors pose major issues against successful long-term therapy; the way the virus multiplies daily, the noticeable drug-to-drug interactions, and the coexistence of other diseases complicate treatment.

2.4 Nevirapine

Nevirapine (NVP) is an example of an antiretroviral drug commonly used to shield the immune system by reducing the amount of virus in the body thus hindering the progression of the AIDS disease.[11] NVP primarily functions to prevent babies' infection from HIV-infected mothers during delivery so that babies just born from ladies whose infection status is not completely known, will benefit from such administration. A routine of two doses a week lowers the risk of infection during lactation, but monotherapy is recommended because resistance to therapy develops early.[12] Hence, costly combined treatment with zidovudine is adopted.[29] Nevirapine has a high daily consumption by HIV-positive patients in South Africa and is stubbornly persistent at elevated concentrations in wastewater.[13]

NVP connects to the exterior of the HIV, inhibiting viral duplication, inactivating cell-free virions located in the genital tract and hence found present in human milk.[14] The drug molecules are easily absorbed orally, extensively dispersed, enter the blood-brain/blood-cerebrospinal fluid (CSF), and since it is lipophilic, get quickly transported across the placenta.[15] Even since significant amounts of Nevirapine are present in breast milk, there is not enough evidence of teratogenicity and extensively metabolized by the cytochrome P450 isoenzyme system in the liver; its half-life of 40-60hours when treatment is launched initially.[16] NVP potency is lowered in the bodies of patients using rifampicin but not disturbed in patients using a host of other pharmaceutical drugs such as cimetidine, erythromycin, and fluconazole.

Severe skin redness and early reversible liver dysfunction are among the extreme side effects often seen among patients using Nevirapine. With the high rate of HIV/AIDS infections, it is expected that a growing concentration of HIV drug compounds will be

detected in water samples analyzed from almost every local major surface water (river and dam). Nevirapine[13, 17], figure 2.1a, Lopinavir[13] (figure 2.1b), and Zidovudine[13, 17] (figure 2.1c) are the most commonly occurring compounds while combinations of Stavudine[13], Nevirapine[13] and Zidovudine[13] revealed high averages even though their concentrations are in a lower range. Therefore, some of these contaminants survive conventional drinking water treatment processes and appear in potable water, and pose a danger as continuous ingestion of these contaminated waters will cause a toxin tolerance to active pharmaceutical ingredients leading to drug resistance when such HIV drugs are used in future medical treatment. Studying the persistence of pharmaceutical compounds and other organic contaminants at wastewater treatment plants (WWTPs) serves as an indicator of the plant's technical performance.[18]

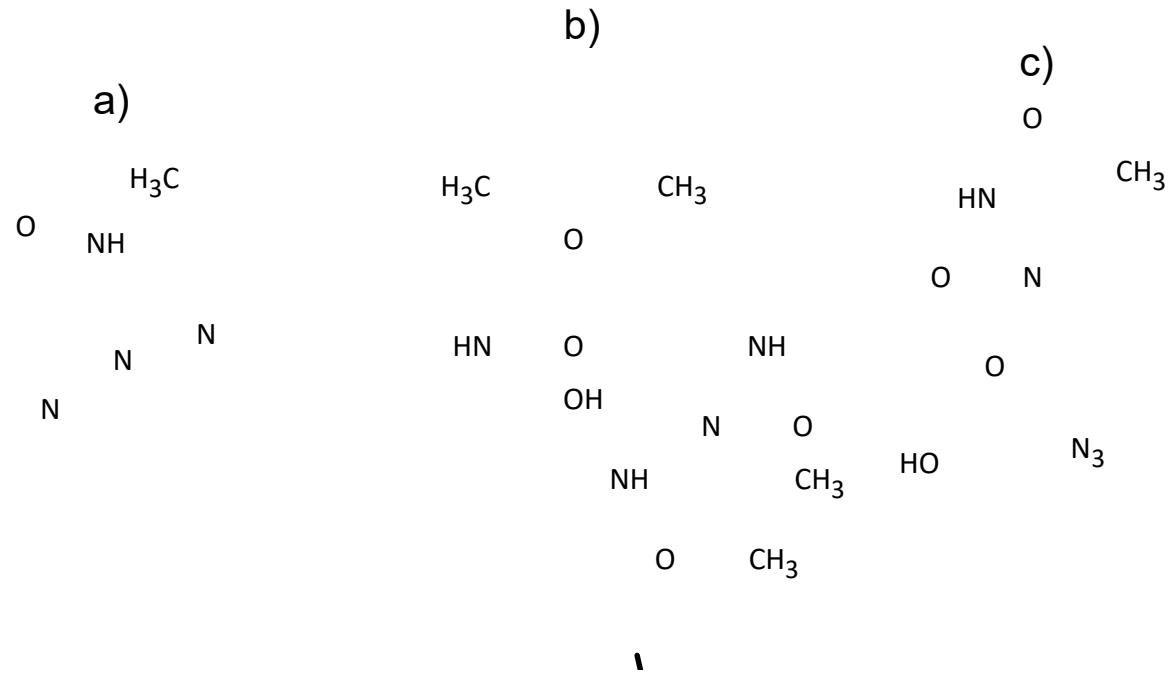

Figure 2.1: The chemical structures of common antiretroviral drugs; a) Nevirapine, b) Lopinavir, and c) Zidovudine

Active pharmaceutical ingredients (APIs) toxicity may have antimicrobial activity against a variety of certain gram-negative intestine bacteria, such as Escherichia coli, which is also used for effluent treatment in WWTPs.[19] Since WWTPs are not specifically designed to remove them, they are likely to be present in effluents from WWTPs even at trace levels thus contributing as major point sources of HIV drug APIs

to the aquatic environment. To elucidate the potential impacts and implications of HIV drug APIs for the safe and efficient operation of WWTPs requires an understanding of the pollutant's fate and behavior in such systems.[20] To continue investigating the stability of NVP in wastewater, selected parameters such as pH and electrical conductivity were considered in a study where WWTP effluent was closely monitored; with Nevirapine as well as without Nevirapine.[21] A report on the investigation of the stability of NVP in wastewater at various pH and electrical conductivity revealed that an increase in the gradual concentration of NVP increased the acidity of the wastewater effluent. However, a strange trend of the decline in alkalinity of the wastewater at the highest concentration of Nevirapine was observed. While a sudden decrease in electrical conductivity was observed in the values at the initial levels of Nevirapine spiked wastewater. At the highest concentration of NVP treated wastewater, high values were noted but settled at a lower value at the end. This phenomenon cannot be convincingly explained thus it remains crucial to monitor the level of Nevirapine in wastewater treatment plants. To achieve efficient monitoring; selective, fast, cost-effective, and low detection methods are vital. This will enable the detection of trace amounts and carry out routine analysis. Therefore, the development of these analytical methods is a necessity.

2.5 Analytical methods for Nevirapine

The inherited high polarity of several pharmaceutical drugs has led to liquid chromatography (LC) being the preferred analytical technique to determine concentrations. Hence, why current chromatography methods are the dominant techniques used in Nevirapine analysis. Such laboratory protocols are high-performance liquid chromatography (HPLC)[22], cost-effective thin layer chromatography, and hyphenated liquid chromatography with mass spectroscopy (LC-MS/MS)[25]. However, the application of TLC shows poor results in the monitoring of Nevirapine in saliva.[23] The technique was expected to be sensitive and specific, but the local temperature and humidity severely affected the TLC plates which caused poor assays. Furthermore, it also became debatable whether drug penetration into saliva takes place because of molecular size and lipid solubility of the drug after oral administration. Among the most suitable detector for samples with biological matrices is mass spectrometry (MS) due to its adequate sensitivity and selectivity to perform

measurements of pharmaceutical compounds in complex biological matrices at trace levels. Increased resolution and accuracy of mass spectrometry permit it to be operated in full scan mode to overcome the shortcomings of target type analyses and an added benefit is that MS including MS/MS detection facilitates individual or simultaneous analyses.[24] Absorption and fluorescence detection modes with liquid chromatography have been used to determine efavirenz and NVP.[25] Careful sample preparation for the determination of NVP in human plasma[24] is essential for reproducible results. Among the mentioned chromatography methods, very few have a low enough lower limit of quantification (LLQ) and in addition to this, the analysis time of a single run for these methods is extremely long. Optimizing the sample injection volume was used to influence the analysis time and sensitivity of the detection.[22] In comparison to protein precipitation, solid-phase extraction (SPE) proved to be much more effective to obtain a clean aliquot of NVP and directly introducing it into the LC-MS/MS system without the evaporation step. However, these methods are awkward when it comes to, gradient elution, run time, and mobile phase polarity switching. To overcome meticulous sample preparation regimes, a harmonized LC-MS/MS technique was developed to measure lamivudine, zidovudine including Nevirapine in human plasma for a clinical pharmacokinetic study.[26] The final results of the cocktail containing the three drugs, revealed that lamivudine and zidovudine were eluting in the void volume due to them being highly polar and not retained in the reverse phase column. Matrix effects are further indicated to be the root cause of improper separation of analytes since Nevirapine is lyophilic and bound tightly to the reverse phase column, causing it to elute late. These techniques have been extensively used in pharmaceutical pollution water analysis and reports on HIV drug residues analysis in South African waters including by German researchers show levels of significant deposits of waste and surface water.[27] In Kenya, research involved an investigation into the levels of pollution of the Nairobi River Basin by antibiotics and antiretrovirals. Water samples containing lamivudine, NVP, and zidovudine were all prepared through solid-phase extraction followed by liquid chromatography-electrospray ionization tandem mass spectrometry (SPE LC-ESI/MS/MS), to identify their environmental risk.[25] The high antibiotic and antiretroviral loads in the river water confirmed that the contamination is significant, due to urbanization and poor wastewater management systems.[25] Additionally, did the study reveal that such levels of antiretrovirals are higher than reported globally and aquatic species will be

influenced negatively.[25] The analytical laboratory method however involved much time specifically for sample preparation.

An ultraviolet/visible (UV/vis) spectrometry method was used to measure quantitatively NVP present in various pharmaceutical formulations and required tetrathiocyanatocobalt (II) as a reagent to complete optimum reaction conditions to ensure suitable sensitivity as well as selectivity.[27] Analytical parameters such as molar absorptivity, the limit of detection, and limit of quantification, are needed to comply with standards according to the International Council for the harmonization of technical requirements of pharmaceuticals for human use (ICH); a manner in which to promote method reliability and reduce analyte interferences. Other practical criteria for the analysis were the correct preparation of the reagent ion, choosing the optimum volume of the reagent, confirming the stability of the analyte-reagent complex over time, and hence calculating the stability constant of the complex. In this analytical method, the selectivity towards other species that are present in formulations became even more vital and their relative solubilities. The potential interferences like talc, starch, and glucose contribute to light scattering.[28]

The impact of Nevirapine in maternal plasma and breast milk was considered in therapeutic scenarios using a rapid automated enzyme immunoassay test developed by Ark™ Diagnostics incorporated, a company that designs, manufactures, and distributes in-vitro diagnostic devices for biological samples. The technique is based on the binding of the analyte to a drug-labelled enzyme but has a detection limit and is more feasible to determine the presence or absence of NVP. The study also furthermore presented evidence that the selectivity of the technique towards the analyte needs to be heavily optimised.[29]

The plasma of infants who received 14 weeks of extra Nevirapine or NVP in addition to Zidovudine was analyzed with ViroSeq HIV genotyping system and through LigAmp sensitive point-mutation assay to determine Nevirapine resistance.[30] These techniques were only able to present proof of frequency and persistence of Nevirapine resistance, limitations to quantification as well as only a single method available for NVP resistance analysis. Statistically, similar frequencies in Nevirapine resistance

mutations using ViroSeq and LigAmp were found, and it was concluded that mutation studies are complex to do without clinical trials to evaluate several treatment strategies in infants who were exposed to HIV drugs before the commissioning of HIV treatment.

Electrochemical sensing technologies are used in HIV treatment monitoring purposes to confirm binding as well as recognition proceedings on the analytical surface because of biomolecules.[31] Furthermore, does a broad class of biosensors have a few advantages like simplicity and reasonable signal-to-noise ratio thus small electrical interference related to biological sample matrices. Figure 2.2 captures essential elements produced when modifying an electrode surface to be relevant to a specific application. Electrochemical platforms can monitor the capture of biomolecules due to an electrode interface development linked to prompting changes in current, resistance impedance, or voltage. Strategies to quantify such signals are amperometric, voltammetric, potentiometric or impedance where the first two approaches mainly measure an electrochemical reaction that is promoted by the generation of redox current while the latter considers resistance relative to the redox behavior. Peak current density related to direct oxidation or reduction of target molecules immobilized on the electrode surface, becomes measurable with biosensors. In situations involving affinity sensing tactics, antigen species are trapped by specific antibodies which act as recognition elements on the electrode surface. The result of this is an electrochemical reaction that affects electron transfer and lowers the output current. This lessening in output current is easily quantified and proportional to the captured target molecules. To determine potential or charge accumulation due to electroactive molecules, potentiometric biosensors are recommended since they are equipped with ion-selective electrodes. Impedance biosensors can follow the electrical resistance of an interface in an alternating current steady-state through the application of a sinusoidal voltage at a certain frequency noting the produced analytical current response. The net current-to-voltage ratio observed in electrochemical impedance studies offers the impedance signal and allows precise monitoring of consequent conductivity concluding that the electrode’s biomolecules interaction causes the electrochemical reaction which has its respective resistivity as well as charging capacity.

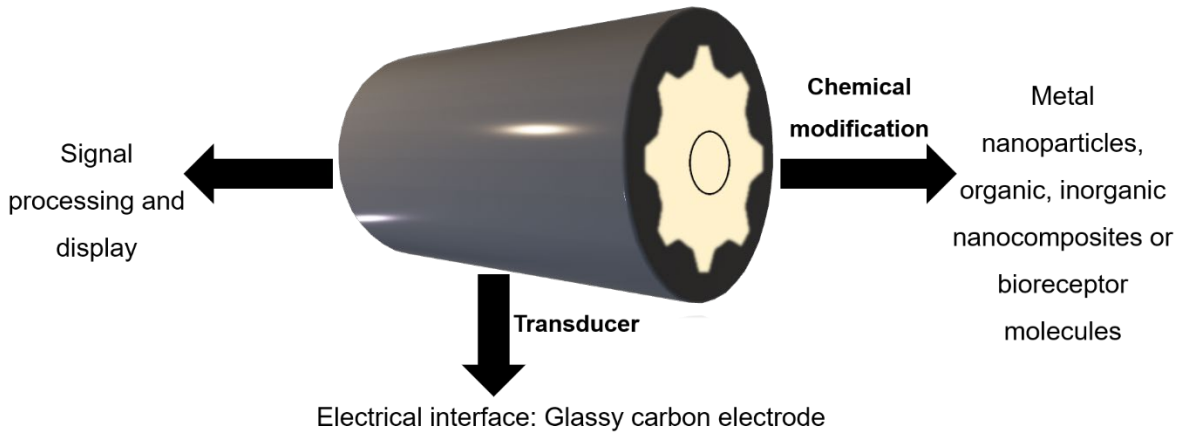

Figure 2.2: The chemical modification of a glassy carbon electrode in sensor fabrication

2.6 The use of electrochemical detection in HIV drug monitoring

Capillary electrophoresis is a useful analytical technique for routine testing of samples or more complex mixtures. It is automated, requires little analysis time, and performs highly efficient separation of sample components. A variety of analyte molecules can be determined with the techniques including small organic ions to macromolecular protein complexes as well as DNA.[32] The capillary tube in which electrophoresis takes place plays a major role in the entire technique because of its diameter size and length. In the case of capillary zone electrophoresis, the sample is introduced into a capillary filled with buffer solution electrokinetically and at low voltage conditions. The ends of the capillary and electrodes are then immersed in a buffer solution which is governed by the high voltage that permits the migration of analyte molecules through the capillary tube and beyond the detection window to quantify the signal. Micellar electrokinetic chromatography is a mode of electrophoresis that separates compounds based on charge to give the analyte partitioning between micelles from a surfactant so that complex mixtures of charged and uncharged species can be separated realistically. Single HIV drug components have been analyzed with a vast number of analytical techniques and thus led to an investigation of the simultaneous determination of lamivudine, didanosine, and saquinavir in human serum using capillary electrophoresis.[33] All three of the pharmaceutical drugs were successfully separated and measured with capillary zone electrophoresis taking into consideration the effect of buffer concentration.

Cyclic voltammetry (CV) is a great and commonly preferred electrochemical mode to study the reduction and oxidation of activities of several molecules. It is also very practical to research electron transfer promoted chemical reactions such as catalysis.[34] CV is grounded on a linear waveform where potential applied changes as a function of time whereas the rate of change in potential with time is referred to as scan rate. The simplest electrochemical mode that uses such a waveform is known as linear sweep voltammetry (LSV) which involves only a single linear sweep from the lower potential limit to the upper limit.[35] CV and LSV are techniques that are less used but are relevant for understanding the redox mechanisms. To improve the speed and sensitivity of the electrochemical experiment, various arrangements of the potential modulation have been made available and in doing so have led to the development of pulse techniques namely normal pulse voltammetry (NPV), differential pulse voltammetry (DPV), and square gave voltammetry (SWV).[36] NVP uses several potential pulses of rising amplitude proceeded by current measurements close to the end of every pulse so that sufficient time is left for the decay of the charging current The experiment takes place at a dropping mercury electrode (DME) interface and the resulting voltammogram plot shows sampled current against potential relative to pulse steps. DPV is closely related to NPV because potential is scanned with little pulses but also differs largely since in DPV each potential is fixed at small amplitudes and superimposed on a slow-changing bias potential. In SWV mode, the symmetrical square-wave pulse of amplitude has a staircase form, and the net charge current is established by taking the difference between the forward and reverse currents which are rooted in the redox potential. In an analytical sense, the current peak height is proportional to the concentration of the redox species thus is DPV and SWV good modes for the assay of pharmaceutical drugs and biological samples.

Another electrochemical method used to determine lamivudine in human serum and plasma involved Clark-Lubs buffer as an electrolyte with a hanging mercury drop electrode. Determining trace amounts of the drug in such a manner was feasible in pharmaceuticals also.[37] The hanging mercury drop electrode is the working electrode, Ag/AgCl as the reference electrode, and platinum wire acted as an auxiliary/counter electrode while both CV and DPV modes were utilized to obtain voltammograms. A

separate study to measure zidovudine in serum including urine, also led to the use of a hanging mercury drop electrode which allowed the examination as well of azidopyrimidine analogs that form part of DNA and RNA function.[38] Square wave voltammetry was selected as electrochemical mode and determinations extended to the keratinocyte cells. The electro-oxidative determination of emtricitabine, an HIV drug, in an aqueous solution was performed on a gold disc electrode and in the linear sweep mode.[39] A well-defined irreversible anodic signal corresponded to the oxidation of emtricitabine. Polypyrrole film which has been infused with conductive gold nanoparticles was synthesized on a glassy carbon electrode and applied as a platform for CYP3A4 enzyme immobilization to fabricate a biosensor to accurately detect indinavir, a protease inhibitor.[40] Abacavir is a drug that belongs to the nucleoside reverse transcriptase inhibitor class and required a trusted method for its reduction behavior.[41] The findings in a protic-rich environment revealed electro reduction and proton transfers in various sequences based on electrochemical parameters. Many electrochemical techniques for zidovudine have been reported due to its fast responsiveness, inexpensiveness, and sensitivity except for the case of using the electrodeposition technique. Silver nanofilm was to be deposited onto a glassy carbon electrode modified with a multiwalled carbon nanotube and demonstrated its electrolytic performance observed in the presence of the analyte.[42]

For raised stability and sensitivity, modifying the surfaces of electrodes is providing better selectivity which supports the advantages of developing electrochemical techniques.[43] Improving electrode surfaces in this manner gives more opportunity for the development of innovative analytical testing in cases of crucial electrochemical investigations and electroanalytical approaches. Making electrodes specific to analytes facilitates better discrimination in the sample matrix, enhanced electron transfer, and consistent signals due to analyte presence which would otherwise be difficult with bare glassy carbon electrodes.[44] Electrochemical methods have been proven to show added responsiveness and reliability for measuring quantities of electroactive compounds like NVP. Furthermore, does the simple device configuration, low cost, and rapidness of the technique, create a sought-after option where personnel technical skill is lacking. Because of mercury's toxicity, it carries the risk of contaminating the environment despite a mercury thin film electrode's suitability

in adsorptive stripping voltammetry being suitable for determining Nevirapine.[45] At trace analytical levels, better electrical conductivity, and larger measuring surface area can be acquired for NVP by modifying electrodes.[46]

2.7 Electroanalytical detection methods for Nevirapine

Reports indicate that several materials have been used to modify electrodes to quantify Nevirapine in samples such as human serum including pharmaceutical formulations. Uracil covalently grafted carbon paste electrode was created by electro-deposition of uracil onto the carbon paste electrode surface.[47] The S/N ratio of 3, a detection limit of 0.05μM as well as a linear relationship between analyte concentration and oxidation peak current between 0.1 to 70.0μM were achieved after optimal conditions for the method were established. Adenine and guanine reacted with uracil which negatively influenced this modified electrode's current response. The electrochemical oxidation of NVP at a bare glassy carbon electrode surface was promising because, in phosphate buffer, the linearity of the method was in the range of 5.0 to 350 μM, and the limit of detection was 1.026 μM, and the limit of quantification was 3.420 μM. Oxidation of the analyte due to adsorption resulting in the fouling of the electrode lowered Nevirapine peak current significantly when obtaining multi-sweep voltammograms.[1] Utilizing sodium hydroxide supporting electrolyte, a linear current density response for NVP concentration was reached with a carboxylated multiwalled carbon nanotube and synthesized 11-mercaptoundecanoyl hydrazine carbothioamide coated with silver nanoparticles composite modified glassy carbon electrode.[48] The amperometric method was applied at a constant potential showing that AgNPs have some of the best catalytic properties and its decoration with organic or inorganic composite exhibits a synergistic effect on the analyte. The drawback of this electrode modification however is that NVP could not be oxidized under acidic media. Pharmaceutical and blood serum samples were examined for NVP with multiwalled carbon nanotube/poly (methylene blue)/gold nanoparticles composite modified graphite electrode[49] and confirmed that with increasing NVP concentration there is proportionality with oxidation peak current. To support electron transfer, an electrode modifier consisting of an organic dye such as methylene blue, π to π electronic interactions between organic compounds and carbon nanotube which possess a π conjugative arrangement was suggested to measure Nevirapine. The issue incurred

though with this biosensor is physically adsorbed methylene blue monomer that clogged the electrode surface. At the increase of NVP concentration, a comparative trend in oxidation peak current was noticed when MoS_2 quantum dots decorated Pd@rGO acted as electrode modifiers.[50] Two-dimensional (2D) graphene oxide provides a good matrix but despite this, MoS_2 has structural defects like point defects that may play a negative role during biomedical assays.

Biomolecules at the surface of an electrochemical sensor are responsible for binding and are used to recognize events during HIV treatment.[33] Minimal electrical interference because of biological specimen medium, reasonable signal-to-noise ratio, and ease of use are among the benefits of a wide group of biosensors. Impedance, potentiometric, voltammetric, and amperometric measurements give changes in electrical impedance, voltage, and current that is related to occurrences at the electrode surface due to biomolecules taking part in an electrochemical reaction. The generation of redox current is prompted by the electrochemical reaction measured in the case of amperometric or voltammetric strategies thus direct reduction or oxidation relative to current is recorded by biosensors. Output current is reduced if a resulting electrochemical reaction blocks electron transfer when for example as specific antibodies capture antigen molecules in affinity-based sensors. Charge or potential generation on the electrode surface is measured by potentiometric biosensors and can consist of a reference electrode, including an ion-selective electrode that reacts specifically to analyte species. Measuring biomolecules activity at the electrode surface is made possible by the signal transduction approach since current response can be monitored when the sinusoidal voltage at a certain frequency is applied to create an interface in alternating current steady-state, to track for example electrical impedance. Biomolecules interaction is confirmed when electrochemical reactions cause changes in electrical properties and hence current to voltage ratios are affected.

2.8 Zinc oxide application

Nano zinc oxide (ZnO) is a very versatile compound due to its remarkable physiochemical characteristics such as consistency and photo-stability.[51] It offers a solution to corrosion protection, surface coatings, electronics, computers, sunscreen protection, medicine, diagnostic techniques, and antibacterial band-aids. Surface

reaction activity, environmental friendliness, and large surface-area-to-volume ratio improve the field of electroanalysis because of the qualities of ZnO. [52] High electron mobility attributed to large exciton binding energy and appreciative bandgap are the properties of an n-type semiconductor such as zinc oxide. ZnO is an innovative material and can act as a cost-effective alternative in many disciplines. It exists in single crystals as bulk as well as thin films. Synthesizing ZnO in crystalline form involves generating it from seed (precursor) level or onto other substrates; both of specific quality, possessing electrical and optical properties.[53] Different synthesis routes of ZnO can certainly impact its particle size, shape, crystal structured particle size distribution, and dispersion. Preparation techniques of ZnO are spray pyrolysis, wet polymerization, chemical vapor deposition, solvothermal, microemulsion, hydrothermal process, direct precipitation, and sol-gel chemical hydrolysis.[54, 55] Reaction conditions such as precursor concentration, temperature, and time have a significant effect on the nature of resulting ZnO. ZnO can be used in many different applications like in pharmaceutical industries, glass manufacturing as well as other technical supplies. This is linked to the fact that ZnO is seen as a solution to composites that have poor metal stability and controls the heterogeneous distribution of nanocrystals.[56] Reducing mechanical stress in proteins or ceramics can be reached with superior piezoelectric qualities influenced by rigidity and hardness which zinc oxide has. Reinforcements to concrete can be made through enhancing cement pore structure, and flexural and tensile strength which is heavily constituted by ZnO.[57] Furthermore is the kinetic properties of ZnO noticeable when measuring the radiation absorption forming new compounds. Nanoclay ZnO hybrids can be prepared by alkaline ion exchange which involves simple synthetic steps, no solvent, and a relatively short experiment time.[58] Furthermore, has ZnO received considerable research interest in its purpose in electrochemical sensors. The research was done to develop a novel electrochemical sensor using a glassy carbon electrode modified by graphene, AgNPs-ZnO, and methylene blue for the sensitive and selective detection of L-tryptophan. Due to the great electrochemical performance of the methylene blue/AgNPs-ZnO/graphene composite, enhanced voltammetric response to L-tryptophan was noticed on the modified electrode.[59] Research has been documented on a biosensing composite made up of 1,4 benzoquinone, ZnO multiwalled carbon nanotube to quantify xanthine. Such a composite gave enhanced response characteristics towards xanthine due to the combined action of the various

components of the electrode modifying composite.[60] The number of other ZnO-based composites as per figure 2.3, that have been prepared for use in electrochemical sensors is vast and includes fusions with polymers, other metal nanoparticles, biological molecules, graphene derivatives, and carbon nanotubes.

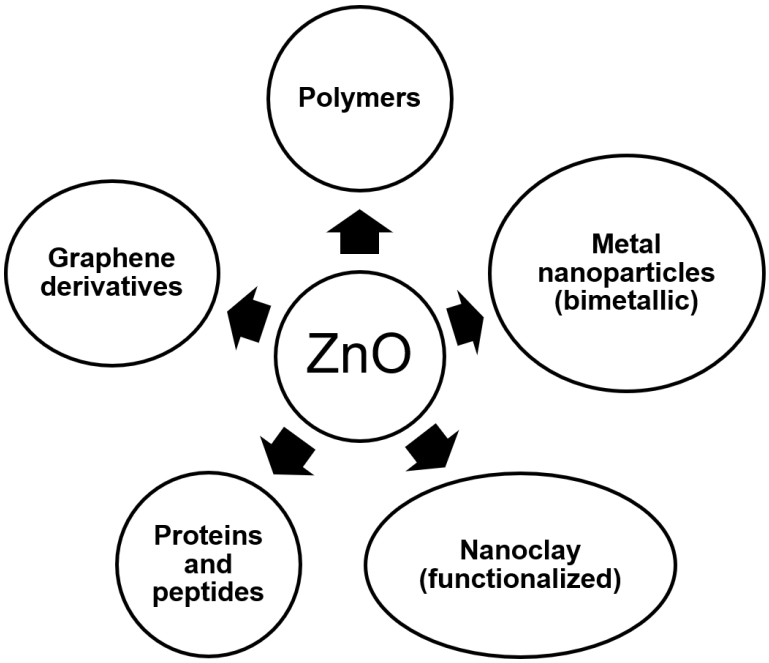

Figure 2.3: The materials which can form composites with ZnO

2.9 Nanoclay

Nanoclay particles have been proved to be a preferred material for important applications because of their rare properties such as being inexpensive, can be modified by other materials, and their surface allowing preconcentration of other species. Interchangeable cations reside in the interlayers of smectite in bentonite mineral clay that can be replaced by other cations through ion exchange to result in layered silicates becoming modified.[61] Nanoclay particles are extremely useful because of their small size, swelling capability, porosity, and ease of controlling their structure through modification containing silicates as well as aluminum hydroxide, Si_2O_5, and $Al_2(OH)_4$, to achieve nano-scaled structure layers. Features like particle size distribution, specific surface area, and crystalline structure as well as containing quartz and feldspar make bentonite a very useful hydrated aluminosilicate mineral clay.[62] Pore volume and surface area can be reduced, and new cracks and surface pores created by replacing different mineral ions situated in surface cavities by

changing the surface nature through nanoclay modification. These particles have been widely said to be responsible for viable uses in catalysis and catalyst support because the immobilization of complex catalysts in clay structures influences the eventual specificity of catalysts.[63] Composite material's chemical and physical properties are substantially through bentonite or organoclay improved by the addition of little quantities. A self-assembled bentonite clay/human serum albumin (HSA) nanocomposite shown in figure 2.4, was observed by a desolvation method involving water.[64]

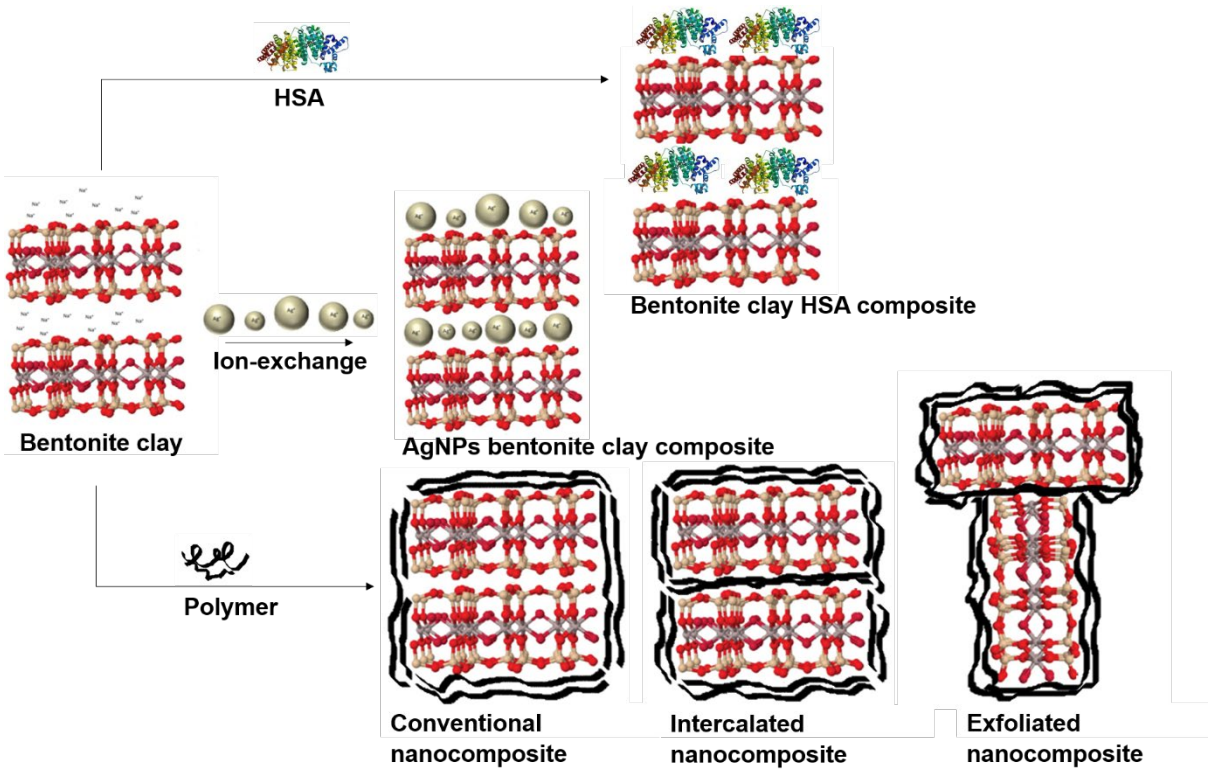

Figure 2.4: The ways that nanoclay can be functionalized with surface modifiers

The dropwise addition of ethanol proceeded after glutaraldehyde was added to the nanocomposite made up of bentonite clay containing a hydroxyl group. The amine ends of lysine in the serum structure experienced crosslinking when human serum albumin was mixed with bentonite clay. The bentonite/human serum albumin nanocomposite was used to modify the surface of disposable pencil graphite electrodes in the application of cytosensing. Synthetic steps have been followed to prepare an AgNPs (silver nanoparticles)/bentonite clay composite as per figure 2.4, to

develop a testing platform for hydrogen peroxide.[65] Clay-based nanocomposites generate an overall enhancement in performance with materials of note like epoxy, nylon, and water-based polymers (figure 2.4), and due to its wide affinity, it is exceptional for pollution control and drug delivery purposes.

2.10 Human serum albumin

Forming composites with polymer conjugates, acting as stabilizers, scaffolds, nanocarriers, and biological templates are pronounced functions of human serum albumin which is the most abundant protein in human plasma.[66] Physiological functions of serum albumin include transport, buffering and nutrition in the body therefore its interaction with minerals in the body is essential to consider due to surface effects impacting serum albumin's bioactivity. Serum albumins are the top circular proteins playing a key role in the spread of lipophilic metabolites and pharmaceutical agents and it is said that nanoparticles in the body reacting lead to many pharmacokinetic as well as pharmacodynamic activities.[67] Drugs, hormones, and metal ions are among some materials to occupy potential binding sites as confirmed by HSA studies thus acting as a versatile natural carrier in blood plasma as well as biocompatible with non-immunogenic characteristics. Voltammetric results indicate that two enantiomers can easily and remarkably be discriminated by an electrode surface modifying composite including HSA.[68] The fabrication of indium tin oxide (ITO) electrodes surface with modifiers including (3-Aminopropyl) triethoxysilane (APTES) molecule, graphene oxide (GO), and human serum albumin (HSA) for the detection of D and L-tryptophan showed pleasing results. In a case reported, the clinical application of a pharmaceutical drug was monitored by electrochemical studies and found that the presence of HSA would also inevitably influence the drug's activity. The electrochemical method concludes that more research will promote wider elucidation of understanding of the true interaction of HSA and direct drug treatment adherence.[69] The measure of adsorption on the surface of different protein layers impacts charge transfer strongly by considering electrical impedance studies of various solid surfaces exposed to macromolecules of biological interest when performing adsorption studies.[70]

2.11 Conclusion

This chapter deliberated the goal behind antiretroviral drugs to restrict the growth of HIV, the known mechanism of Nevirapine, and the issues with conventional laboratory methods when testing it. Reported electroanalytical detection techniques for antiretroviral drug monitoring have revealed limitations in terms of selectivity and sensitivity as well as the complexity of instrument design. There is a need for more specific voltammetry methods with the purpose of point-of-care diagnostics and transducers consisting of materials such as ZnO, nanoclay, and HSA as analytical responsive platforms so that the electrochemical behavior of the analyte is enhanced through the composite's better mass transport, higher effective surface, and catalytic properties.

2.12 References

1. Nagappa Laxman Teradal, Shankar Narayan Prashanth, Jaldappagari Seetharamappa. Electrochemical studies of Nevirapine, an anti-HIV drug, and its assay in tablets and biological samples. J. Electrochem. Sci. Eng. 2(2) (2012) 67-75
2. Muhammad Daniyal, Muhammad Akram, Abdul Hamid, Allah Nawaz, Khan Usmanghani, Saeed Ahmed and Leena Hameed. A comprehensive review on the treatment of HIV. Pak. J. Pharm. Sci., Vol.29, No.4, July 2016, pp.1331-1338
3. Vaidya KA, Kadam AV and Nema V. Anti-Retroviral Drugs for HIV: Old and New. Austin J HIV/AIDS Res. Volume 3 Issue 2-2016
4. Eric J. Arts and Daria J. Hazuda. HIV-1 Antiretroviral Drug Therapy. Cold Spring Harb Perspect Med 2012;2
5. Vassil St. Ceorgiev and John J. McGowan. AIDS: Anti-HIV agents; therapies and vaccines. Annals of the New York Academy of sciences. Volume 616
6. Graeme Meintjes, Michelle A. Moorhouse Sergio Carmona. Adult antiretroviral therapy guidelines 2017. S Afr J HIV Med. 2017;18(1), a776
7. Da-Yong Lu, Hong-Ying Wu, Nagendra Sastry Yarla, Bin Xu, Jian Ding and Ting-Ren Lu. HAART in HIV/AIDS Treatments: Future Trends. Infectious Disorders-Drug Targets, 2018, Vol. 18, No. 1

8. Pomerantz, RJ; Horn, DL. Twenty years of therapy for HIV-1 infection. Nat Med. 2003, 9, 867-873 [2]
9. Lu, DY; Lu, TR. High active antiretroviral therapy for HIV/AIDS, progress and drawback. Adv. Pharmacoepidemiol. Drug Saf., 2012, 1 (6) e115 [3]
10. Lu, DY; Lu, TR; Wu, HY; Che, JY. Challenges for HIV/AIDS therapy. Adv. Pharmacoepidemiol. Drug Saf., 2013, 2 (4), e120
11. Elahe Ahmadi, Mohamad Reza Eyvani, Vahid Riahifar, Hossein Momeneh and Changiz Karami. Amperometric determination of Nevirapine by glassy carbon electrode (GCE) modified with c-MWCNTs and synthesized 11-mercaptoundecanoyl hydrazine carbothioamide coated silver nanoparticles. Microchemical Journal 146 (2019) 1218-1226
12. Chinmoy Ghosh, Shashank Gaur, Ajay Singh, Chandrakanta P. Shinde, and Bhaswat S. Chakraborty. Estimation of Nevirapine from Human Plasma by LC-ESI-MS/MS: A pharmacokinetic Application. J Bioequiv Availab 2011, 3:1
13. Timothy Paul Wood, Cornelia S.J. Duvenage, Egmont Rohwer. The occurrence of anti-retroviral compounds used for HIV treatment in South African surface water. Environmental Pollution 199 (2015) 235-243
14. Taha E Taha, Newton I Kumwenda, Amanda Gibbons, Robin L Broadhead, Susan Fiscus, Valentino Lema, George Liomba, Chiwawa Nkhoma, Paolo G Miotti, Donald R Hoover. Short postexposure prophylaxis in newborn babies to reduce mother-to-child transmission of HIV-1: NVAZ randomized clinical trial. The Lancet. Vol 362. October 11, 2003
15. Kirsten Salado-Rasmussen, Zahra P. Theilgaard, Mercy G. Chiduo, Ib C. Bygbjerg, Jan Gerstoft, Margrethe Lüneborg-Nielsen, Martha Lemnge, Terese L. Katzenstein. Nevirapine, Sodium Concentration and HIV-1 RNA in Breast Milk and Plasma among HIV Infected Women Receiving Short-Course Antiretroviral Prophylaxis. PLos One 10(3): e0121111.
16. Sanjay S. Patel and Paul Benfield. Nevirapine. Clinical Immunotherapeutics. October 1996
17. C Swanepoel, H Bouwman, R Pieters & C Bezuidenhout. Presence, concentrations, and potential implications of HIV antiretrovirals in selected water resources in South Africa. Water Research Commission. Report number: WRC Report No 2144/1/14

18. Paul E. Stackelberg, Edward T. Furlong, Michael T.Meyer, Steven D. Zaugg, Alden K.Henderson, Dori B. Reissman. Persistence of pharmaceutical compounds and other organic wastewater contaminants in a conventional drinking-water treatment plant. Science of the Total Environment 329 (2004) 99-113
19. J. Brooks Jackson, James Dick, Tsigereda Tekle, Antoine Simmons, Karen C. Carroll. Lack of antimicrobial activity by the antiretroviral drug Nevirapine against common bacterial pathogens. Antimicrobia; agents and chemotherapy. August 2009, p. 3606-3607
20. C. Schoeman, M. Dlamini, O.J. Okonkwo. The impact of a Wastewater Treatment Works in Southern Gauteng, South Africa on efavirenz and Nevirapine discharges into the aquatic environment. Emerging Contaminants 3 (2017) 95-106
21. Lawrence Obidike and Jean Mulopo Effect of High Concentration of Nevirapine on the Growth of E. Coli in Wastewater Treatment. Proceedings of the World Congress on Engineering and Computer Science 2018 Vol II
22. Chinmoy Ghosh, Shashank Gaur, Ajay Singh, Chandrakanta P. Shinde, and Bhaswat S. Chakraborty. Estimation of Nevirapine from Human Plasma by LC-ESI-MS/MS: A pharmacokinetic Application. J Bioequiv Availab 2011, 3:1
23. Mohammed Lamorde, Quirine Filleke, Kim Sigaloff, Cissy Kityo, Allan Buzibye, Joshua Kayiwa, Concepta Merry, Lillian Nakatudde-Katumba, David Burger, and Tobias F Rinke de Wit. Therapeutic drug monitoring of nevirapine in saliva in Uganda using high-performance liquid chromatography and a low-cost thin-layer chromatography technique. BMC Infectious Diseases 2014, 14:473
24. Purnima Hamrapurkar, Mitesh Phale, Priti Patil and Nitul Shah. Determination of Nevirapine in human plasma by high-performance liquid chromatography with ultraviolet detection. Int. J. Pharm Tech Res. 2010, 2 (2)
25. Elijah Ngumba, Anthony Gachanja, Tuula Tuhkanen. Occurrence of selected antibiotics and antiretroviral drugs in Nairobi River Basin. Kenya Science of the Total Environment 539 (2016) 206-213
26. Mohammed Lamorde, Quirine Filleke, Kim Sigaloff, Cissy Kityo, Allan Buzibye, Joshua Kayiwa, Concepta Merry, Lillian Nakatudde-Katumba, David Burger, and Tobias F Rinke de Wit. Therapeutic drug monitoring of nevirapine in saliva

in Uganda using high-performance liquid chromatography and a low-cost thin-layer chromatography technique. BMC Infectious Diseases 2014, 14:473

27. T.V. Sreevidya and B. Narayana. Spectrophotometric determination of Nevirapine using tetrathiocyanatocobalt(II) ion as a reagent. Ecl. Quím., São Paulo, 35-3: 93-102, 2010
28. Kirsten Salado-Rasmussen, Zahra P. Theilgaard, Mercy G. Chiduo, Ib C. Bygbjerg, Jan Gerstoft, Margrethe Lüneborg-Nielsen, Martha Lemnge, Terese L. Katzenstein. Nevirapine, Sodium Concentration and HIV-1 RNA in Breast Milk and Plasma among HIV Infected Women Receiving Short-Course Antiretroviral Prophylaxis. PLoS ONE 10(3)
29. J. Fogel, D.R. Hoover, J.I.N. Sun, L.M. Mofenson, M.G. Fowler, A.W. Taylor, N. Kumwenda, T.E. Taha, and S.H. Eshleman. Analysis of nevirapine (NVP) resistance in HIV-infected infants who received extended NVP or NVP/zidovudine prophylaxis. AIDS 2011, Vol 25 No 7
30. Burcin Bozal, Bengi Uslu and Sibel A. Ozkan. A Review of Electroanalytical Techniques for Determination of Anti-HIV Drugs. International Journal of Electrochemistry Volume 2011, Article ID 343947
31. James P. Landers. Clinical Capillary Electrophoresis. Clin. Chem. 41/4, 495-509 (1995)
32. Burcin Bozal, Bengi Uslu and Sibel A. Ozkan. A Review of Electroanalytical Techniques for Determination of Anti-HIV Drugs. International Journal of Electrochemistry Volume 2011, Article ID 343947
33. Noemie Elgrishi, Kelley J. Rountree, Brian D. McCarthy, Eric S. Rountree, Thomas T. Eisenhart, and Jillian L. Dempsey. A Practical Beginner’s Guide to Cyclic Voltammetry. J. Chem. Educ. 2018, 95, 197−206
34. Service Department. Instruction manual for Basi Epsilon for electrochemistry. 2000-2009 Bioanalytical Systems
35. Samuel P. Kounaves. Voltammetric Techniques. Handbook of Instrumental Techniques for Analytical Chemistry. Tufts University, Department of Chemistry
36. Katia Christina Leandro, Josino Costa Moreira, Pércio Augusto Mardini Farias. Differential Pulse Voltammetric Studies on Lamivudine: An Antiretroviral Drug. American Journal of Analytical Chemistry, 2013, 4, 47-51

37. Jan Vacek, Zdenek AndrysÌk, Libuse Trnkova, Rene Kizek. Determination of Azidothymidine-an Antiproliferative and virostatic drug by Square-Wave Voltammetry. Electroanalysis 2004, 16, No. 3
38. Balaji B. Mulik, Sambhaji T. Dhumal, Rajkumar R. Harale, Kiran R. Kharat, and Bhaskar R. Sathe. Electrochemical Studies of Anti-HIV Drug Emtricitabine: Oxidative Determination and Improved Antimicrobial Activity. Chem Electro Chem 2018, 5, 1-7
39. Natasha Ross, Nicolette Hendricks-Leukes, Rachel Fanelwa Ajayi, Priscilla Baker, and Emmanuel I. Iwuoha. Conductive Composite Biosensor System for Electrochemical Indinavir Drug Detection. Journal of Chemistry Volume 2015, Article ID 630408
40. Burcu Dogan, Bengi Uslu, Sibel A. Ozkan and Petr Zuman. Electrochemical Determination of HIV Drug Abacavir Based on Its Reduction. Anal. Chem. 2008, 80, 209-216
41. Amir Abbas Rafati and Ahmadreza Afraz. Amperometric sensing of anti-HIV drug zidovudine on Ag nanofilm-multiwalled carbon nanotubes modified glassy carbon electrode. Materials Science and Engineering C 39 (2014) 105–112
42. Daniel Apath, Mambo Moyo, and Munyaradzi Shumba. TiO_2 Nanoparticles Decorated Graphene Nanoribbons for Voltammetric Determination of an Anti-HIV Drug Nevirapine. Volume 2020, Article ID 3932715
43. Saeed Shahrokhian, Razieh Kohansal, Masoumeh Ghalkhani, and Mohammad K. Amini. Electrodeposition of Copper Oxide Nanoparticles on precasted Carbon Nanoparticles Film for Electrochemical Investigation of anti-HIV Drug Nevirapine. Electroanalysis 2015, 27, 1989 – 1997
44. Juan J Pina, Abel I Balbin, Carmen ana M Esteva, Elias Blanco, Quintana, Pedro Hernandez. Determination of Nevirapine in the presence of cucurbit (7) uril with a gold electrode. J. Electrochem. Sci. Eng. 4(1) (2014) 37-44
45. Camila Alves de Lima, Edson Roberto Santana, Jamille Valéria Piovesan, Almir Spinelli. Silver nanoparticles-modified electrode for the determination of nitro compound-containing pesticides. Anal Bioanal Chem (2016) 408: 2595-2606
46. Fenfen Zhang, Li Li, Liqiang Luo, Yaping Ding, Xiao Liu. Electrochemical oxidation and determination of antiretroviral drug Nevirapine based on uracil-modified carbon paste electrode. J.Appl Electrochem (2013) 43:263-269

47. Elahe Ahmadi, Mohamad Reza Eyvani, Vahid Riahifar, Hossein Momeneh and Changiz Karami. Amperometric determination of Nevirapine by glassy carbon electrode (GCE) modified with c-MWCNTs and synthesized 11-mercaptoundecanoyl hydrazine carbothioamide coated silver nanoparticles. Microchemical Journal 146 (2019) 1218-1226
48. Mohammad Bagher Gholivand, Elahe Ahmadi, and Mozhdeh Haseli. A novel voltammetric sensor for Nevirapine, based on modified graphite electrode by MWCNs/poly (methylene blue)/gold nanoparticles. Analytical Biochemistry 527 (2017) 4-12
49. Preeti Tiwari, Narsingh R. Nirala, and Rajiv Prakash. Determination of the Anti-HIV Drug Nevirapine Using Electroactive 2D Material Pd@rGO Decorated with MoS_2 Quantum Dots. Chemistry Select 2018, 3, 5341-5347
50. Shambhu Sharan Kumar. Chemical synthesis of zinc oxide nanoparticles by precipitation method. International journal of engineering and technological research (IJETR). Volume 2012, January-June 2012
51. Yu Ya, Cuiwen Jiang, Tao Li, Jie Liao, Yegeng Fan, Yuning Wei, Feiyan and Liping Xie. A zinc oxide nanoflower-based electrochemical sensor for trace detection of sunset yellow. Sensors 2017, 17, 545
52. Anderson Janotti and Chris G van de Walle. Fundamentals of zinc oxide as a semiconductor. Rep. Prog. Phys. 72 (2009) 126501
53. Ravangave L.S. and Shaikh R.S. Influence of pH on structure, morphology, and UV/visible spectra of ZnO nanorods. International journal of engineering science invention, volume 6 Issue 11, November 2017, p76-79
54. A. Khorsand Zak, R. Razali, W.H. Abd Majid, Majid Darroudi. Synthesis and characterization of the narrow size distribution of zinc oxide nanoparticles. International journal of nanomedicine 2011:6, 1399-1403
55. Sherif Mohamed, Abdel Salam KESHK, Mohamed Saad HAMDY. Preparation of physicochemical characterization of zinc oxide/sodium cellulose composite for food packaging. Turkish Journal of chemistry 2019, 43:94-105
56. Mohammed Reza Arefi and Saeed Rezaei-Zarchi. Synthesis of zinc oxide nanoparticles and their effect on the compressive strength and setting time of self-compacted concrete as cementitious composites. Int. J. Mol. Sci. 2012, 13, 4340-4350

57. N. Garshasbi, M. Ghorbanpour, A. Nouri, and S. Lotfiman. Preparation of zinc oxide-nanoclay hybrids by alkaline ion-exchange method. Brazilian journal of chemical engineering. Vol. 34, no. 04, pp. 1055-1063, October-December 2017
58. Yao Wang, Dan Li, Junfeng Kang, Shiye Guan and Daoxin Wu. An electrochemical sensor Based on MB/Ag-ZnO/Graphene modified glassy carbon electrode for determination of L-Tryptophan in Biofluid Samples. Int. J. Electrochem. Sci., 14 (2019) 5448-5461
59. Berna Dalkıran, Ceren Kaçar, Pınar Esra Erden and Esma Kılıç. Electrochemical xanthine biosensor based on Zinc oxide nanoparticles-multiwalled carbon nanotubes-1,4-benzoquinone composite. JOTCSA. 2018; 5(1): 317-332
60. A. Abu R Abi-Stankovic, A. Milutinovic-Nikolic, N. Jovic-Jovic IC, P Bankovic, M.Z. Unic, Z. Mojovic and D. Jovanovic. p-Nitrophenol electro-oxidation on a $BTMA^{+}$ bentonite modified electrode. Clays and Clay Minerals, Vol. 60, No. 3, 291–299, 2012
61. B. S.Surendra, H.P. Nagaswarupa, K.S. Anantharaju, M.R. Anil Kumar, H. Nagabhushana, Krushitha Shettya. Acid Activation of Bentonite Clay under Microwave Irradiation: Characterization, Cyclic Voltammetry, and Photocatalytic activity. Materials Today: Proceedings 5 (2018) 22643–22651
62. Vladimir Borek and Matthew J. Morra. Cyclic Voltammetry of Aquocobalamin on Clay-Modified Electrodes. Environ. Sci. Technol. 1998, 32, 2149-2153
63. Wanju Zhang, Qingbo Zhang, Fang Wang, Lian Wang, Lian Yuan, Ziqiang Xu, Fenglei Jiang, and Yi Lu. Comparison of interactions between human serum albumin and silver nanoparticles of different sizes using spectroscopic methods. Luminescence 2015; 30. 397-404
64. Yesim Tugce Yamana, Oznur Akbala and Serdar Abacia. Development of clay-protein-based composite nanoparticles modified single used sensor platform for electrochemical cytosensing application. Biosensors and Bioelectronics 132 (2019) 230-237
65. Dharmendra Kumar Yadav, Rupali Gupta, Vellaichamy Ganesan, Piyush Kumar Sonkar, Pankaj Kumar Rastogi. Electrochemical sensing platform for hydrogen peroxide determination at low reduction potential using silver nanoparticle-incorporated bentonite clay. J Appl Electrochem (2016) 46:103–112

66. Wanju Zhang, Qingbo Zhang, Fang Wang, Lian Wang, Lian Yuan, Ziqiang Xu, Fenglei Jiang and Yi Lu. Comparison of interactions between human serum albumin and silver nanoparticles of different sizes using spectroscopic methods. Luminescence 2015; 30. 397-404
67. Mohd. Sajid Ali, Hamad A. Al-Lohedan, Ayman M. Atta, Abdelrahman O. Ezzat, Sami A.A. Al-Hussain. Interaction of human serum albumin with silver nanoparticles functionalized with polyvinylthiol. Journal of molecular liquids 204 (2015), 248-254
68. Erhan Zor, Imren Hatay Patir, Haluk Bingol, Mustafa Ersoz. An electrochemical biosensor based on human serum albumin/graphene oxide/3-aminopropyl triethoxy silane-modified ITO electrode for the enantioselective discrimination of D- and L-tryptophan Biosensors and Bioelectronics 42 (2013) 321–325
69. Jing Zhao, Xiaofeng Zheng, Wei Xing, Junyi Huang, and Genxi Li. Electrochemical Studies of Camptothecin and Its Interaction with human serum albumin. Int. J. Mol. Sci. 2007, 8, 42-50

CHAPTER THREE: ZnO synthesis and characterization

3.1 Summary

The following chapter presents the use of metal oxide nanoparticles like zinc oxide, synthesis methods, and characterization of ZnO. This is followed by the methodology used in the study as well as the respective characterization protocol. The results and discussion described the findings while the conclusion highlights the major findings.

3.2 Introduction

Nanoparticles of transition metal oxides are researched due to their variety of sizes, shapes, and compositions. The valence state of these metals and defect structures in the oxygen lattice permits the modification for electrical, optical, magnetic, mechanical, and chemical purposes.[1] Therefore, nanostructured ZnO is an extremely coveted compound for its potential applications in wider areas such as nanoscale devices, light-emitting diodes, ultraviolet lasers, and gas sensors.[2] ZnO is exceptionally good in advanced catalytic applications and is drawing interest in the field of photo-catalysis.[3] Lowered porosity is achieved through firmer microstructure when ZnO acts as nano-filler and nano reinforcer because it is so reactive. Furthermore, it accelerates cement hydration when it serves as heterogenous nuclei in cement pastes. The pore assembly, flexural and tensile power of concrete is enhanced when integrating ZnO.[4] Reports show that ZnO is resilient against infection due to its anti-inflammatory response. This has led to findings that it promotes healing in skin wounds in pigs as well as resisting intestinal sickness by being a protective agent. Managing post-weaning diarrhea in piglets has been achieved pharmacologically using ZnO.[5] Many forms of nanostructured ZnO can be synthesized like nanowires, nanorods, nanosheets, or nanoflowers and are related to unique applications. These numerous morphological options are dependent upon laboratory synthesis conditions and involve techniques like hydrothermal, solvothermal process, sol-gel, wet chemistry precipitation method, and polyol process.[2] Figure 3.1 is the grouping of the experimental ZnO synthesis protocols.

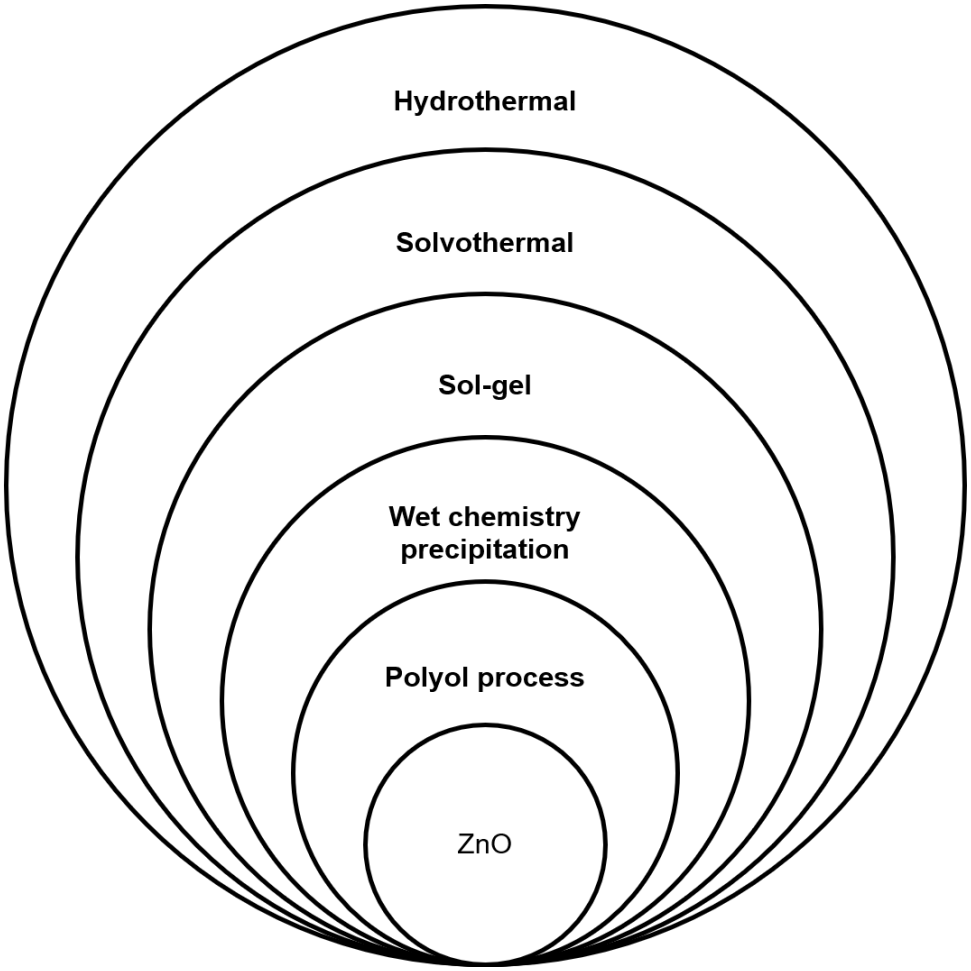

Figure 3.1: The list of various ZnO synthetic laboratory methods

3.3 ZnO synthesis methods

3.3.1 Hydrothermal

The hydrothermal method was a simple and environmentally friendly process since no grinding or calcination were required. The reaction was performed in a Teflon-lined stainless steel autoclave[6,7] where zinc salt precursors like $Zn(NO)_3$, $Zn(CH_3COO)_2$ or $ZnCl_2$, and an inorganic base such as NaOH[6,7] were heated to temperatures between 60 and 220^oC[7,8] with substantial stirring for 2 to 12 hours. The resulting product was cooled down to room temperature.

3.3.2 Solvothermal

In the solvothermal method, ZnO was synthesized by a reaction where a precursor such as $Zn(CH_3COO)_2$ or $ZnSO_4$ got converted in the presence of solvents such as ethylene glycol, ethanol, LiOH, NaOH, or Na_2CO_3 [1,9] while temperatures of 120 to

200°C were maintained. The batch reactor[10] for such a process remained closed and pressure conditions were regulated for 12 to 72 hours. After the reaction, the nanoparticles formed were collected, further washed, and allowed to dry in air.

3.3.3 Sol-gel method

In the sol-gel synthesis technique, ZnO was produced using the transformation of the zinc precursor which was $Zn(NO)_3$ or $Zn(CH_3COO)_2$ solution [11,12], solvents like 2-amino ethanol, 2-methoxy ethanol, ethanol, polyethylene glycol 2000, ethylene glycol or polyvinyl alcohol and base components like NaOH or ammonia solution. After a sol was added and strong stirring applied, a colloidal suspension was formed followed by washing and the inclusion of gelatine. The mixture was heated between 50 to 80°C[13] to evaporate the solvent for 2 to 4 hours and underwent calcination to collect the ZnO product. A reaction container that allowed for clear visibility was required.

3.3.4 Wet chemistry precipitation

The wet chemistry method for ZnO was rapid[2,14] and involved the zinc salt precursor such as $Zn(NO)_3$, $Zn(CH_3COO)_2$, or $ZnCl_2$ solution that was treated with a reducing agent in the form of NaOH, KOH, or $NaNO_3$ at room temperature. The experiment took place in water media and involved vigorous mixing[15] over about 2 hours, the precipitate was cooled to room temperature, washed, and centrifuged. The critical experimental parameters were the concentration of reagents, rate of adding a reducing agent, and reaction temperature.

3.3.5 Polyol process

With the polyol procedure, ZnO was prepared with a zinc salt precursor like $Zn(NO)_3$ or $Zn(CH_3COO)_2$ in the absence of water[16] but rather solvent environments such as ethylene glycol, 1,2 propane diol, butane diol, tetra ethylene glycol or p-toluenesulfonic acid monohydrate [17], due to their high boiling points (> 100°C). In the reaction, the zinc salt precursor was dissolved entirely for 10 minutes to 12 hours and subjected to reflux or sonication[18] to achieve the final product.

3.4 ZnO characterization tools

Several analytical techniques can be utilized when having to characterize zinc oxide nanoparticles based on their structure and composition. Due to valuable information obtainable from characterization methods, they can be categorized into electron microscopy, spectroscopy, particle properties analysis, thermal analysis, and electrochemical as per figure 3.2. It is effective to combine the different results from them to discuss the properties of nanoparticles fully.

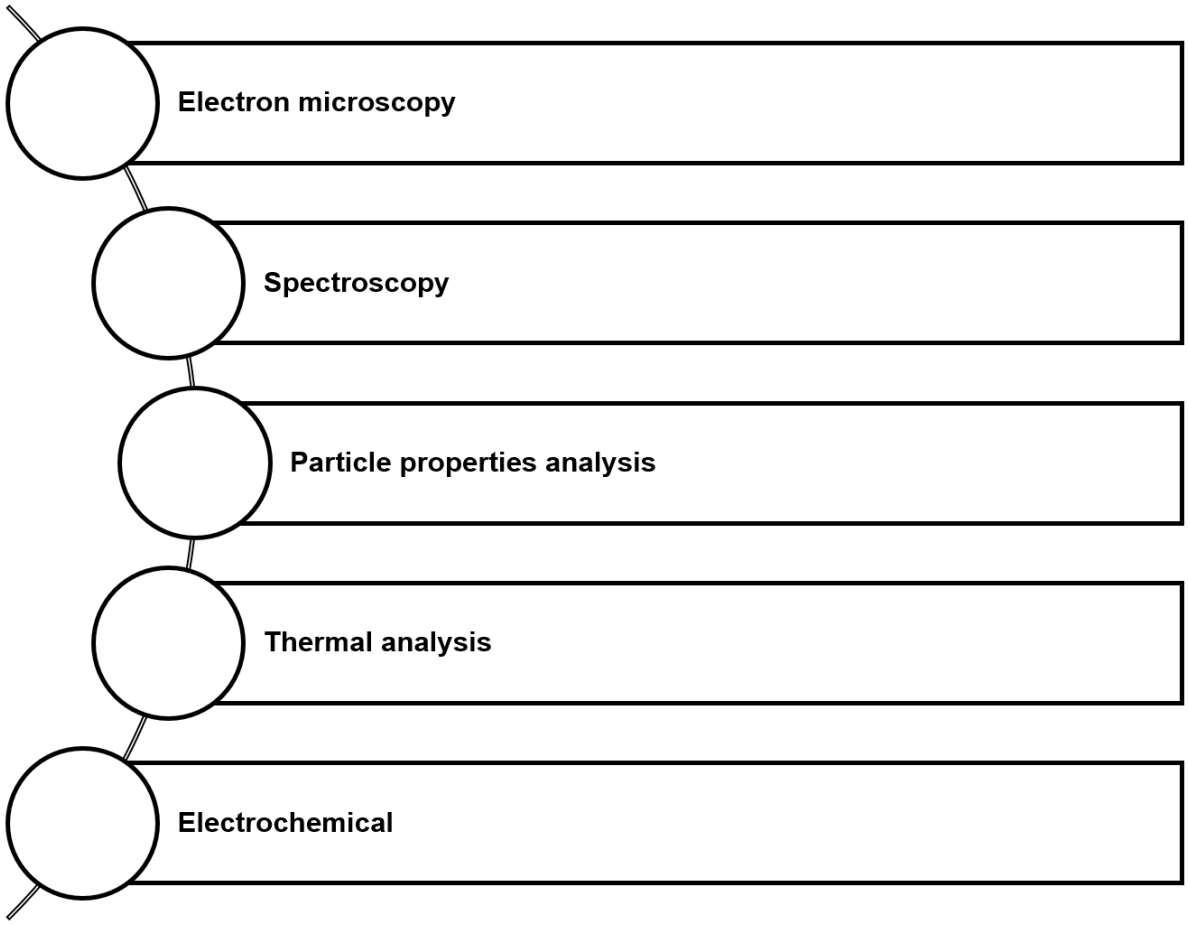

Figure 3.2: The categories of analytical characterization for nanoparticles

3.4.1 Electron microscopy

3.4.1.1 Scanning electron microscopy and transmission electron microscopy

Among this category are techniques involving scanning electron microscopy (SEM) and transmission electron microscopy (TEM). It serves to determine morphology, microstructure, shape, and crystallinity. In SEM and TEM an electron beam is used to

image a sample with resolution down to nanometre level and in the case of TEM, these are powerful techniques for material science because of the high energy electron beam which creates interactions between the electrons and the atoms. This results in the ability to observe features like crystal structure, dislocations, or grain boundaries. Electron microscopy can be used to study the growth of layers, the consequent composition, and defects in nanoparticles. The selected area electron diffraction (SAED) patterns obtainable for a sample are facilitated through electrons which are scattered by electrostatic potential because of constituent atoms in the sample.

3.4.2 Spectroscopy

Spectroscopic techniques involve the irradiation of the sample to understand its response as a function of chemical composition. Elemental composition, consistency, functionality, molecular states, absorption, and emission behavior is confirmed.

3.4.2.1 Ultraviolet/visible

Ultraviolet/visible (UV/vis) spectroscopy takes place when the sample in a cuvette is exposed to light in the UV/vis region and if completely in solution, the atomic molecules shall absorb the radiation quantitatively. That radiation that passes through the sample is transmitted light and the ratio between this and the light absorbed indicates a concentration of analyte species present. This relationship of absorbance related to concentration is given by the Lambert-Beer law.

3.4.2.2 Fourier transform infrared

Fourier transform infrared (FTIR) spectroscopy considers the sample's ability, through the molecules absorbing light in the infrared region, to convert it to molecular vibrations. This behavior is related to characteristic absorption by chemical bonds present in the sample that results in an infrared spectrum which presents a molecular fingerprint that is used to identify organic or inorganic species.

3.4.2.3 X-ray diffraction

In the x-ray diffraction (XRD) technique, an x-ray beam hits the sample and interacts with electrons in the atoms that leading to photons from the incident beam that is

deflected wayward from the original path. Such deflected photons that have unchanged wavelengths are said to be elastically scattered but retain their energy and are quantified in diffraction protocol since they possess information about electron distribution in the sample. The XRD peaks which are collected relate to atomic distances through the Braggs law.

3.4.2.4 Raman

Raman spectroscopy involves looking at the inelastic light scattering in a sample where the incoming radiation translates energy by atoms to molecular vibrations. This scattered light can be detected to represent a chemical impression of a sample utilizing the spectral information that is used to correctly identify the classification of the sample.

3.4.2.5 Photoluminescence

Photoluminescence (PL) spectroscopy occurs when light energy stimulates the emission of a photon from molecules when it is directed onto a sample. Light is absorbed and leads to a process called photo-excitation and it is seen that such molecules elevate to a higher electronic state and release energy (photons) as it returns to lower energy, Such emission of light or luminescence observed is photoluminescence.

3.4.2.6 Energy dispersive x-ray

Energy dispersive x-ray (EDX) spectroscopy is a surface analytical technique where an electron beam collides with the sample causing existing electrons near the nucleus followed by more distant electrons to drop energy levels to fill the resulting cavities created. Every element emits a different set of x-ray frequencies as their empty lower energy states are refilled therefore determining such emissions will provide both qualitative (spectral) as well as quantitative information about the near-surface topography of a sample.

3.4.3 Particle properties analysis

3.4.3.1 Zetasizer

Specific surface area, average particle size, polydispersity, and Zeta potential can be established by considering the nature of particle properties. Zetasizer is a technique that performs size measurements using a process known as dynamic light scattering or called photon correlation spectroscopy. It determines Brownian motion and is connected to particle dimensions. This occurs due to illuminating the particles with a laser and analyzing the intensity fluctuations in scattered light. Zeta potential and related parameters are established through calculating electrophoretic mobility including the application of the Henry equation. The velocity of the particles is established through laser doppler velocimetry.

3.4.4 Thermal analysis

Thermal analysis techniques are used to carefully investigate the change in mass because of temperature as well as other physical properties over a certain period.

3.4.4.1 Thermogravimetry and differential thermal analysis

Thermogravimetry and differential thermal analysis (TG/DTA) is a simultaneous method in which TG and DTA are combined and measured at the same time by one instrument. Thermogravimetry measures the mass change in a sample and it is used to detect evaporation, decomposition, oxidation, and other effects due to controlled temperature changes. The differential thermal analysis involves a reference material relative to a sample in a specified temperature atmosphere.

3.4.4.2 Differential scanning colorimetry

Differential scanning colorimetry (DSC) allows for thermal analysis of a sample compared to a reference which enables measurements of transitions like glass transition, melting, and crystallization. Furthermore, the chemical reaction such as thermal curing, heat history, specific heat capacity, and purity analysis are measurable. The technique is exceptional since it can perform quantitative temperature difference measurements of heat on the surface of the sample and reference.

3.4.5 Electrochemical characterization

The behavior of electroactive molecules at a glassy carbon electrode surface helps to determine whether electrochemical reactions can be explained through kinetics because the transportation of such redox molecules would be seen as rate determined.[19] Growing diffusion tempos allow for effective determination of electron transfer kinetics through electroanalytical methods due to such tempos reaching limits.[20] When scan rates are considerably high, the electron transfer rate which is strongly influenced by the diffusion of electroactive molecules, elevates these diffusion tempos.[21] Diffusion governed by electron transfer in voltammetry determinations leads to rates that are measurable with a small electrode surface. Establishing the constants responsible for rapid oxidation and reduction reactions can now be grasped more clearly.[22] The movement of redox molecules becomes a major characteristic if the likelihood of such species colliding with the glassy carbon electrode surface before it drifts away is considered. Glassy carbon electrodes are known to be adequate small surfaces for electron transfer reactions since it permits the migration of oxidized molecules.[23] When a few factors affect the tempo of electron transfer, the electrochemical reaction i.e., the process is called kinetically controlled.[24]

The redox potential, E_o, (equation 3.1) represents the mean value of anodic including cathodic peak potentials while the cell potential, ΔEp, is determined (equation 3.2) by the difference between anodic and cathodic peaks. At slower scan rates E_o can be carefully observed causing ΔEp to become a low value; E_o also needs the potential of the reference electrode, Ag/AgCl in this study, to be comparable to E_o values tabulated where for example the normal hydrogen electrode applies.[25]

$$E_0 = \frac{1}{2}\{E_p(cathodic) + E_p(anodic)\} \quad 3.1$$

$$\Delta E_p = E_p(anodic) - E_p(cathodic) = \frac{0.059}{n} \quad 3.2$$

To understand the tempo of reactions at the electrode/electrolyte interface including modified electrode surfaces, the kinetic parameters linked to these events will provide

substantial information. Current is measured by considering the rate of the reaction and transport of the reacting species to the interface including noting the electrode potential where this behavior is taking place; the electrode potential is proportional to features of ZnO. The type of the redox activity taking place at the ZnO modified GCE can be determined by plotting current, Ip against scan rate, v, including Ip against the square root of scan rate, √v, to inspect the correlation between these variables. Good linearity between Ip and v implies that the electrochemical process is adsorption controlled while acceptable linearity of Ip against √v, suggests that the diffusion takes place at the surface. Through making use of the Randle-Sevcik equation, equation 3.3, the diffusion coefficient, D, together with the slope of the plot of current against scan rate. Equation 3.5 is a derived version of Equations 3.3 and 3.4.

$$Ip = 0.4463nFAC(\frac{nFvD}{RT})^{1/2} \quad 3.3$$

$$slope_{Randle-Sevcik} = \left[0.4463nFAC\left(\frac{nFD}{RT}\right)^{\frac{1}{2}}\right] \quad 3.4$$

$$Therefore, D = (\frac{slope_{Randle-Sevick}}{0.4463nFAC})^2 \frac{RT}{nF} \quad 3.5$$

The species adsorbed to an electrode surface can be determined by considering k_s, the heterogenous standard rate constant, using the Laviron method. There are however key criteria to consider that limit the application of the method such as α, and electron transfer coefficient, from the cyclic voltammetry results. Calculating α involves equation 3.6 and the slope of the variation of the plot of the electrode potential against the log of the scan rate. The other variables in the expression are F which is the Faraday constant (96485 C/mol), n, the electron transfer number, T, temperature (298 K), and R, the universal gas constant (8.314 J/mol/K).

$$slope_{Laviron} = \frac{2.3RT}{\alpha nF} \quad 3.6$$

Equation 3.7 can then be applied to determine the heterogenous standard rate constant.

$$Log\ k_s = \propto \log(1-\propto) + (1-\propto) log \propto - \log\left(\frac{RT}{nFv}\right) - \propto (1-\propto)\frac{nF\Delta E_p}{2.3RT} \qquad 3.7$$

Mass transport, m_{trans}, at the modified electrode surface can essentially be activities to and from the working electrode. Since the standard rate constant is related to electrode potential an increase in current density is expected. A depleted layer results when electroactive species reacting at an electrode surface lessens since there is a decrease in concentration at a particular potential. Equation 3.8 is a breakdown of mass transfer.

$$m_{trans} = \left[\frac{(\pi nFDv)}{(RT)}\right]^{\frac{1}{2}} \qquad 3.8$$

The maximum amount of current can be interpreted as a charge per unit of time and will be limited by the diffusion of species at the modified surface. The diffusion fluctuation is governed by the concentration gradient near the measuring electrode surface and affects the rate at which species diffuses through the electrochemical cell. At higher scan rates there exists a larger concentration incline leading to a higher current i.e., a maximum current provided by equation 3.3. Equation 3.9 is used to test whether the peak currents *I*p for the forward and reverse reactions are the same.

$$\frac{Ip_{red}}{Ip_{ox}} = 1 \qquad 3.9$$

Chemical reversibility implies that one of the redox partners is present after the chemical reaction at the electrode surface while electrochemical reversibility states that the electron transfer is unhindered throughout the activities at the electrode surface. Due to this, a dimensionless parameter, Λ, known as the Nickelson parameter

relates the standard rate constant to mass transport to estimate the transition between reversible and irreversible electrochemical reaction by equation 3.10.

$$\Lambda = \frac{k_s}{m_{trans}} \qquad 3.10$$

3.5 Experimental

3.5.1 Reagents and materials

Distilled water was cleaned by a Milli-Q system from Merck. Zinc nitrate; $Zn(NO_3)_2$ (Merck, 98%), zinc acetate; $Zn(CH_3COO)_2$ (Merck, 98%), zinc chloride; $ZnCl_2$ (Merck, 98%), sodium hydroxide; NaOH, (Merck, 99%), hydrochloric acid (HCl) different micropipettes and 2ml Eppendorf tubes.

3.6 Methodology

3.6.1 Zinc oxide nanoparticles (ZnO NPs) synthesis

Wet chemistry precipitation was used to prepare ZnO NPs from 100ml of 0.2M solutions of each of the zinc salt precursors. These solutions were each heated to approximately 80^{o}C and stirred vigorously. An amount of 10ml of 1M NaOH was added dropwise to each of the precursor solutions and kept at 80^{o}C with vigorous stirring. Each reaction was monitored for changes and allowed to proceed for two hours. After this period, each reaction vessel was removed from heat & stirring and allowed to cool down to room temperature. The formed products were transferred to amber containers to preserve the quality. The respective ZnO products were labelled following the salt precursor used; $ZnNO_3$ (nitrate), ZnAC (acetate), and ZnCl (chloride).

3.6.2 Sample preparation

The D1008 microcentrifuge from DLab Scientific Inc. at a setting of 5000rpm and 2ml Eppendorf tubes were used to wash the ZnO products so that ionic species are dissolved, discriminate between suspended particles, and collect the nanoparticles quantitatively. Further sample preparation was done relative to what characterization techniques require.

3.6.3 Characterization

3.6.3.1 Scanning electron microscopy (SEM)

The Tescan MIRA SEM was used to view the microstructure, distribution of nanoparticles, and homogeneity of the ZnO samples. The samples were mounted on standard pin stubs and lightly carbon coated. Accelerating voltage of 5kV, as well as magnifications of 20.0 and 50.0kx, were sufficient to observe images clearly, while the field of view was respectively 10.4 and 4.15μm. The working distance for the different precursors were 4.96, 5.04, and 5.07mm whereas the detector used was for secondary electrons.

3.6.3.2 Ultraviolet/visible spectroscopy

An 1800 Shimadzu model UV/vis (ultraviolet/visible) spectrometer was used for measuring the differences in absorbance between 200 and 800nm of ZnO concerning different precursors. Measurements took place in a 10mm wide glass cuvette and the blank sample was Milli Q pure water. ZnO product samples were centrifuged and washed three times with Milli Q water to collect supernatant before the analysis protocol. The resulting solution was measured without any further dilution.

3.6.3.3 Fourier transform infrared spectroscopy

The Perkin Elmer Spectrum II FTIR, (Fourier transform infrared) sensitive in the frequency range of 400-4000cm^{-1}, monitored the presence of functional groups characteristic of ZnO samples. The sample preparation of the respective ZnO product solutions involved centrifuging and washing three times with Milli Q water, filtering with filter paper, and filter funnel to obtain the respective ZnO solids. Further drying at room temperature was allowed before each measurement.

3.6.3.4 X-ray diffraction spectroscopy

The BRUKER AXS D8 Advance (from Germany) diffractometer was used to analyze samples for crystallinity and phase composition of ZnO product samples. The LynxEye detector is the position type detector, the tube Cu-Ka radiation (I Ka_1 = 1.5406Å) and θ to θ scanning was carried out in locked coupled style. The variable slits were V20, tube current 40mA, and tube voltage 40kV for all measurements. BRUKER supplied

EVA software to handle the data, ICDD pdf database 1999 to analyze data while the 2θ range from 10° to 80° were at 2θ (0.034°) increments. The sample preparation involved centrifuging and washing three times with Milli Q water of the different ZnO product solutions, filtering with filter paper and filter funnel to obtain the respective ZnO solid powders. Further drying at room temperature was allowed before the analysis of these samples.

3.6.3.5 Zetasizer and pH

The Malvern Zetasizer Nano Z was used to determine particle size, polydispersity index, Zeta potential, and conductivity of the ZnO product solutions from different precursors. The ZnO product samples were centrifuged and washed three times with Milli Q water for supernatant before testing as well as no additional dilution. The samples were measured using disposable plastic cuvettes for particle size and polydispersity index while a 20µL measuring cell was used for Zeta potential and conductivity determinations. A pH meter from Hanna instruments was used to determine pH levels of ZnO product solutions which were centrifuged and washed three times with Milli Q water.

3.6.3.6 Electrochemical characterization

Preparation involving 1, 0.3, and 0.05 µm alumina slurries were used to polish glassy carbon electrodes (GCE) to clean the surface for electrochemical characterization followed by thorough rising with water and ultrasonication at room temperature for approximately 15 minutes. The ZnO product solutions were centrifuged and washed once with Milli Q water to gather enough nanoparticles suspended. About 20µL of this was used in each ZnO product's case to drop-coat on the GCE surface to form a thin film and allowed to dry overnight. The in cyclic voltammetry and differential pulse voltammetry modes respectively. Cyclic as well as differential pulse voltammetry were the major modes of experiments performed for electrochemical characterization with the Autolab PGSTAT 101 supplied from Metrohm South Africa. The reference electrode was silver/silver chloride in 3M KCl, counter electrode platinum wire, and supporting electrolyte 0.1mM HCl. Various scan rates were applied to the cell. Electrochemical impedance studies (EIS) of each of the ZnO product thin films formed

were carried out with Impedance analyzer STAT I-400 also from Metrohm South Africa.

3.7 Results and discussion

3.7.1 Scanning electron microscopy

The information from this technique is high-resolution imaging that is helpful to evaluate surface properties and give a broader scope of crystallinity. Observation of ZnO samples at appropriate magnification provided exact qualitative chemical analysis. Figure 3.3a the SEM image of synthesized ZnO from $ZnNO_3$ at different magnifications and showed regions throughout the nanocrystal that are related to spherical-shaped particles. This morphology reveals agglomeration[4] and the appearance of specific cavities.[4] The $ZnNO_3$ precursor is converted to $Zn(OH)_2$ colloids because of basicity[6] which is then followed by the $Zn(OH)_2$ colloids dissolving in Zn^{2+} and OH^- species. It is reported that the round-shaped nanoparticles may include rod-like features due to nucleation[8] that results in the crystal growth phase; it is further also notable that this microstructure improves the particles' properties.[11] Figure 3.3b represents ZnO from ZnAC that strongly resembles rods[9] that are elongated in some areas. The flower fashion zones are related to the basicity of the nanoparticles as the concentration of Zn^{2+} and OH^- reaches supersaturation and it is the ZnO nuclei[10] that generates the observed morphology. This attributes also to the thickness of layers, vertical alignment of the particles, and therefore nanoneedles. Figure 3.3c depicts ZnO from ZnCl which is uniform in size[4], and nanorods but is shorter due to the acidity. Previous research suggests that the ZnCl precursor proceeds to ZnO sheets[8] and the presence of this related nanostructure is confirmed. The roughness of the nanoparticle surface is affected by this and serves as well as an explanation for the corrugated three-dimensional arrangement that is visible.

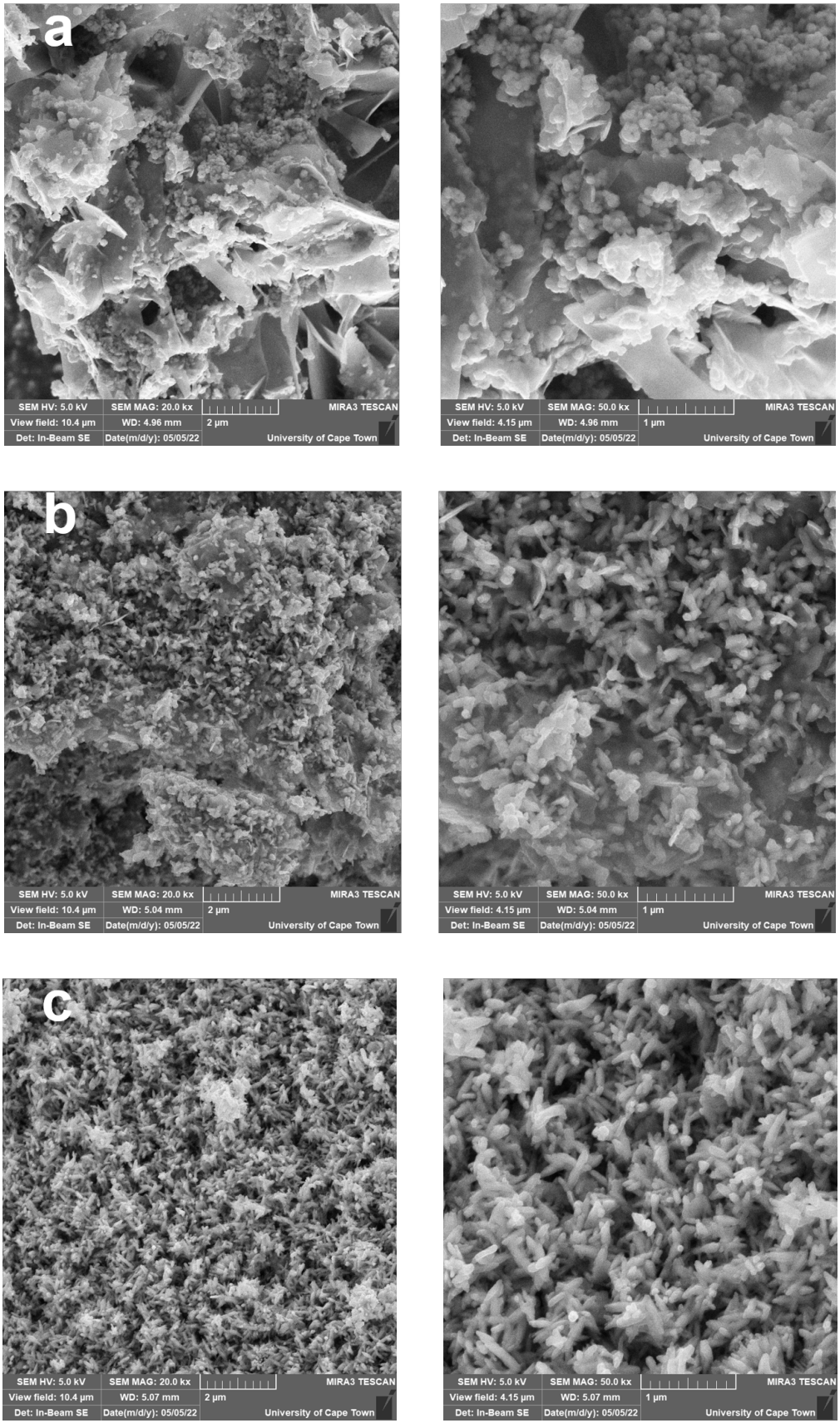

Figure 3.3: The scanning electron microscopy images of ZnO synthesized from a) $ZnNO_3$, b) ZnAC and c) ZnCl.

3.7.2 Ultraviolet/visible spectroscopy

UV/vis spectra were used to establish the relationship between absorbance at a certain wavelength of comparable intensity due to maximum ZnO absorbance. Synthesized samples from different precursors were investigated with the technique.

It is known that absorbance due to ZnO nanoparticles occurs between the 300 and 400 nm range and it is contributed by the surface plasmon resonance in ZnO.[2] In figure 3.4a synthesis using $ZnNO_3$, results in absorbance at 302nm of 1.87 intensity units is observed while with ZnAC 352nm with 0.70 intensity units while ZnCl resulted in 355nm with 0.35 intensity units. The very sharp absorbance band using $ZnNO_3$ is due to ZnO nanoparticle confinement.[26] The electron transition O_{2p}>Zn_{3d} is from the valence band to the conductance band and causes fundamental band-gap absorption of ZnO which reduces absorbance intensity, and redshift but increases wavelength; ZnAC however lowers the energy. In the case of using ZnCl a further lowering in absorbance intensity and more shift in wavelength is associated with the broader ZnO nanoparticles distribution in size such that wider absorbance bands take place and agglomeration of the nanoparticles.[27] The respective optical energy bandgap values as per figure 3.4b are $ZnNO_3$ (3.74eV), ZnAC (3.28eV), and ZnCl (3.34eV) showing that the precursors contributed to particles in the region of 3.37eV[1] which is the standard value for bulk ZnO, confirming effective synthesize.

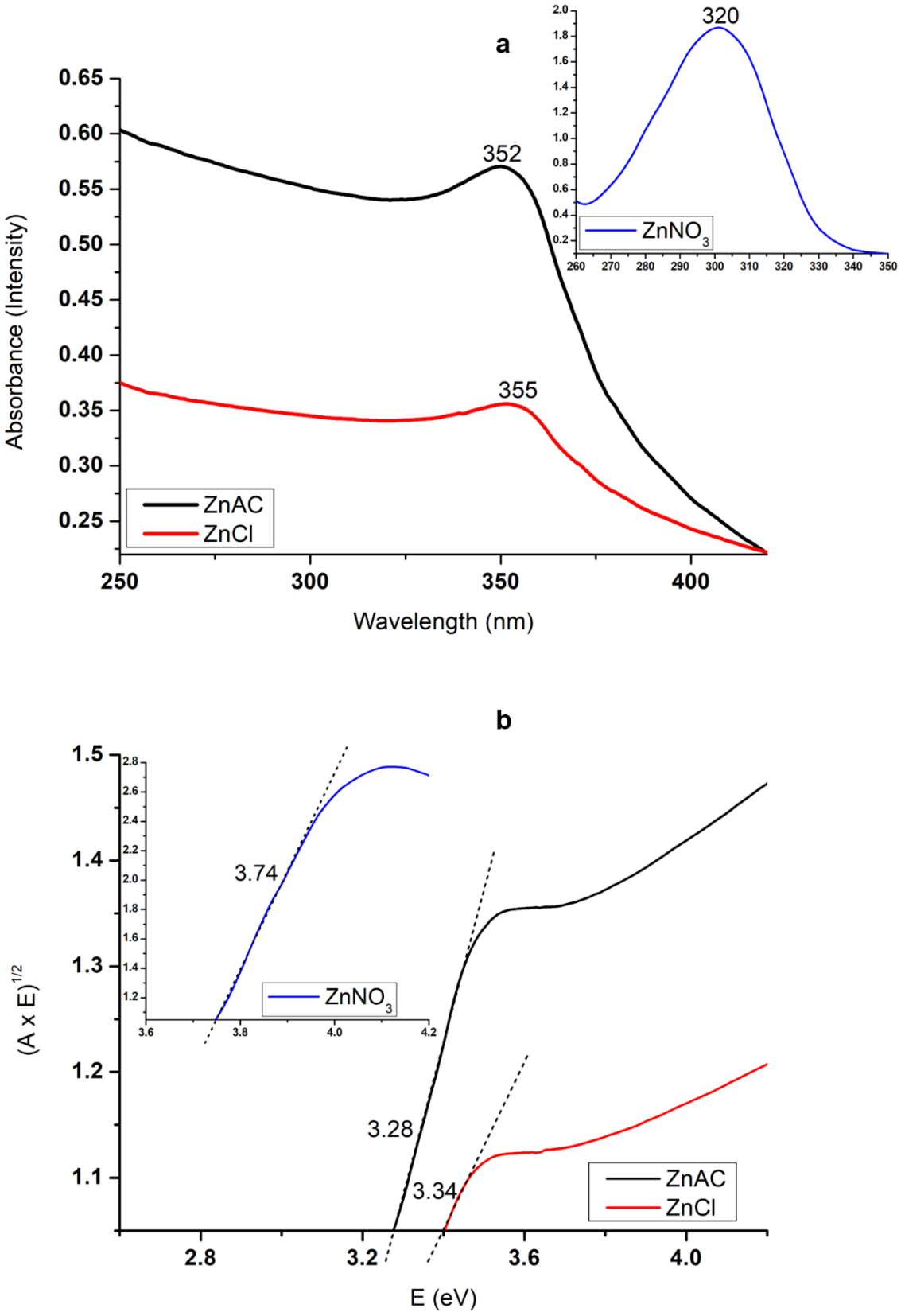

Figure 3.4: This caption is showing a) Ultraviolet/visible spectra and b) Tauc plot of ZnO synthesized from various precursors

3.7.3 Fourier transform infrared spectroscopy

It was important to look at how phase morphology was affected by the various precursors by examining specific functional groups in ZnO samples with the FTIR technique. Figure 3.5 is the spectral information of ZnO synthesis where the important Zn-O bond vibration is observed at 610, 620, and 641cm^{-1} respectively from each precursor, consistent with previously reported work.[3, 18]

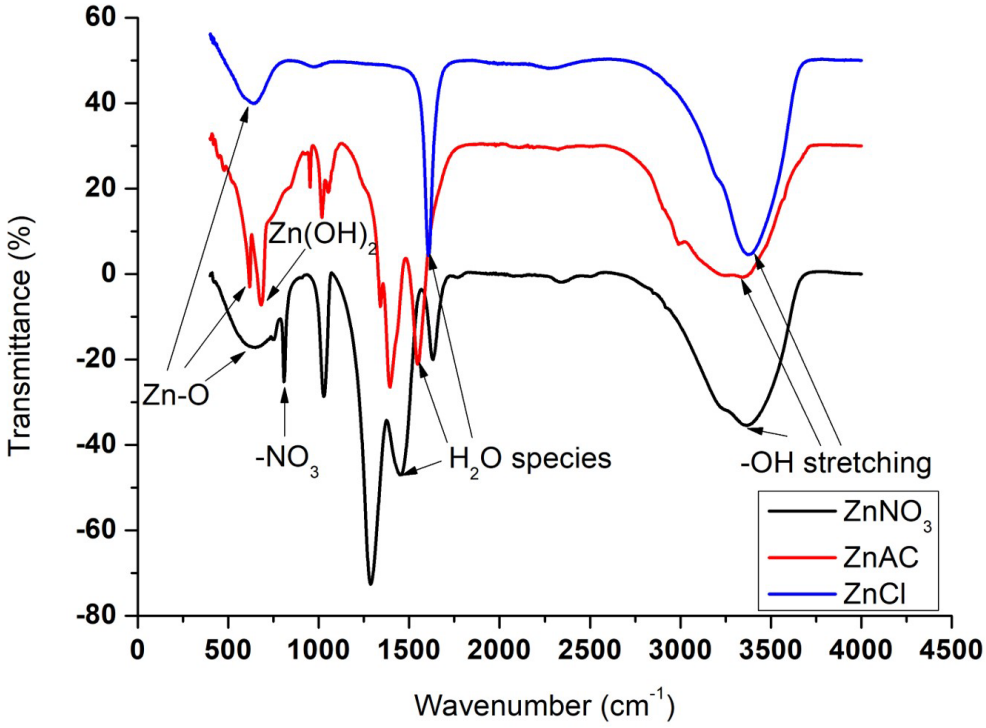

Figure 3.5: The Fourier transform infrared spectral data of ZnO synthesized from various precursors

Nitrate group stretching is seen when using $ZnNO_3$ by 811 and a frequency for the formation of the $Zn(OH)_2$ intermediate[3] is achieved with ZnAC at 685 cm^{-1}. At 1456, 1543 and 1611cm^{-1} are frequencies selectively for $ZnNO_3$, ZnAC, and ZnCl, due to bending vibrations of water species. Frequencies at 3384, 3360, and 3394 cm^{-1}are the effect of -OH stretching vibrations of layer hydroxyls.[28]

3.7.4 X-ray diffraction spectroscopy

XRD traces of synthesized ZnO using $ZnNO_3$, ZnAC, and ZnCl were measured to investigate surface crystallinity and consider which phases are present in the respective ZnO products influenced by the precursors.

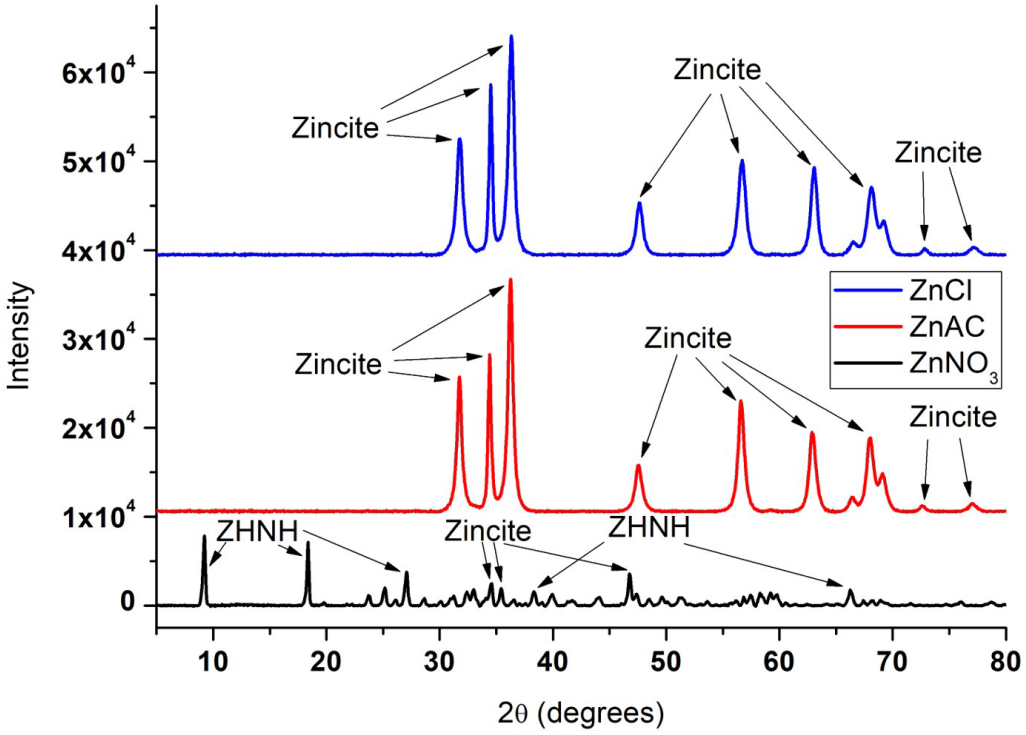

Figure 3.6: The x-ray diffraction patterns of ZnO synthesized from various precursors

The XRD patterns of the ZnO products in figure 3.6, feature the result of $ZnNO_3$ with diagnostic peaks at 2θ 9.24° (200), 18.40° (110), 27.08° (020), 38.33° (421) and 66.25° (713) for the presence of zinc hydroxide nitrate hydrate (ZHNH), an intermediate compound when forming ZnO influenced by the precursor. Zincite, which is a very pure form of ZnO revealed matches at 33.01° (002), 35.44° (101), and 46.76° (102). Both ZnAC and ZnCl showed strong presence of zincite at positions 31.77° (100), 34.42° (002), 36.25° (101), 47.54° (102), 56.60° (110), 62.86° (103), 67.96° (112), 72.56° (004) and 76.96° (202). From this information, ZnAC and ZnCl possess more crystalline phases since at the same diffraction angles the presence of ZnO in $ZnNO_3$, is lower. The qualities of ZnAC and ZnCl are confirmed by detectable peaks indexed

to the ZnO wurtzite structure which supports lattice parameters like crystalline sizes and their respective planes.[29] High intensity and sharp diffraction peaks are an indication of well-crystallized ZnO together with little impurities.[30] The shape of ZnO NPs from ZnAC compared to ZnCl will still be different based on the intensity of the signals due to the peaks representing the preferred growth of ZnO crystals along specific planes; this can further be used to establish dimensions (one, two or multi) of ZnO nanostructure and hence shape (particles, rods, stars, etc.).[31]

3.7.5 Zetasizer

Zetasizer was used to measure particle size properties of the ZnO samples since they are colloidal. The impact of precursors on particle size disruption was monitored because ZnO NPs n this study were dispersed since the sample particles in this study were dispersed by an aqueous solvent. From these trends, ZnO surface properties can act as a guide to bulk material character.

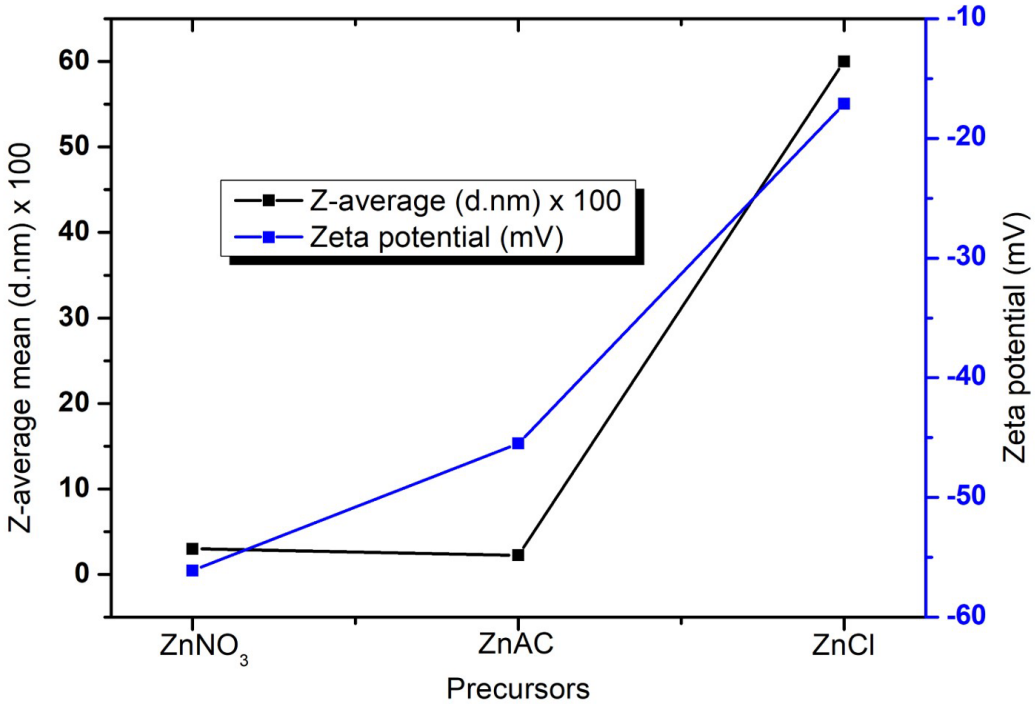

Figure 3.7: The Zeta potential and Z-average of ZnO synthesized from various precursors

The Zeta potential of ZnO nanoparticles synthesized from $ZnNO_3$, ZnAC, and ZnCl is depicted in figure 3.7. It is measured in mV describing the amount of electrostatic repulsion or attraction between ZnO nanoparticles and hence stability. Values obtained for the precursors are in the manner of increasing value, $ZnNO_3$<ZnAC<ZnCl, supporting that the smallest (negative) value shows the nanoparticles are creating the prospect of weakened reversible adhesion of particles due to a secondary minimum created. Brownian motion cannot even break up these loosely clumped masses of fine particles due to their stability. ZnAC has a value bigger (more positive) but still confirms that electrostatic stabilization leads to stable nanoparticles due to particle interaction and distribution of charge in the suspension. ZnCl has the greatest value (most positive) revealing unstable ZnO nanoparticles because of it being polydisperse in aqueous media.[32-38] The Z-average mean size in figure 3.7 of the ZnO products is a parameter used in dynamic light scattering measurements when nanoparticles assemble and is reported in the units diameter nanometer is in the order of increasing value, ZnAC<$ZnNO_3$<ZnCl. It can be deduced that ZnAC produced more monodispersed ZnO nanoparticles than $ZnNO_3$ keeping in mind that water is the common dispersant and the same concentration of zinc salt precursor was used. Using ZnCl, a high Z-average value for ZnO NPs clearly shows that the particles have a very broad distribution hence explaining the immediate precipitate during synthesis which leads to particles aggregating. The Z-average mean results thus are a guide to say which precursor forms consistent ZnO nanoparticles.[36-42]

The polydispersity index with a dynamic light scattering of the ZnO products each precursor is an analytical indicator to understand the extent of dispersity. The respective values obtained from the precursors given in figure 3.8 are in the order of decreasing value, ZnCl>$ZnNO_3$>ZnAC their respective ZnO solutions. There are no units for polydispersity index and it is suggested that values smaller than 0.05 are dedicated for highly monodisperse nanoparticles while values greater than 0.70 are for nanoparticles that have a greatly broad size distribution. ZnCl produced ZnO nanoparticles with a broad size distribution, $ZnNO_3$ narrower size distribution, and ZnAC with the least narrow size.[39-42]

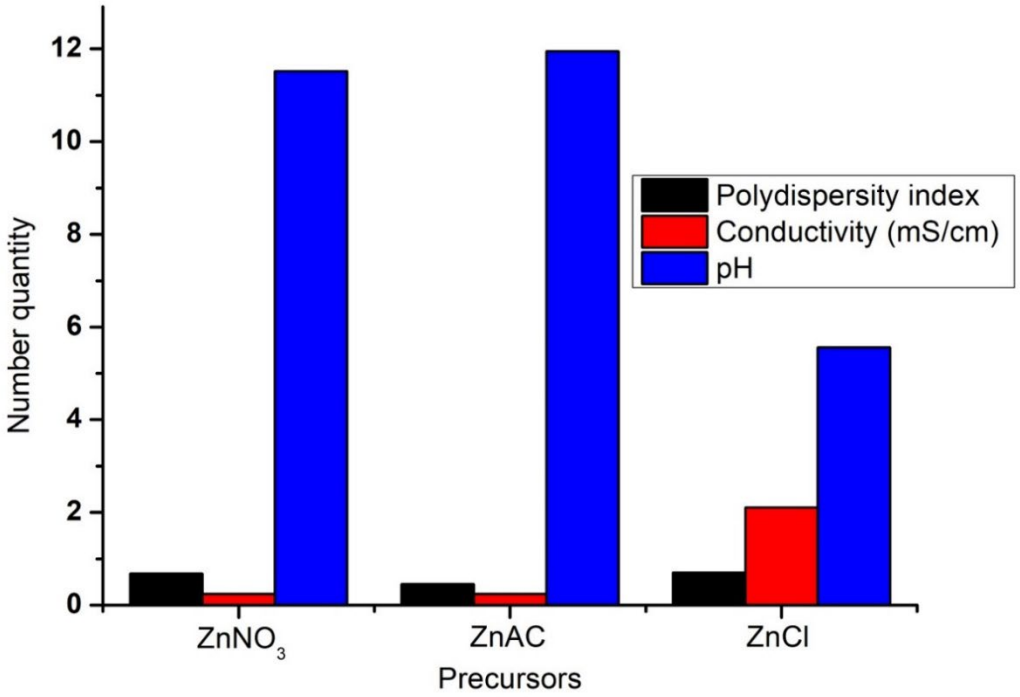

Figure 3.8: The polydispersity index, conductivity, and pH of ZnO synthesized from various precursors

The conductivity of ZnO nanoparticles synthesized with $ZnNO_3$, ZnAC, and ZnCl is provided in figure 3.8. $ZnNO_3$ and ZnAC are identical magnitudes but ZnCl is the largest. The fact that the formed ZnO NPs contribute to the conductivity of the suspensions in aqueous media can be justified by all the values. A double layer thickness affects Zeta potential, therefore, is there a difference between in conductivity of ZnO products from $ZnNO_3$ and ZnAC compared to that of ZnCl. The stability against aggregation for $ZnNO_3$ and ZnAC will be greater than ZnCl because of the adsorption of ions at the particle/liquid (solvent) interface, noting the Z-average mean was the greatest for ZnCl.[32-38] The pH of ZnO products using $ZnNO_3$, ZnAC, and ZnCl was determined and plotted in figure 3.8. The respective values are in the order of ZnCl<$ZnNO_3$<ZnAC. The Zeta potential of nanoparticle solutions is influenced by the corresponding pH and is associated with the isoelectric point. The isoelectric point is a measure of pH and it is said that the isoelectronic point is the pH at which a molecule or material carries the average net charge of zero. Bearing in mind that ZnCl compared to $ZnNO_3$ and ZnAC, had the Zeta potential closest to zero, it does have minimum

stability and minimal solubility in water explaining why it coagulates and precipitates at lower pH. ZnO solutions from $ZnNO_3$ have a higher pH, confirming its stability, dispersity, and a fair size distribution while that from ZnAC indicated the highest pH, is monodisperse, shows the narrowest size distribution and greater nanoparticles consistency.[3, 29]

3.7.6 Electrochemical characterization

3.7.6.1 Cyclic voltammetry

The electrochemical features of the bare GCE (glassy carbon electrode) compared to ZnO-modified electrodes fabricated from various precursors, involved cyclic voltammetry measurements to determine the effect of surface chemistry on the electron transfer performance.

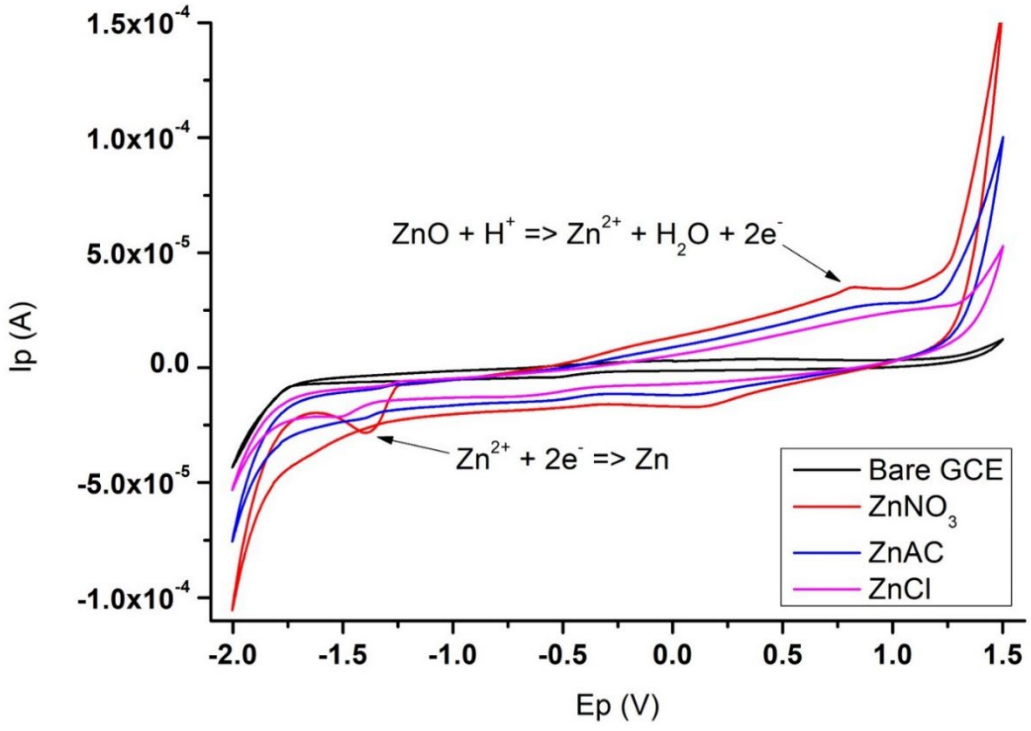

Figure 3.9: The cyclic voltammogram overlay of bare GCE and ZnO synthesized from various precursors at 60mV/s

Table 3.1: The observed electrochemical parameters of ZnO synthesized from various precursors at 60mV/s

Electrochemical parameters	ZnO precursors		
	$ZnNO_3$	ZnAC	ZnCl
Epa (V)	0.8423	1.172	1.191
Epc (V)	-1.406	-1.492	-1.460
E_o (V)	0.2224	0.1877	0.1886
ΔEp (V)	0.5640	0.3198	0.2686

The overlay cyclic voltammogram of ZnO using different precursors is presented in figure 3.9 and shows no response by the bare glassy carbon electrode while the oxidation of Zn is given by the anodic peak and corresponding reduction, by the cathodic peaks. The corresponding redox and cell potentials were calculated with equations 3.1 and 3.2 respectively and are tabulated in table 3.1; a pattern in which $ZnNO_3$ has the lowest oxidation (anodic) potential followed by ZnAC and then ZnCl. A sharp cathodic peak for the reduction process proves that no decomposition of ZnO took place at the used experimental conditions and is in the manner of ZnCl most negative followed by $ZnNO_3$ and then ZnAC. Literature values such as -1.261 and -0.920V[43] with a zinc sulfate precursor have been reported and in another case -0.81 and -1.4V[44] was recorded where zinc acetate was the precursor, using identical reference electrode and electrolyte. In a previous study, the electrochemical reduction of ZnO precursors, resulted in Zn catalysts that are very dynamic, discriminating as well as steady in the application of selective reduction of CO_2 to CO[45]; in such case, the crystal shape of ZnO had a relatable impact on the rate of overall reduction contributing towards minimum surface energy, slower ZnO reduction at more positive potentials and larger hexagonal crystals causing slower crystallization tempo due to low porosity. The precursors of a ZnO layer are related to the distribution of nucleus centers because of the Zn^{2+} concentration which will influence ultimately the electrochemically active surface area of ZnO-based electrodes. How the ZnO crystals grew during synthesis in terms of particle size and shape gave a high degree of

stability to such films as well as better optical and electrochemical qualities which are strongly dependent on precursors.[46] From the precursors used for ZnO, it is clear that the current density is a function of electrode potential and also scan rate; the excitation signal during charging of the electrode interface capacitance through the electron transfer process impacts the shape of cyclic voltammograms.[47] The surface area of the ZnO modified electrode is impacted by the pore size of the film-coated electrode thus the rate of electron transfer can be said to be the potential difference between oxidation and reduction peaks in cyclic voltammetry.[48] Roughness of ZnO film coated on the electrode influences mechanisms of affected by precursors and [49] and additional factors to this are film thickness, ZnO crystal structure and extend of drop coating.[50]

3.7.6.2 Electrochemical kinetics

Figure 3.10 is a compilation of cyclic voltammograms of ZnO films prepared using $ZnNO_3$, ZnAC, and ZnCl with 0.1mM HCl as supporting electrolytes at various scan rates. Factors that influence any change in potential when raising scan rate are related to kinetic limitations brought about when the electrode surface is modified. This is a direct consequence of the ZnO film interrupted by electrolyte, uneven reaction site distribution of the film, and electrostatic forces at the electrode surface. Variables such as the speed at which the potential is scanned, diffusion coefficient, the number of electrons transferred, electrode material, bulk concentration of the analyte, and temperature conditions are proportional to current density in cyclic voltammetry of ZnO as given in figure 3.11.[51] The dominant anodic reaction is diffusion-controlled for ZnO precursors with the best linearity of the variables belonging to ZnAC followed by ZnCl and then $ZnNO_3$. Together with the slope of the plot from Ep against log v in figure 3.12, equation 3.6 was used to calculate values of the electron transfer coefficient, α, and found to be the highest for ZnCl, followed by $ZnNO_3$ then ZnAC, while n is established to at least be 1 since all α values are in the region of 0.5, making the electrode process due to the ZnO films, reversible.

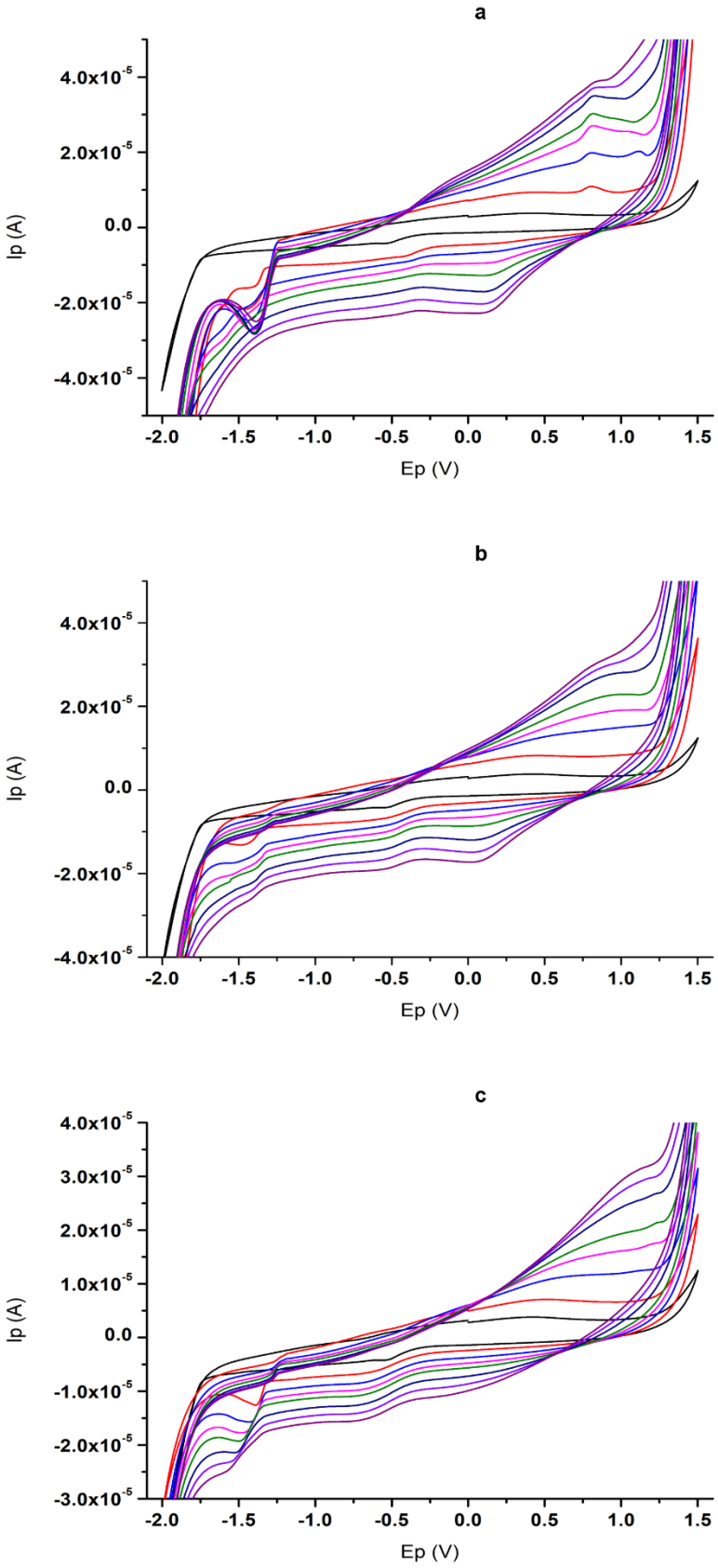

Figure 3.10: The cyclic voltammogram overlay of ZnO modified GCE using, a) $ZnNO_3$, b) ZnAC and c) ZnCl as precursor at scan rates 10 to 100mV/s

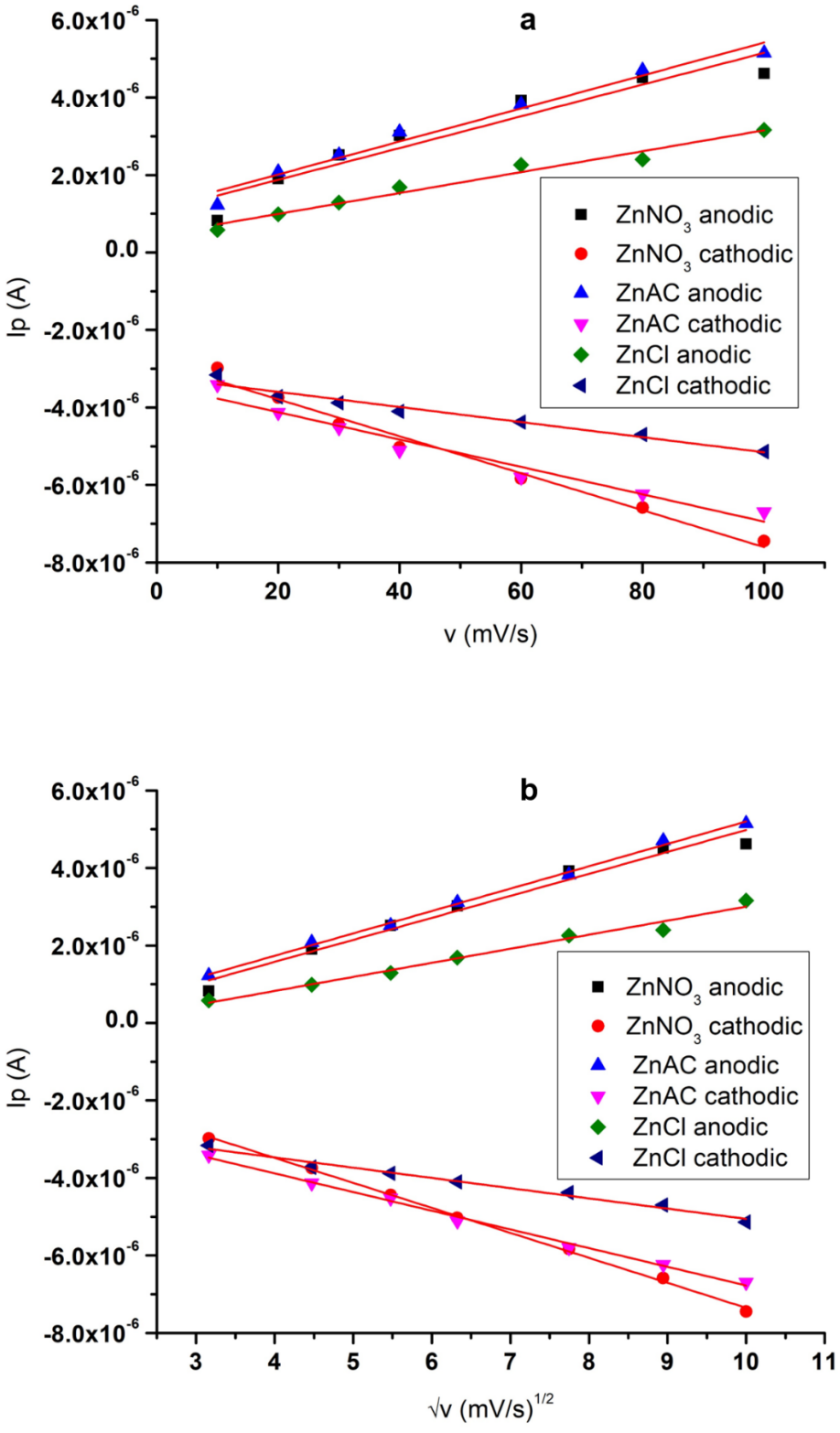

Figure 3.11: Plot of the Ipa and Ipc vs a) v as well as b) √v of ZnO modified GCE synthesized from various precursors

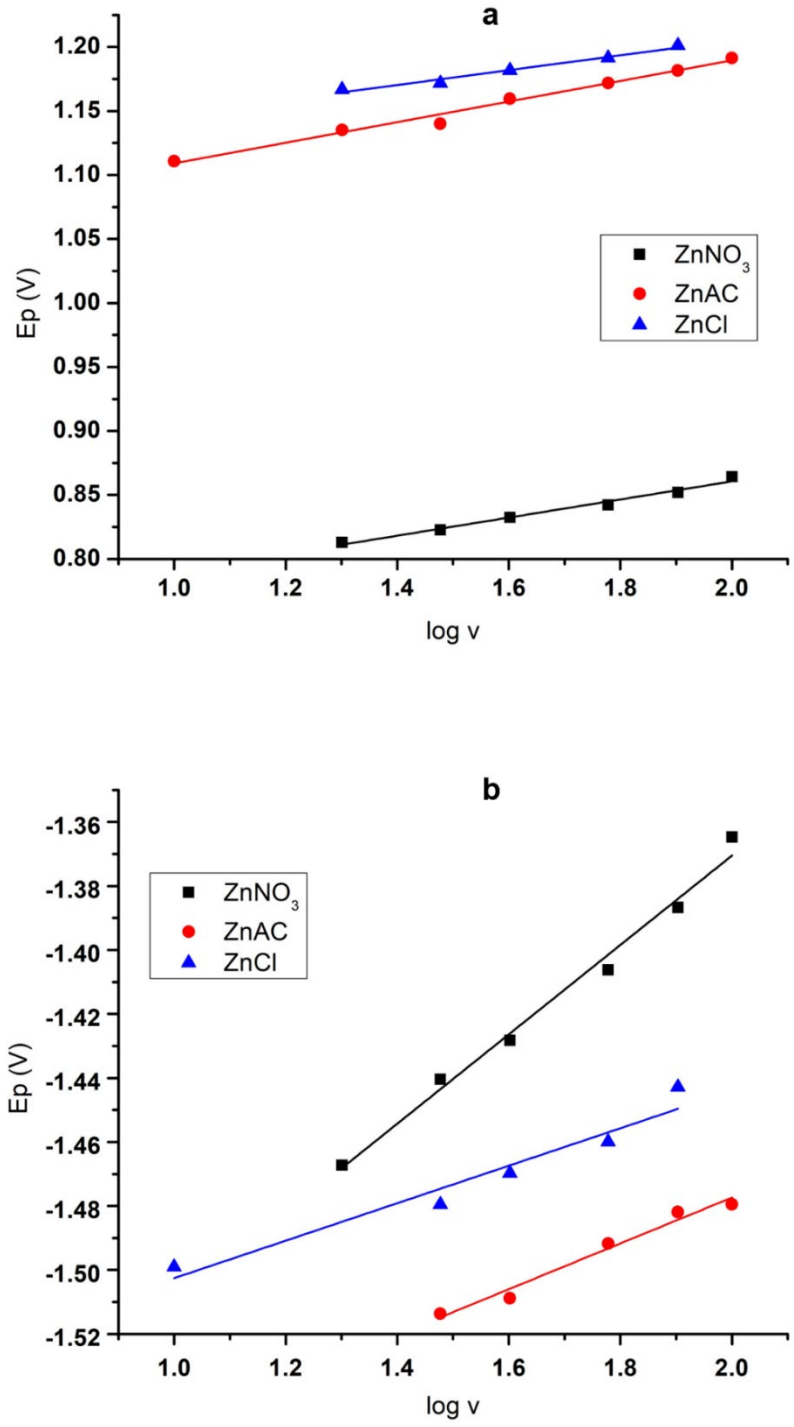

Figure 3.12: The variation of a) Ep anodic and b) Ep cathodic vs logarithm v of ZnO modified GCE synthesized from various precursors

Table 3.2: The electrochemical parameters of ZnO modified GCE synthesized from various precursors at 40mV/s

Electrochemical parameter	ZnO precursors		
	$ZnNO_3$	ZnAC	ZnCl
Slope fig. 3.10b $x10^{-7}$ (Slope fig. 3.11 a)	5.68 (0.0708)	5.78 (0.0805)	3.63 (0.0580)
R^2 fig. 3.10b (R^2 fig. 3.11a)	0.98 (0.99)	1 (0.99)	0.98 (0.99)
D ($cm^{2/}s$) $x10^{-15}$	3.12	3.12	1.39
α	0.42	0.38	0.51
k_s (s^{-1})	0.019	2.50	5.69
m_{trans} (s^{-1}) $x10^{-6}$	5.51	5.51	3.69
Ip (A) $x10^{-6}$	3.78	3.78	0.80
Ip_{red}/Ip_{ox}	0.91	0.90	0.92
Λ $x10^3$	3.39	456	1540

Table 3.2 is the overall summary of all other crucial electrochemical parameters. Interpreting the diffusion coefficient of ZnO precursors determined with equation 3.5, is the highest when using $ZnNO_3$ and ZnAC followed by ZnCl, suggesting that the mobility of ZnO is most efficient with the two first mentioned. The effect of scan rate on ZnO observed shows that faster scan rates reduce the size of the diffusion layer and further contribute to higher current density measured.[52] An increase in current at constant electrode potential indicates the high electrocatalytic activity of the ZnO modified GCE.[53]

The ZnO modified electrodes using different precursors resulted in the heterogeneous standard rate constant, k_s values in the order of $ZnNO_3$<ZnAC<ZnCl respectively determined with equation 3.7 and according to the kinetics of electron transfer processes, if the heterogenous standard rate constant is larger than $1x10^{-2}$, the electron transfer process will be very fast, therefore, the electrode reaction is reversible and in situations where the value is between $1x10^{-4}$ and $1x10^{-2}s^{-1}$, the electrode reaction is quasi-reversible. Thus, ZnO facilitates reversible electrode

reactions with all precursors. The texture of ZnO influences electrochemical parameters and hence the experimental values of D too.[54] An extended reason behind this observation comprises the depletion of OH^- ions close to the electrode when $Zn(OH)_3^-$ forms including the occurring Zn to $Zn(OH)_4^{2-}$ oxidation.[55] The combined effects of ZnO nanostructures, electrolyte ionic strength, film coating thickness, and the electrode contact area, influence the electrode's performance.[56] The diffusion of Zn in ZnO shows a stable signal and thus greater through less structural regions of ZnO.[57] Zn^{2+} transportation is a measure of good anodic and cathodic peak separation, great mass transfer and better chemical reactivity in the ZnO modified electrode.[58]

The mass transport determined with equation 3.8 of the ZnO films at the electrode surface influenced by the different precursors was the quickest with $ZnNO_3$ and ZnAC followed by ZnCl. Such behavior is attributed to the movement of electrons through the electrode, through the solution of the electroactive species to the modifier, and the movement of electrons across the interface due to the electrode reaction.

The greatest current possible through equation 3.3 due to ZnO precursors were $ZnNO_3$ and ZnAC followed by ZnCl. The reduction activity through equation 3.9 of the ZnO films using ZnCl is the highest followed by $ZnNO_3$ and then ZnAC.

Based on the Nickelson parameters from equation 3.10 of the ZnO films, using zinc precursors, the order of increasing values is $ZnNO_3$, ZnAC then ZnCl, resulting in a reversible electron transfer process because of values being greater than 10 and these processes are diffusion controlled.

3.7.6.3 Differential pulse voltammetry

The differential pulse voltammogram plot in figure 3.13 shows a strong reduction peak at around -1.2 and -1.3V vs Ag/AgCl for all precursors. $ZnNO_3$ showed the best current signal response for ZnO coated on GCE, followed by ZnCl and ZnACl at electrode potential -1.292V. Microstructure and the density regulating electronic states caused by electrode modifying material nature near the semiconducting ZnO Fermi level which promotes the redox reactions play important roles in the electron transfer process.[59]

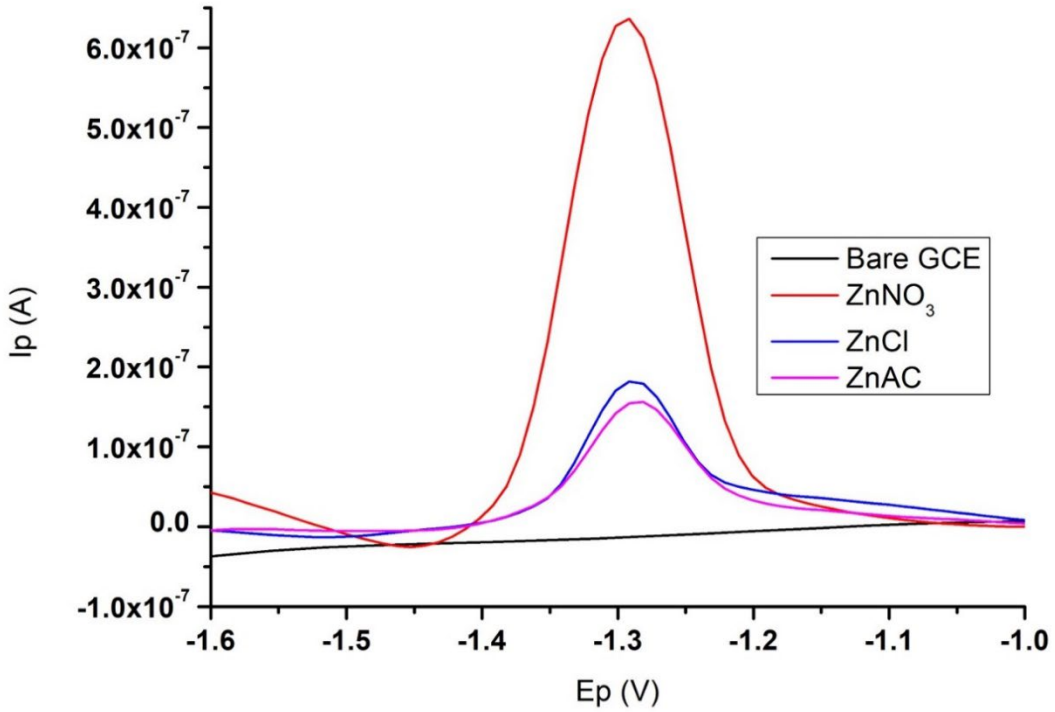

Figure 3.13: The differential pulse voltammogram overlay of bare GCE and ZnO modified GCE synthesized from various precursors at 30mV/s

3.7.6.4 Electrochemical impedance studies

Further electrochemical characteristics of ZnO were considered using electrochemical impedance studies (EIS). This was performed to confirm the redox behavior of the ZnO modifier films, establish the superior transfer of electrons and investigate the enhancement of the electrode's overall catalytic ability because of nanostructured ZnO.[60] In the Nyquist plot together with the inset of an equivalent circuit for $ZnNO_3$ only, figure 3.14, the diameter of the semicircle section located at bigger frequencies is related to charge transfer resistance, R_{ct}, that governs electron transfer kinetics because the ZnO film, the electrode boundary and solution resistance, R_s, the resistance at the ZnO modifier film and electrolyte interface. R_s values indicated that the bare GCE has a high solution resistance followed by ZnAC, $ZnNO_3$ then ZnCl., therefore the introduction of this ZnO encouraged electron flow relative to the electrolyte.

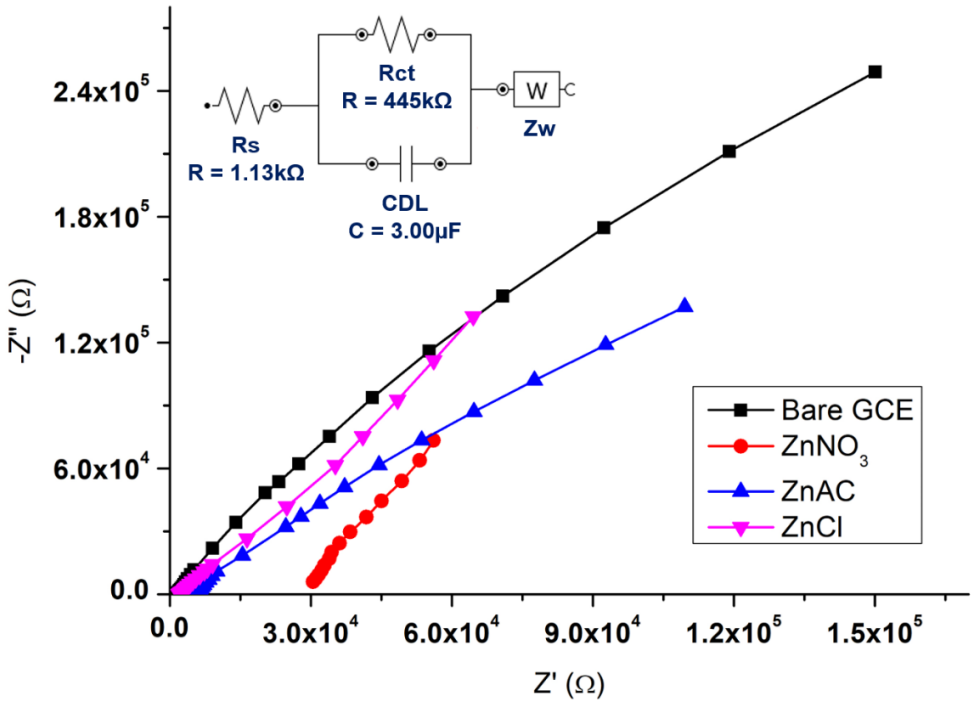

Figure 3.14: The Nyquist curves of bare GCE and ZnO modified GCE synthesized from various precursors as well as the inset of Randles equivalent circuit using $ZnNO_3$ precursor

Table 3.3: The elements of equivalent Randles circuit values from electrochemical impedance studies of bare GCE and ZnO modified GCE synthesized from various precursors

Elements of Randles circuit		ZnO precursors		
	Bare GCE	$ZnNO_3$	ZnAC	ZnCl
R_s (kΩ)	1.73	1.13	5.15	1.95
R_{ct} (kΩ) x10^3	0.252	0.445	1.12	3.47
CPE (F) x10^{-6}	5.13	3.00	5.62	0.45
n value	0.998	0.997	0.996	0.996

Table 3.3 is a compilation of the major elements in the Randles circuit describing the electrode's impedance due to modification; the estimated % error was low for each measurement. Values higher than the bare GCE are related to diffusion-limited charge

transfer at the electrode-electrolyte interface.[61] Dimensional aspect ratio like particle size (average length and diameter) of ZnO from the precursors used in this study is a crucial consideration cause adhesion and robustness of ZnO nanostructures will affect film charge transfer resistance and thus explain the increase in the values[62]; R_{ct} values measured are the biggest for ZnCl, followed by ZnAC then $ZnNO_3$ compared to that of the bare GCE surface that was smallest of them all pointing towards the fact that the ZnO films presence are significant and explained by a hindrance to electron transfer due to insulating species.[63] Another possible reason can be linked to the existence of functional groups on the ZnO surface which are negatively charged that restrict interfacial charge movement behavior between a modified electrode and supporting electrolyte.[61]

3.8 Conclusion

The observed SEM images provided essential information about the synthesized zinc oxide nanoparticles which have distinctive patterns due to the influence of various precursors. There is furthermore confirmation of particles that are spherical-shaped, experience agglomeration, have cavities, are rod-like, and have surface layer thickness as well as roughness. The UV-vis, FTIR, Zetasiser, and electrochemistry results collectively confirmed the presence of ZnO in the synthesized nanoparticles samples. Using different precursors, ZnO formed showed characteristic UV/visible absorbance in addition to a slight shift in wavelength and changes in intensity. With FTIR, the Zn-O bond diagnostically was consistent with all precursors, but the rest of the frequencies were due to precursors. Zetasizer testing of ZnO produced Z-average values showing noticeable variation due to precursors affecting the aggregation of particles. The polydispersity indexes of ZnO were affected by the nature of the precursors since it represents the size distribution while the varying Zeta potential established showed that changes in electrostatic stabilization affect the stability of particles due to precursors. The conductivity of only two of the ZnO solutions was identical while it was the case as well when the pH was measured from which it can be concluded that precursor conditions strongly influence double layer thickness and particles consistency. XRD analysis showed the potential shape of ZnO relative to the precursors based on the preferred crystal growth plane which can be seen by the diffraction patterns caused by precursors. Electrochemistry of ZnO from various

precursors revealed anodic and cathodic peaks at electrode potentials that were noticeable and distinct compared to a bare glassy carbon electrode. Cyclic voltammetry and 0.1mM HCl as electrolyte at various scan rates showed comparable results to previously reported that which can be linked to the ionic strength of electrolyte together with ZnO porosity as the influence of precursor is obvious with change in current density. According to the Nickelson parameters of ZnO, using all zinc precursors results in reversible electron transfer processes and this is confirmed since k_s is larger than m_{trans}, implying that electron transfer by ZnO is faster than mass transport. The DPV technique confirmed the impact of precursors on current density while EIS is useful to indicate the binding efficiency between ZnO films to the electrode surface and hence the precursors' impact on resistance suggesting that the nitrate precursor caused a ZnO film with superior features.

3.9 References

1. Tandra Ghoshal, Subhajit Biswas, Manidipa Paul, and S. K. De. Synthesis of ZnO Nanoparticles by Solvothermal Method and Their Ammonia Sensing Properties. Journal of Nanoscience and Nanotechnology Vol.9, 5973-5980, 2009
2. Shambhu Sharan Kumar. Chemical synthesis of Zinc oxide nanoparticles by precipitation method. International Journal of Engineering and Technical Research (IJETR). Volume-2012, January-June 2012
3. Maroua Mrad, Bilel Chouchene and Tahar Ben Chaabane. Effects of Zinc Precursor, Basicity and Temperature on the Aqueous Synthesis of ZnO Nanocrystals. S. Afr. J. Chem., 2018, 71, 103–110
4. Mohammad Reza Arefi and Saeed Rezaei-Zarchi. Synthesis of Zinc Oxide Nanoparticles and Their Effect on the Compressive Strength and Setting Time of Self-Compacted Concrete Paste as Cementitious Composites. Int. J. Mol. Sci. 2012, 13, 4340-4350
5. C. H. Hu, Z. C. Qian, J. Song, Z. S. Luan, and A. Y. Zuo. Effects of zinc oxide-montmorillonite hybrid on growth performance, intestinal structure, and function of broiler chicken. 2013 Poultry Science 92:143-150

6. Thanakorn Wirunmongkol, Narongchai O-Charoen, and Sorapong Pavasupree. Simple Hydrothermal Preparation of Zinc Oxide Powders Using Thai Autoclave Unit. Energy Procedia 34 (2013) 801-807
7. P. M. Aneesh, K. A.Vanaja, M. K. Jayaraj. Synthesis of ZnO nanoparticles by hydrothermal method. Proc. of SPIE Vol. 6639 66390J
8. Wuxing Zhang and K. Yanagisawa. Hydrothermal Synthesis of Zinc Hydroxide Chloride Sheets and Their Conversion to ZnO. Chem. Mater. 2007, *19,* 2329-2334
9. M. Segovia, C. Sotomayor, G. Gonzalex, E. Benavente. Zinc Oxide Nanostructures by Solvothermal Synthesis, Mol. Cryst. Liq. Cryst., Vol. 555: pp. 40-50, 2012
10. Widiyastuti Widiyastuti, Siti Machmudah, Tantular Nurtono, Sugeng Winardi, Ratna Balgis, Takashi Ogi, Kikuo Okuyama. Morphology and Optical Properties of Zinc Oxide Nanoparticles Synthesised by Solvothermal Method. Chemical Engineering Transactions, 56, 955-960
11. Hanan ABD El Zaher ABD EL Wahab, Omar Nur, Magnus Willander, Aida ABD EL Karim Salama, ABD El Menem El Saeid, and I. K. Battisha. Growth of Zinc Oxide Nano-Rod Thin Film for Hemoglobin Biosensor Applications Prepared Using Sol-Gel and Aqueous Chemical Growth. International Journal of Engineering and Innovative Technology (IJEIT) Volume 4, Issue 1, July 2014
12. Y. L. Zhang, Y. Yang, J. H. Zhao, R. Q. Tan, P. Cui, W. J. Song. Preparation of ZnO nanoparticles by a surfactant-assisted complex sol-gel method using zinc nitrate J Sol-Gel Sci Technol (2009) 51:198-203
13. J.N. Hasnidawani, H.N. Azlina, H. Norita, N.N. Bonnia, S. Ratim, E.S. Ali. Synthesis of ZnO Nanostructures Using Sol-Gel Method Procedia Chemistry 19 (2016) 211-216
14. Ravichandran. S, Franklin. D. Raja, Kalyan. U. Effect of capping agent on the synthesis of zinc oxide nanoparticles by precipitation and chemical reaction methods. National Journal on ChemBiosis, Vol. 1, No.2, October 2010
15. Rudeerat Suntako. Effect of zinc oxide nanoparticles synthesized by a precipitation method on mechanical and morphological properties of the CR foam. Bull. Mater. Sci., Vol. 38, No. 4, August 2015, pp. 1033-1038
16. Buong Woei Chieng, Yuet Ying Loo. Synthesis of ZnO nanoparticles by modified polyol method. Materials Letters 73 (2012) 78-82

17. M.R. Philip, Hieu P. T. Nguyen, R. Babu, V. Krishnakumar, and Thang H. Q. Bui. Polyol Synthesis of Zinc Oxide-Graphene Composites: Enhanced Dye-Sensitized Solar Cell Efficiency. Current Nanomaterials, 2018, Vol. 3, No. 1
18. A. Anzlovar, K. Kogej, Z. Crnjak Orel, M. Zigon. Polyol mediated nano-size zinc oxide and nanocomposites with poly(methyl methacrylate). Express Polymer Letters Vol.5, No.7 (2011) 604-619
19. Ryan J. White, Henry S. White. A random walk-through electron transfer kinetics. American Chemical Society, Analytical Chemistry, June 2005
20. Bard, A. J.; Faulkner, L. R. Electrochemical Methods, 2nd ed.; Wiley & Sons: New York, 2001.
21. Girault, H. H. Analytical and Physical Electrochemistry; Marcel Dekker: New York, 2004.
22. Watkins, J. J.; et al. Anal. Chem. 2003, 75, 3962-3971.
23. Watkins, J. J.; White, H. S. Langmuir 2004, 20, 5474-5483
24. Smalley, J. F.; et al. J. Phys. Chem. 1995, 99, 13,141-13,149
25. N. Aristov, and A. Habekost, Cyclic Voltammetry-A Versatile Electrochemical Method Investigating Electron Transfer Processes. World Journal of Chemical Education, Vol. 3, no. 5 (2015): 115-119
26. U. Srinivas Raoa, G. Srinivas and T Prasada Rao. Influence of precursors on morphology and spectroscopic properties of ZnO nanoparticles. Procedia materials science 10 (2015) 90-96
27. Awodugba Ayodeji Oladiran, Ilyas Abdul-Mojeed Olabisi. Synthesis and characterization of ZnO nanoparticles with zinc chloride as zinc source. Asian Journal of Natural and Applied sciences. Vol. 2 No. 2, June 2013
28. Swati S. Kulkarni Swa. Sawarkar Mahavidyalaya Beed, Mahendra D. Shirsat, Babasaheb Ambedkar Marathwada. Optical and Structural Properties of Zinc Oxide Nanoparticles. International Journal of Advanced Research in Physical Science (IJARPS) Volume 2, Issue 1, January 2015, PP 14-18
29. A. Maikap, K. Mukherjee, B. Mondal and N. Mandal. Zinc oxide thin film-based nonenzymatic electrochemical sensor for the detection of trace-level catechol. RSC Adv., 2016, 6, 64611-64616
30. Derjaguin, B.V. and Landau, L. (1941). Acta Physiochim. URSS, 14, 633.
31. Verway, E.J.W., and Overbeek, J. Th.G. (1948) Theory of the Stability of Lyophobic Colloids, Elsevier, Amsterdam.

32. Hunter, R.J. (1988) Zeta Potential in Colloid Science: Principles and Applications, Academic Press, UK.
33. Shaw, D.J. (1992) Introduction to Colloid and Surface Chemistry, Butterworth Heinemann, UK.
34. Everett, D.H. (1994) Basic Principles of Colloid Science, The Royal Society of Chemistry, UK.
35. Ross, S. and Morrison, I.D. (1988) Colloidal Systems and Interfaces, John Wiley and Sons, USA.
36. Lyklema, J. (2000) Fundamentals of Interface and Colloid Science: Volume 1 (Fundamentals), Academic Press, UK.
37. International Standard ISO22412 Particle Size Analysis-Dynamic Light Scattering, International Organisation for Standardisation (ISO) 2008.
38. Dahneke, B.E. Measurement of Suspended Particles by Quasielastic Light Scattering, Wiley, 1983.
39. Pecora, R. Dynamic Light Scattering: Applications of Photon Correlation Spectroscopy, Plenum Press, 1985.
40. Washington, C. Particle Size Analysis In Pharmaceutics And Other Industries: Theory and Practice, Ellis Horwood, England, 1992.
41. Johnson, C.S. Jr., and Gabriel, D.A. Laser Light Scattering, Dover Publications, Inc., New York 1981
42. Roman Marsalek. Particle size and Zeta potential of ZnO. Apcbee Procedia 9 (2014) 13-17
43. Emad Salaam Abood, Amer Mousa Jouda, and Muthana Saleh Mashkoor, Zinc Metal at a New ZnO Nanoparticle Modified Carbon Paste Electrode: A Cyclic Voltammetric Study. Nano Biomed. Eng., 2018, 10(2): 149-155
44. Blessing Tatenda Shedeke, Mangaka Matoetoe. Bactericidal efficacy of wound gauze treated with chitosan nanomaterial hybrids of zinc, silver, and copper on common wound bacteria. Cape Peninsula University of Technology, Cape Town 2018
45. Wen Luo, Qin Zhang, Jie Zhang, Emanuele Moioli, Kun Zhao, Andreas Züttel. Electrochemical reconstruction of ZnO for selective reduction of CO_2 to CO. Applied Catalysis B: Environmental 273 (2020) 119060

46. Carmen M. López and Kyoung-Shin Choi. Electrochemical Synthesis of Dendritic Zinc Films Composed of Systematically Varying Motif Crystals. American Chemical Society. Langmuir 2006, 22, 25, 10625-10629
47. Noluthando Mayedwa, Ali Talha Khalil, Nametso Mongwaketsi, Nolubabalo Matinise, Zabta Khan Shinwari, and Malik Maaza. The Study of structural, physical, and electrochemical activity of ZnO nanoparticles synthesized by green natural extracts of *Sageretia Thea.* Nano Research and Applications 2017. Vol. 3 No. 2: 9
48. Agne Sulciute, Keita Nishimura, Evgeniia Gilshtein, Federico Cesano, Guido Viscardi, Albert G. Nasibulin, Yutaka Ohno, and Simas Rackauskas. ZnO nanostructures application in electrochemistry: Influence of morphology. J. Phys. Chem. C 2021, 125, 1472-1482
49. Mazabalo Banetoa, Alexandru Enescab, Yendoubé Larea, Koffi Jondoa, Kossi Napoa, Anca Dutab. Effect of precursor concentration on structural, morphological, and optoelectric properties of ZnO thin films prepared by spray pyrolysis. Ceramics International 40 (2014) 8397-8404
50. Foudil Rahal and Djamila Abdi. Effects of solution precursor on structural, morphological, and photoelectrochemical properties of ZnO layers deposited by recurrent cyclic voltammetry. Journal of Electronic materials. Vol. 49, No. 8, 2020
51. Paul M.S. Monk. Fundamentals of Electroanalytical chemistry. Analytical techniques in the sciences. John Wiley & Sons Ltd. 2001
52. Noemie Elgrishi, Kelley J. Rountree, Brian D. McCarthy, Eric S. Rountree, Thomas T. Eisenhart, and Jillian L. Dempsey. A Practical Beginner's Guide to Cyclic Voltammetry. J. Chem. Educ. 2018, 95, 197−206
53. Feng Zhang and Danni Li. Development of a Graphene Oxide-ZnO Nanorod Composite for Sensitive Determination of Catecholamine. Int. J. Electrochem. Sci., 13 (2018) 3643-3650
54. Nazrin Abdullayeva, Cigdem Tuc Altaf, Merve Mintas, Ahmet Ozer, Mehmet Sankir, Hamza Kurt & Nurdan Demirci Sankir. Investigation of Strain Effects on Photoelectrochemical Performance of Flexible ZnO Electrodes. Scientific Reports (2019) 9:11006

55. Shuxi Dai, Yinyong Li, Zuliang Du, and Kenneth R. Carter. Electrochemical deposition of ZnO hierarchical nanostructures from hydrogel coated electrodes. Journal of The Electrochemical Society, 2013 160(4): D156-D162
56. S. Ashok Kumar and Shen-Ming Chen. Nanostructured Zinc Oxide Particles in Chemically Modified Electrodes for Biosensor Applications. Analytical Letters, 41: 141-158, 2008
57. EA Sacco. Diffusion of Zn in ZnO. Can. J. Chem. Vol. 39 (1901)
58. Yaojian Zhang, Zheng Chen, Huayu Qiu, Wuhai Yang, Zhiming Zhao, Jingwen Zhao, and Guanglei Cui. Pursuit of reversible Zn electrochemistry: a time-honored challenge towards low-cost and green energy storage. NPG Asia Materials (2020) 12:4
59. Junjun Jia, Aiko Takasaki, Nobuto Oka, and Yuzo Shigesatoa. Experimental observation on the Fermi level shift in polycrystalline Al-doped ZnO films. Graduate School of Science and Engineering, Aoyama Gakuin University, 5-10-1 Fuchinobe, Chuo, Sagamihara, Kanagawa 252-5258, Japan. Journal of applied physics 112, 013718 (2012)
60. Chelladurai Karuppiah, Selvakumar Palanisamy, Shen-Ming Chen, Vediyappan Veeramani and Prakash Periakaruppan. Direct electrochemistry of glucose oxidase and sensing glucose using a screen-printed carbon electrode modified with graphite nanosheets and zinc oxide nanoparticles. Microchim Acta (2014) 181:1843-1850
61. Sajid B. Mullani, Ananta G. Dhodamani, Annadanesh Shellikeri, Navaj B. Mullani, Anita K. Tawade, Shivaji N. Tayade, Julien Biscay, Lynn Dennany & Sagar D. Delekar. Structural refinement and electrochemical properties of one dimensional (ZnONRs)1−x(CNs)x functional hybrids for serotonin sensing studies. Scientific Reports (2020) 10:15955
62. S. Ashok Kumar, Shen-Ming Chen. Nanostructured Zinc Oxide Particles in Chemically Modified Electrodes for Biosensor Applications. Analytical Letters, 41:2, 141-158. 2008
63. R. M. Bashami, A. Hameed, M. Aslam, Iqbal M. I. Ismail, and M. Tahir Soomro. The suitability of ZnO film-coated glassy carbon electrode for the sensitive detection of 4-nitrophenol in the aqueous medium. Anal. Methods, 2015, 7, 1794-1801

CHAPTER FOUR: Nanoclay ZnO synthesis and characterization

4.1 Summary

The following chapter's purpose is to present an overview of nanoclays, and functionalization methods including this study's nanoclay ZnO functionalization, synthesized composites characterization with various analytical tools are detailed as well as the affected property changes are discussed.

4.2 Introduction

Nanoclays are among the choice of materials for various nanocomposite uses because of their positive outcomes. They belong to the family of 2:1 layered phyllosilicates since they possess layered silicates ideal for nanocomposites. Figure 4.1 shows magnesium hydroxide sandwiched between two tetrahedral layers of silicon atoms as well as an inner layer that is aluminum and octahedral, to make up its crystal structure. Major ions in the tetrahedral and octahedral sheets are referred to in the first and second bracket terms in the unit cell formula of $Na_{0.4}[Si_8]$ $[Al_{3.6}Mg_{0.4}]O_{20}(OH)_4$. Interlayer spacing is the result of a van der Waals gap often encountered between layers since they have a stacking arrangement.

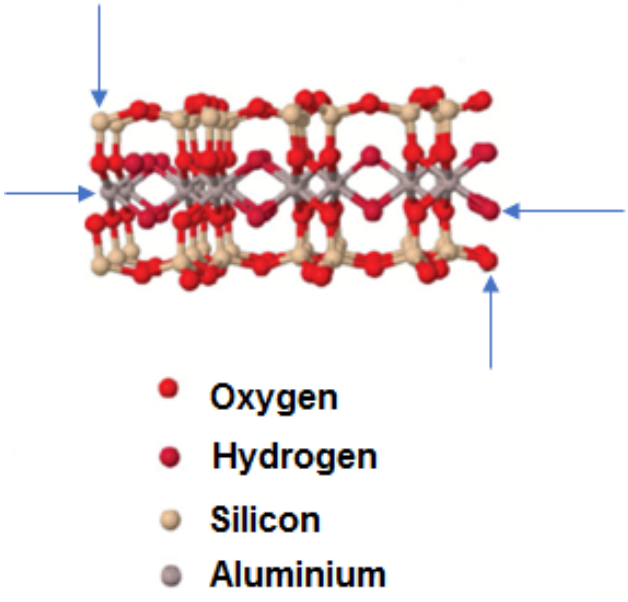

Figure 4.1: The layered mineral silicates of nanoclays

The type of layered silicates will affect the lateral dimensions of layers by 30nm to a few microns while the layer thickness usually is 1nm. The layer ratio, structure, and composition of nanoclays are determined by silicon oxide, aluminum oxide, and magnesium oxide which are then classified as montmorillonite (MMT), saponite, hectorite, vermiculite, mica, talc, and kaolinite. Alkali and alkaline earth metals counterbalance negative charges caused by isomorphic substitution happening in the layers such as Al^{3+} exchanged by Mg^{2+} or Fe^{2+} including Mg^{2+} switching with Li^{+}. Appropriate adsorptive features and cation exchange capacity support MMT in the fabrication of nanocomposites as well as its platelet structure that has an average dimension of 1nm thickness and 70 to 150nm width.[1]

Polyvinyl alcohol (PVA), polyethylene oxide (PEO), fluoropolymers, and hydrophilic molecules are miscible to layered silicates since pristine MMT contains hydrated Na^{+} or K^{+} ions. To achieve hydrophobic conversion with another chemical matrix, the miscibility and compatibility of layered silicates can be modified to suit uses involving hydrophobic nanocomposites. By organically modifying layered silicates and hence nanocomposite materials, the interfacial adhesion is confirmed through two conjugative platelets (intercalated) that have increased interlayer basal spacing. Table 4.1 contains a summary of the modification of pristine nanoclays to create new commercially available organoclays. Alkyl sulphonium organic surfactants, alkyl phosphonium, primary, secondary, tertiary as well as quaternary alkyl ammonium including cationic surfactants can swop with exchangeable ions like Na^{+} and Ca^{2+} located within the layer silicates. Figure 4.2 shows the modification of layered silicates with an alkyl ammonium cation. The modified layered silicates are known as organically modified montmorillonite or simply organoclay. Larger interlayer space results when wetting characteristics of a nanocomposite are improved through modification with specific alkyl ammonium or alkyl phosphonium cations to create layered silicates with low surface energy.

Table 4.1: The modification of pristine nanoclay particles and the subsequent organoclays

Nanoclay	Modification	Organoclay
MMT	• Dimethyl, benzyl, and hydrogenated tallow quaternary ammonium salts • Dimethyl dehydrogenated tallow quaternary ammonium salts • Methyl tallow bis-2-hydroxyethyl ammonium	Cloisite 10A, 15A, 20A, and 30B
	• 35-45% dimethyl dialkyl (C14-C18) amine • 15-35% octadecylamine and 0.5-5% aminopropyl triethoxysilane • 25-30% trimethyl stearyl ammonium	Nanomer 1.30P, 1.31PS, 1.44P, 1.44PS, 1.44PT, and 1.28E
	• Distearyl dimethyl ammonium chloride (dimethyl dehydrogenated tallow ammonium ion)	Nanofil 2, 5, 9, SE 3000, and SE 3010
Hectorite	Alkyl quaternary ammonium salts	Bentone 107, 108, 109, and 2010

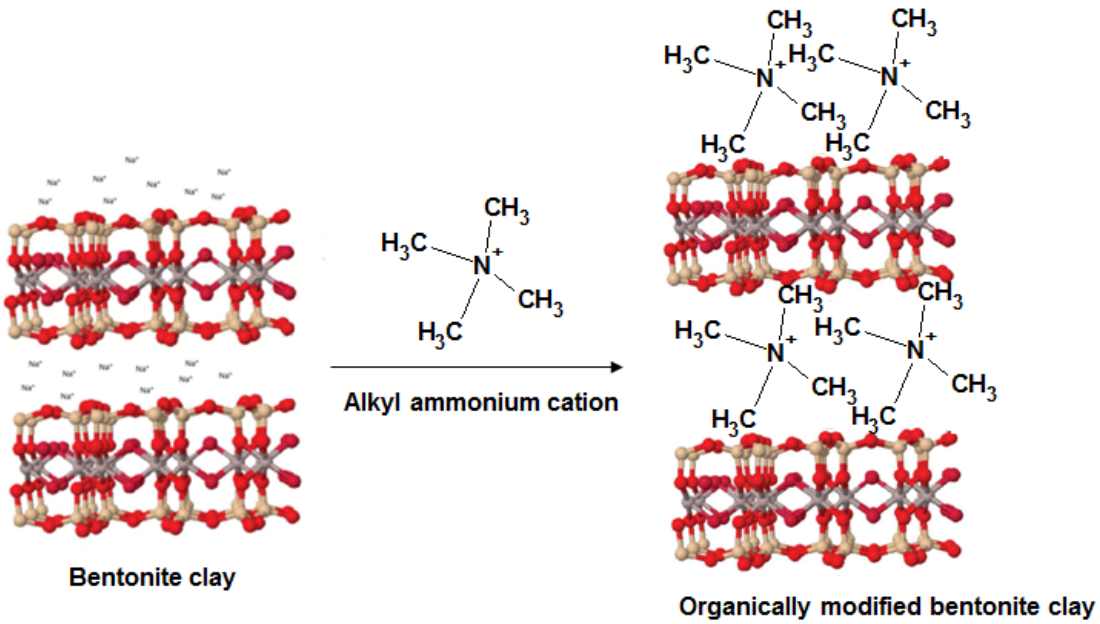

Figure 4.2: The illustration of a modification of bentonite layered silicate to produce the organoclay

Chemical linkage at the interfacial region happens when layered silicates are functionalized by alkyl phosphonium of alkylammonium cations in the fabrication of nanocomposites considering that dispersing into individual layers is a property of layered silicates. The best selection criteria for organoclay depend on the type of nanocomposite properties sought after.[1] The feasibility of nano conversion of layered silicates to form several nanocomposite materials from micro composites has been performed and reports say that innovative approaches such as nano-assembling methods, one-pot reaction synthesis, microwave-assisted, and injection molding are satisfactory. Unlike melt intercalation and other mixing systems involving solution phase or components that exist in colloidal form, the preparation of relatable nanocomposites is becoming flexible to make a wider variety of nanocomposites with clay minerals. Nanoclay composites can be synthesized through melt spinning, melt blending, solvent blending, and ion exchange; these procedures are summarised in figure 4.3.

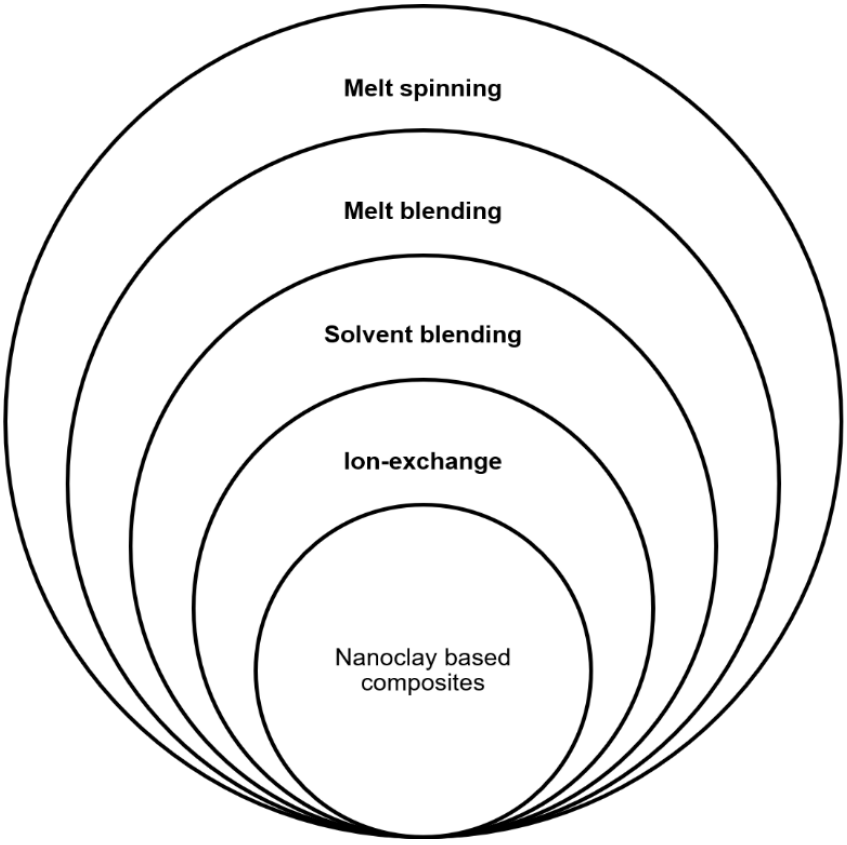

Figure 4.3: A few synthesis methods for nanoclay based composites

4.3 Clay-based nanocomposite synthesis techniques

4.3.1 Melt spinning

Nanoclay/polymer fibers are formed from melt spinning[2] a two or more component composite and using an extrusion system. Precursors like maleic anhydride grafted polypropylene, acrylic acid grafted polypropylene, Nanomer 1.44P or Perkalite F100 are mixed with reagents such as Irganox B225 thermal stabilizer and exposed to temperatures up to 240^{o}C for about 10 minutes. In the extruder heater zones, spinning parameters such as melt draw ratio, speed ratio, the tangential speed of the take-off roller, exit speed from the spinneret, and solid-state draw ratio play a massive role in the product outcome.

4.3.2 Melt blending

Melt blending[3,4] involves manually pre-mixing precursors such as MMT K10, Nanomer PGV, polylactide resin, polycaprolactone, high density polyethylene, Closite C10, C15A, C30B, or Nanomer 1.44P with reagent polyethylene-grafted maleic anhydride compatibilizer at 170-190^{o}C for 10 minutes. The process involves feeding the mixture into an extruder with a specific rotor speed and confirming that the product formed is compression molded at high temperature and extreme force, into sheets to test for tensile strength, flexural, and impact resistance.

4.3.3 Solvent blending

The synthesis involves the formation of nanoclay/polymer composite with styrene monomer, Nanomer 1.28E, 1.30E, 1.44P, or 1.31PS with reagent benzoyl peroxide free radical catalyst at 105^{o}C for 24 hours. The reaction taking place is based on polyremization[5] of the monomer to which the clay particles are added. After stirring, the resulting composite can be dried followed by characterization.

4.3.4 Ion-exchange

Forming a nanoclay ZnO composite involves the alkaline ion exchange of process[6] when immersing several clay particles like MMT K10 or Nanomer 1.31PS, into a solution of zinc salt precursors such as $ZnCl_2$, commercial ZnO nanopowder, or $Zn(CH_3COO)_2$. The inclusion of solvents namely distilled water, THF, ethanol, phenol,

or even surfactant can have a significant effect on the product outcome. Temperature conditions are 70, 120, or 350 to 450^{o}C and the synthesis can take place between 5 minutes and 1 hour. This is proceeded by washing with distilled water of the product, filtration and drying until room temperature. The modification leads thus to fucntionlization[7] of the nanoclay and ultrasoncation[8] causes greater intercalation of molecules between clay layers. Equation 4.1 represents the process taking place.

$$Na - clay_{(s)} + ZnCl_{2(aq)} + H_2O \frac{350,450^{o}C}{\Delta} \rightarrow ZnO - clay_{(s)} + Na^{+}_{(aq)} + 2HCl_{(aq)} \quad 4.1$$

Nanocomposites, where structure is further controlled, can be achieved by using layered silicates like sodium montmorillonite nanoclay due to its large surface area, adsorptive ability, and ion-exchange behavior. Surface modification becomes efficient when the distance between clay layer platelets gets larger since this molecule enters unhindered and proves that nanoclay's dispersion properties are crucial together with its low cost including accessibility. ZnO nanoclay hybrid composites are effectively achieved when porous silica and clay minerals become coated with the metal oxide particles, consequently affecting optical properties majorly of ZnO and nanoclay precursors individually due to the surface modification. Characterization approaches of related clay nanocomposites involve some techniques ranging from electron microscopy, spectroscopy, particle properties, thermal analysis, and electrochemical as per figure 4.4.

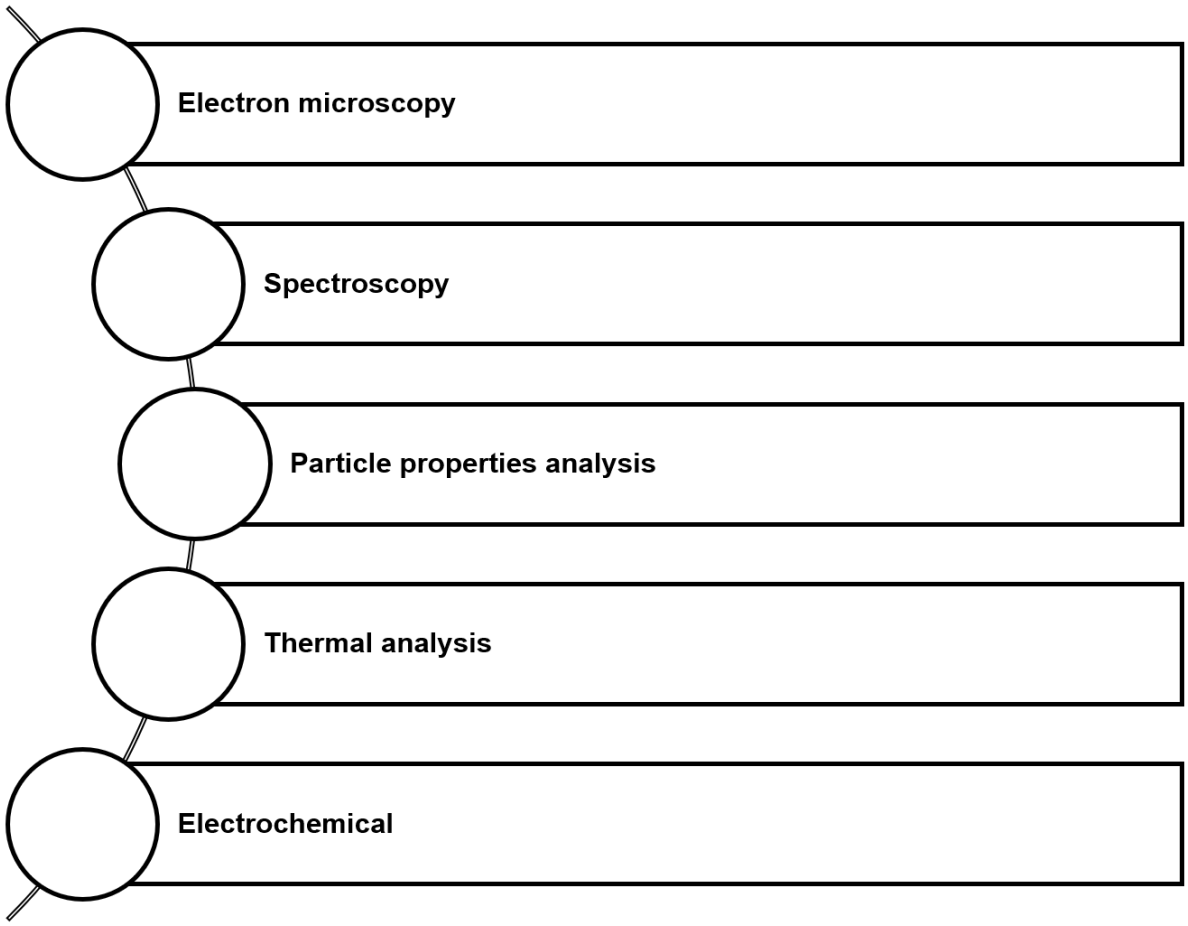

Figure 4.4: The collection of analytical techniques for the characterization of nanoclay composites

4.4 Nanoclay composite characterization methods

Clay-based nanocomposites are effectively characterized to confirm their composition and to establish impregnation by a supposed modifying compound where applicable. Standard laboratory characterization techniques for electron microscopy include SEM and TEM, to confirm the surface shape. Spectroscopy involves FTIR for functional group identification and XRD for crystallinity of the clay regions if pristine but also changes brought about to a sample surface. Dynamic light scattering through Zetasiser can assist in nanoclay particles dimension and further information regarding size distribution, Zeta potential, and dispersity features due to modified surfaces. Thermal stability can be observed with thermal analysis techniques as well as resistance to thermal degradation of pristine nanoclay as well as modified clay surfaces. Electrochemical characterization shall provide details of current density

because of clay exfoliation of conductive nanoparticles and influences electrode potential under consistent conditions as without the presence of nanolcay. Many conclusions can further be made by these few characterization facts of a clay-based nanocomposite like specific surface area, porosity, the solubility of nanoparticles, particle aggregation, hydration or wettability, and adsorption features. Studies such as cation ion exchange capacity, flame retardancy, anti-corrosiveness, swelling capacity, hardness, tear, oxygen permeability, decay resistance, elongation at break, impact, and tensile tests are done on nanlocay composites for quality control purposes.

4.5 Experimental

Reagents and materials

Distilled water was cleaned by a Milli-Q system from Merck. Zinc nitrate; $Zn(NO_3)_2$ (Merck, 98%), sodium hydroxide; NaOH, (Merck, 99%), Nanoclay hydrophilic bentonite (Aldrich, nanomer PGV), Nanoclay surface modified (Aldrich, nanomer 1.44P), hydrochloric acid (HCl), different micropipettes and 2ml Eppendorf tubes.

4.6 Methodology

4.6.1 Nanoclay zinc oxide composites synthesis

Nanoclay zinc oxide nanocomposites were synthesized using the wet chemistry precipitation method by preparing 0.2M solutions of zinc nitrate ($ZnNO_3$) acetate (ZnAC) and chloride (ZnCl) in 100ml quantities. These were kept at a constant heat of 80^oC with vigorous stirring and to these solutions, 1g of PGV and 1g of 1.44P were added in separate beakers. This procedure was followed by 10ml of 1M NaOH drop-wise additions. Each reaction was monitored for changes and allowed to proceed for two hours. After this period, each reaction got allowed to cool down to room temperature with no further stirring. The formed PGV ZnO and 1.44P ZnO products in each case were transferred to amber containers to preserve the quality. In another sequence, only nitrate was used and additional ratios containing 0,5 and 1,5g of PGV and 1.44P respectively were created. The obtained composites were identified in line with the precursors and nanoclay; PGV $ZnNO_3$, PGV ZnAC, PGV ZnCl, 1.44P $ZnNO_3$, 1.44P ZnAC, and 1.44P ZnCl. 0,5g PGV ZnO, 1g PGV ZnO, 1,5g PGV ZnO, 0,5g 1.44P ZnO, 1g 1.44P ZnO and 1,5g 1.44P ZnO are all based on zinc nitrate.

4.6.2 Sample preparation

The D1008 microcentrifuge from DLab Scientific Inc. at a setting of 5000rpm and 2ml Eppendorf tubes were used to wash the PGV ZnO and 1.44P ZnO products to dissolve impurities and obtain nanoparticles quantitatively. Further sample preparation was performed relative to what the characterization techniques necessitated.

4.6.3 Characterization techniques

4.6.3.1 High-resolution transmission electron microscopy

A high-resolution specification transmission electron microscope, model, Tecnai G220 (F20 HR TEM) with SEAD (selected area electron diffraction) was used to analyze solid samples of pristine 1.44P, ZnO from zinc nitrate and a 1.44P ZnO composite to evaluate the morphological nature and changes. Pristine 1.44P, with no purification, was measured as a powder but sample preparation procedures of the ZnO product and 1g 1.44P ZnO composite involved centrifuging, washing three times with Milli Q water, filtering with filter paper, and filter funnel to obtain the respective solids. Additional drying at room temperature was permitted before analysis.

4.6.3.2 Fourier transform infrared spectroscopy

A Fourier transform infrared (FTIR) spectrometer from Perkin Elmer, model Spectrum II, purposed to confirm the presence of characteristic functional groups in the PGV ZnO and 1.44P ZnO composite samples in the frequency range of 400-4000cm^{-1}. The sample preparation of the respective nanoclay ZnO product solutions involved centrifuging and washing three times with Milli Q water, filtering with filter paper, and filter funnel to obtain the respective PGV ZnO and 1.44P ZnO solids. Further drying at room temperature was allowed before each measurement.

4.6.3.3 X-ray diffraction spectroscopy

The BRUKER AXS D8 Advance (from Germany) diffractometer was used to analyze samples for crystallinity and phase composition of ZnO product samples. The LynxEye detector is the position type detector, the tube Cu-Ka radiation (I Ka_1 = 1.5406Å) and θ to θ scanning was carried out in locked coupled style. The variable slits were V20, tube current 40mA, and tube voltage 40kV for all measurements. BRUKER supplied

EVA software to handle the data, ICDD pdf database 1999 to analyze data while the 2θ range from 10° to 80° were at 2θ (0.034°) increments. The sample preparation involved centrifuging and washing three times with Milli Q water of the different 1.44P ratios, filtering with filter paper and filter funnel to obtain the respective 1.44P ZnO powders. Further drying at room temperature was allowed before the samples were tested.

4.6.3.4 Electrochemical characterization

Preparation involving 1, 0.3, and 0.05 μm alumina slurries were used to polish glassy carbon electrodes (GCE) to clean the surface for electrochemical characterization followed by thorough rinsing with water and ultrasonication at room temperature for approximately 15 minutes. The PGV ZnO and 1.44P ZnO product solutions were centrifuged and washed once with Milli Q water to gather enough nanoparticles finely distributed. About 20μL of this was used in each nanoclay ZnO product composite's case to drop-coat on the GCE surface to construct a thin film and let dry overnight. The electrochemical characterization was performed with Autolab PGSTAT 101 supplied from Metrohm South Africa in cyclic voltammetry mode. The supporting electrolyte chosen was 0.1mM HCl while the counter and reference electrodes were platinum wire and Ag/AgCl in 3M KCl accordingly. Various scan rates were applied to the cell.

4.7 Results and discussion

4.7.1 High-resolution transmission electron microscopy

Transmission mission electron microscopy at high resolution (HR TEM), provided electron micrographs of pristine 1.44P, ZnO from $ZnNO_3$ and 1g 1.44P ZnO composite to investigate surface morphology at the level of the crystal lattice of estimated structural changes. SAED (selected area electron diffraction) spots assisted with indicating a single crystal or polycrystalline texture of samples.

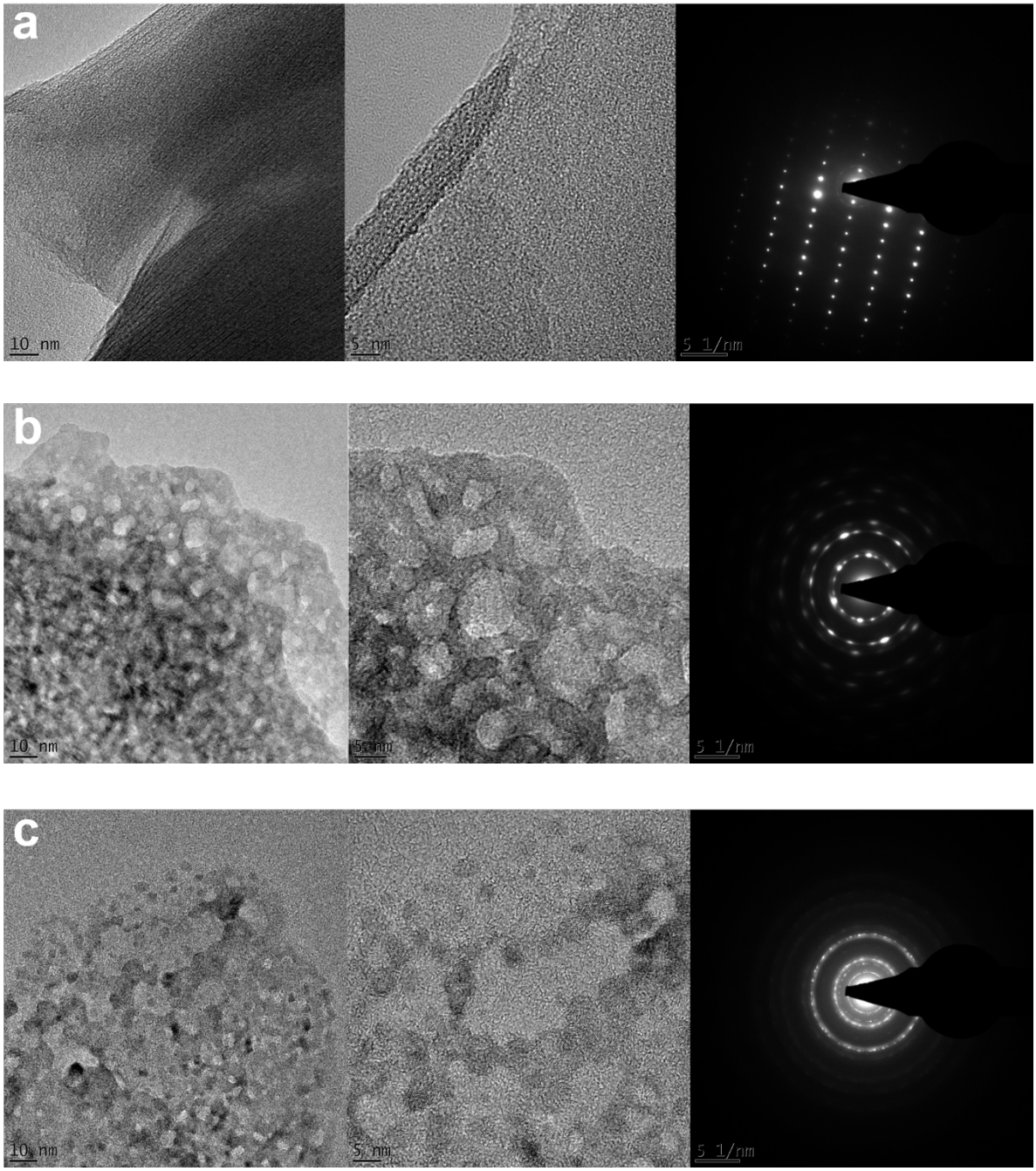

Figure 4.5: The high-resolution transmission electron microscopy images as well as selected area electron diffraction patterns of a) pristine 1.44P, b) ZnO and c) 1g 1.44P ZnO using $ZnNO_3$ as the precursor

At high HR TEM image magnification (10 then 5nm), figure 4.5a, the single layers of pristine 1.44P are revealed as well as a confirmation of laminated clay layers.[2, 9, 10] Furthermore are lattice stripes visible with interlayer spaces establishing the coherence in stacking of adjacent layers which are characteristic features of the

nanoclay edges.[14] The accompanying arrayed bright spots SAED pattern exhibits perfectly ordered crystallinity i.e. single crystal lattice where atoms occur periodically across the entire volume of the clay. Figure 4.5b is the magnified images of the ZnO product which is partially agglomatred[11] and spherical.[16] Additionally, has the ZnO product grown into a form that shows narrow particle size distrubution[15] hence does the intermitted intense SAED outline show that it is a solid which is polycrystalline because of the different crystal growth planes. In figure 4.5c, the 1g 1.44P ZnO composite produced magnified images that describes the delamination of the clay minerals into individual layers onto which ZnO intercalates and gets randomly distributed throughout the clay matrix.[2] This supports the successful formation of the nanocomposite[13] as well as inconsistent particle size distribution.[13] Such exfoliation by the clay affects the distance between ZnO particles[13] thus crystallinity is compromised resulting in an amorphous solid, as depicted by dimmed SAED information.[10]

4.7.2 Fourier transmission infrared spectroscopy

FTIR analysis was used to test whether nanoclay and the related nanoclay ZnO composites have structural consistency, and integrity and can be distinguished. The obtained spectral information becomes a unique fingerprint and allows for functional group characterization, revealing any contamination as well as showing oxidation or decomposition products.

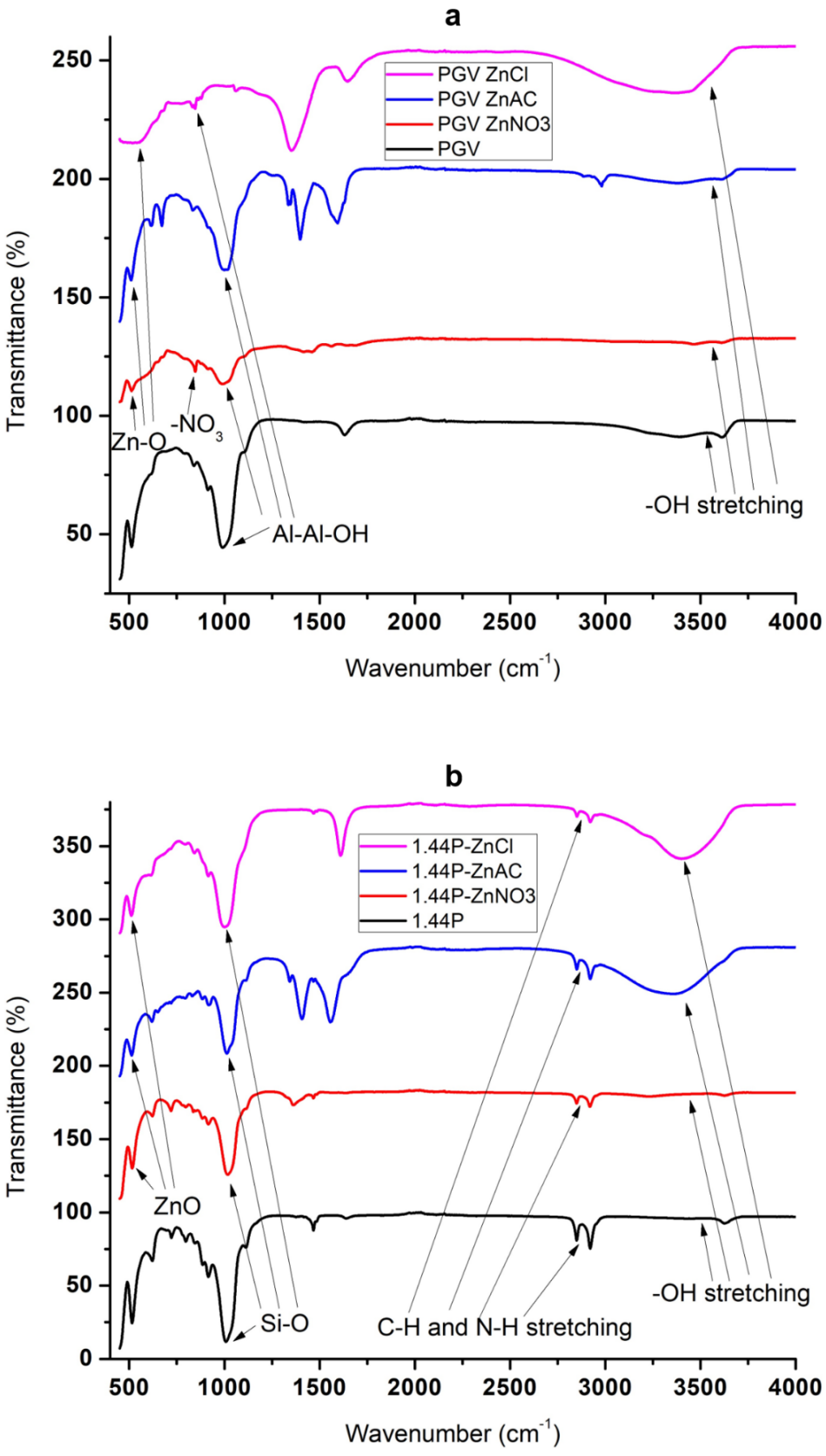

Figure 4.6: The Fourier transform infrared spectral data of a) PGV ZnO and b) 1.44P-ZnO composites synthesized with various precursors

Table 4.2: The observed FTIR functional group frequencies (cm^{-1}) of PGV and 1.44P ZnO composites respectively synthesized with various precursors

Functional group	PGV ZnO			1.44P ZnO		
	$ZnNO_3$	ZnAC	ZnCl	$ZnNO_3$	ZnAC	ZnCl
-OH stretching	3456	3404	3439	3634	3400	3392
C-H stretching				2912	2922	2930
N-H stretching				2859	2852	2851
Si-O				1023	1017	987
Al-Al-OH	1000	1000	1055			
Zn-O	453	455	451	452	451	450

Figure 4.6 is a collection of the FTIR spectral information related to PGV and 1.44P ZnO composites while table 4.2 is comprehensive of the relevant frequencies. Figure 4.6a shows that PGV has a distinctive frequency vibration at 997 due to Al-Al-OH which is part of its clay structure including 3387 cm^{-1} indicating -OH stretching vibrations.[6, 14] PGV with $ZnNO_3$ forms the Zn-O bond around 453, 846 is due to nitrates groups stretching, 1000 due to Al-Al-OH in PGV and 3456 cm^{-1} because of OH stretching vibrations of water molecules. PGV with ZnAC forms the Zn-O bond around 455, has a frequency at 1000 due to Al-Al-OH in PGV and -OH stretching vibrations at 3404 cm^{-1}. PGV with ZnCl creates the Zn-O bond around 451, a frequency at 1055 due to Al-Al-OH and at 3439 cm^{-1} related to -OH stretching vibrations.

The FTIR spectral data assembled in figure 4.6b indicates that 1.44P have characteristic frequencies at 1014 because of Si-O present in its structure and a doublet of peaks in the region of 2921 and 2850 cm^{-1} because of C-H elongation as well as N-H widening from dimethyl dialkyl amine, which is the modifier compound.[5] 1.44P with $ZnNO_3$ leads to vibrational frequencies at 452 due to ZnO, 1023 from Si-O, 2912 and 2859 because of C-H and N-H stretching from dimethyl dialkyl amine and a weak frequency at 3634 cm^{-1} from -OH stretching vibrations of layer hydroxyls. 1.44P with ZnAC leads to vibrational frequencies at 451 due to ZnO, 1017 from Si-O, 2922,

and 2852 because of C-H stretching and N-H stretching from dimethyl dialkyl amine as well as a strong frequency at 3400 cm^{-1} from OH stretching vibrations of layer hydroxyls. 1.44P with ZnCl leads to vibrational frequencies at 450 due to ZnO, 987 from Si-O, 2930, and 2851 because of C-H stretching and N-H stretching from dimethyl dialkyl amine and a strong frequency at 3392 cm^{-1} from OH stretching vibrations of layer hydroxyls.

4.7.3 X-ray diffraction spectroscopy

XRD traces of synthesized ZnO using $ZnNO_3$ from chapter 3 and 1.44P, which is a surface modified version of bentonite also known as montmorillonite (MMT) as well as the corresponding 1.44P ZnO composites were measured to investigate surface crystallinity and consider which phases are present in the pristine 1.44 and after ZnO incorporation. The XRD pattern of synthesized ZnO, figure 4.7a, prepared by a simple precipitation reaction produced diagnostic peaks at 2 theta 9.24^o (200), 18.40^o (110), 27.08^o (020), 38.33^o (421), and 66.25^o (713) for the presence of zinc hydroxide nitrate hydrate (ZHNH), an intermediate compound when forming ZnO, in the sample. A high percentage of the positive match for the ZHNH structure in the sample was confirmed by the instrument software. Additionally, zincite, which is a very pure form of ZnO, serves as a reference and revealed rather weak matches at 2 theta positions 33.01^o (002), 35.44^o (101), and 46.76^o (102) in the synthesized ZnO. ZnO detectable peaks can be indexed to its wurtzite structure which includes lattice parameters like crystalline sizes and their respective planes.[15] High intensity and sharp diffraction peaks are an indication of well-crystallized ZnO together with no characteristic peaks due to impurities.[16] The preferred growth of ZnO along certain planes can be used to confirm dimensions (one, two, or multi) of its nanostructure and hence shape (particles, rods, stars, etc.).[17] The original molecular formula of MMT is approximately $H_2Al_2O_6Si$ thus 1.44P revealed peaks at 19.76^o (101), 35.10^o (107), and 61.84^o (2011), suggesting a hexagonal lattice arrangement. Exchangeable cations residing in the interlayers of MMT were replaced by organic dimethyl dialkyl amine to make layered silicates organophilic giving rise to pristine 1.44P. The presence of SiO_2 in the form of quartz is, therefore, an obvious feature in the crystal lattice and the respective peak positions at 20.27^o (100), 26.62^o (101), 53.94^o (112), 72.89^o (301) confirm a hexagonal crystal lattice. The C, H, and N contents in 1.44P serves as an indictor of the surface

modification of the clay from the parent MMT form, the impact of quartz after the modification, and the nature of the resulting clay layers.[14] A notable feature in comparing sample results to standard XRD diffraction patterns is crystallite size relative to synthesis/manufacturing method when correctly identifying crystalline planes.[19] The lack of any other specific diffraction peaks at 2θ locations can be attributed to the evaporation of water molecules existing in interlayers of the clay due to high operational temperatures.[3] Figure 4.7b indicates the differences in various weights (0,5, 1, and 1,5g) of 1.44P underwent in combination with ZnO. At positions 9 and 18º, a decrease in ZHNH diffraction peak intensity was observed due to 0.5g 1.44P in the composite. An enhancement of the ZHNH diffraction peak with 1g 1.44P became obvious while its presence was again conformed by 1.5g 1.44P. The crystallinity due to zincite reduces with the increasing presence of 1.44P indicating that more nanoclay offers a greater surface area for nanoparticles and will influence overall crystallinity in the composites. As previously reported, ion exchange at the 1.44P ZnO interface is due to the enlargement within the interlayer areas, which consequently promotes impregnation by ZnO species; in addition to this, does the concentration of zinc salt precursor[16] solutions play a key role in ion-exchange at clay surfaces. XRD patterns have shown that pH conditions influence nanostructure properties and hence crystallinity of ZnO as well as related nanocomposites.[10] As per figure 4.7b, the effect of loading is considered in terms of 1.44P due to nanocomposite formation with ZnO. MMT around 19º, 35º, and 61º at 0.5g 1.44P loading is lower in intensity while quartz (SiO_2) in the regions of 20º, 26º, 53º, and 72º at the same quantity of 1.44P is persistent. At 0.5g of 1.44P, there is a slight decrease in intensity of diagnostic diffraction peaks due to MMT while quartz is almost completely diminished. 1g 1.44P produced XRD patterns which show only MMT and not quartz while at 1.5g 1.44P none is observed. The reason behind the shift in MMT diffraction peaks to higher angles in the 0.5g 1.44P ZnO composite is due to poor exfoliation of ZnO, while in 1g 1.44P ZnO, ZnO exfoliation is better and 1.5g 1.44P ZnO indicates a shift to lower angles i.e. comprehensive ion-exchange, because of orderly structured MMT.[21] The prominent peaks in 0.5g 1.44P ZnO indicate 1.44P's crystalline nature, while in 1g 1.44P ZnO, the ZnO unit introduces some amorphic character whereas more incorporations of MMT such as in 1.5g 1.44P ZnO, may potentially lead to complete ZnO ion-exchange. [23]

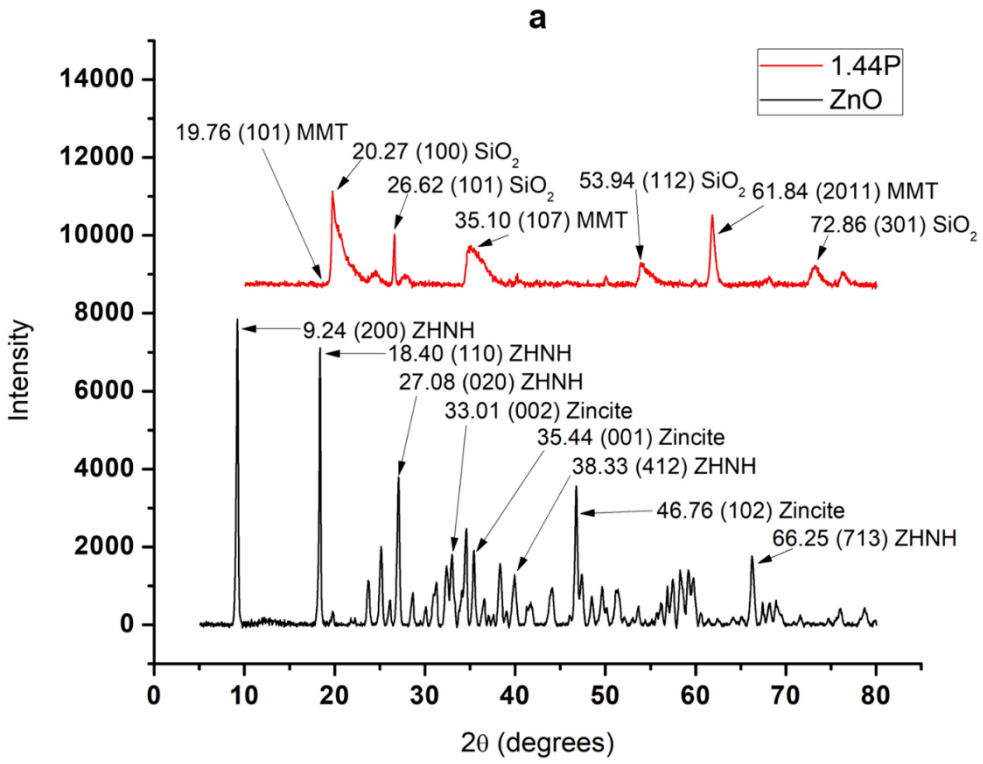
a
1.44P
ZnO
19.76 (101) MMT
20.27 (100) SiO2
26.62 (101) SiO2
35.10 (107) MMT
53.94 (112) SiO2
61.84 (2011) MMT
72.86 (301) SiO2
9.24 (200) ZHNH
18.40 (110) ZHNH
27.08 (020) ZHNH
33.01 (002) Zincite
35.44 (001) Zincite
38.33 (412) ZHNH
46.76 (102) Zincite
66.25 (713) ZHNH
Intensity
2θ (degrees)

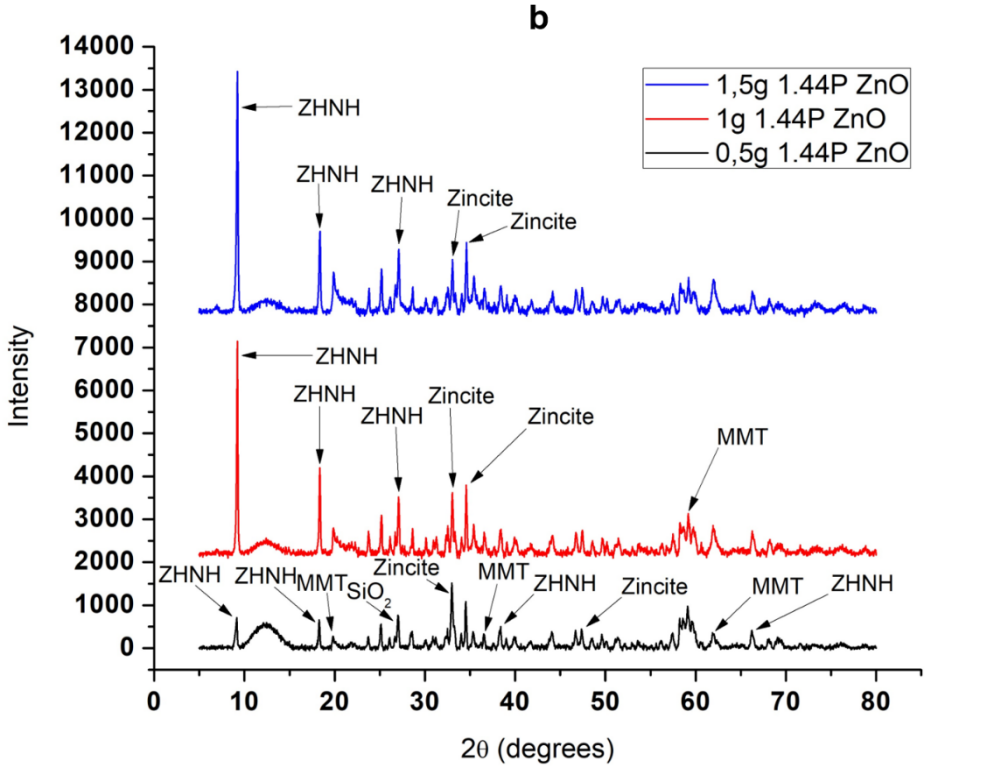
b
1,5g 1.44P ZnO
1g 1.44P ZnO
0,5g 1.44P ZnO
ZHNH
Zincite
MMT
SiO2
Intensity
2θ (degrees)

Figure 4.7: The x-ray diffraction patterns of a) ZnO compared to pristine 1.44P and b) 0.5g 1.44P ZnO, 1g 1.44P ZnO and 1.5g 1.44P ZnO using $ZnNO_3$ as precursor

4.7.4 Electrochemical characterization

Electrochemical characterization was performed on all nanoclay ZnO composites to evaluate the best properties presented in terms of the relevant surface reaction mechanisms, redox potentials, and current density related due to charge transfer. Figure 4.8 is the overlaid cyclic voltammograms of respectively 0,5, 1, and 1,5g of PGV in composites with ZnO showing anodic and cathodic activities, measured in 0.1mM HCl supporting electrolyte at various scan rates. Preparing a hybrid of PGV and ZnO was made possible by knowing the individual features of PGV and ZnO as well as being able to tailor the composition of PGV. The nanostructures of the mesoporous silica and clay mineral become dominated by nanostructures of ZnO.[18] A steady rise of current was observed with an increasing scan rate. As reported before, the presence of ZnO leads to a larger shift towards positive potentials due to reduction as well as the distribution of nucleus centers. It is proven that when metal nanoparticles functionalize the nanoclay platform, the surface morphology changes due to the ion exchange taking place; the purpose of the NaOH reducing agent is evident to reduce particle size for metal nanoparticles to intercalate with surfaces of the clay and influence surface chemistry.[19] Well-defined redox peak behavior and enhanced peak current[20] were observed by the 1.44P ZnO composites, overlaid cyclic voltammograms, figure 4.9, where the composition of the clay was altered by 0.5g, 1g, and 1.5g occasionally resulting in significant electrode potentials. Research supports that operating temperatures[21] and electrolyte choice[21] are among the variables that would affect electrochemical measurements involving electrodes modified nanocomposites where nanoclay is a component but were kept constant when recording these cyclic voltammograms.

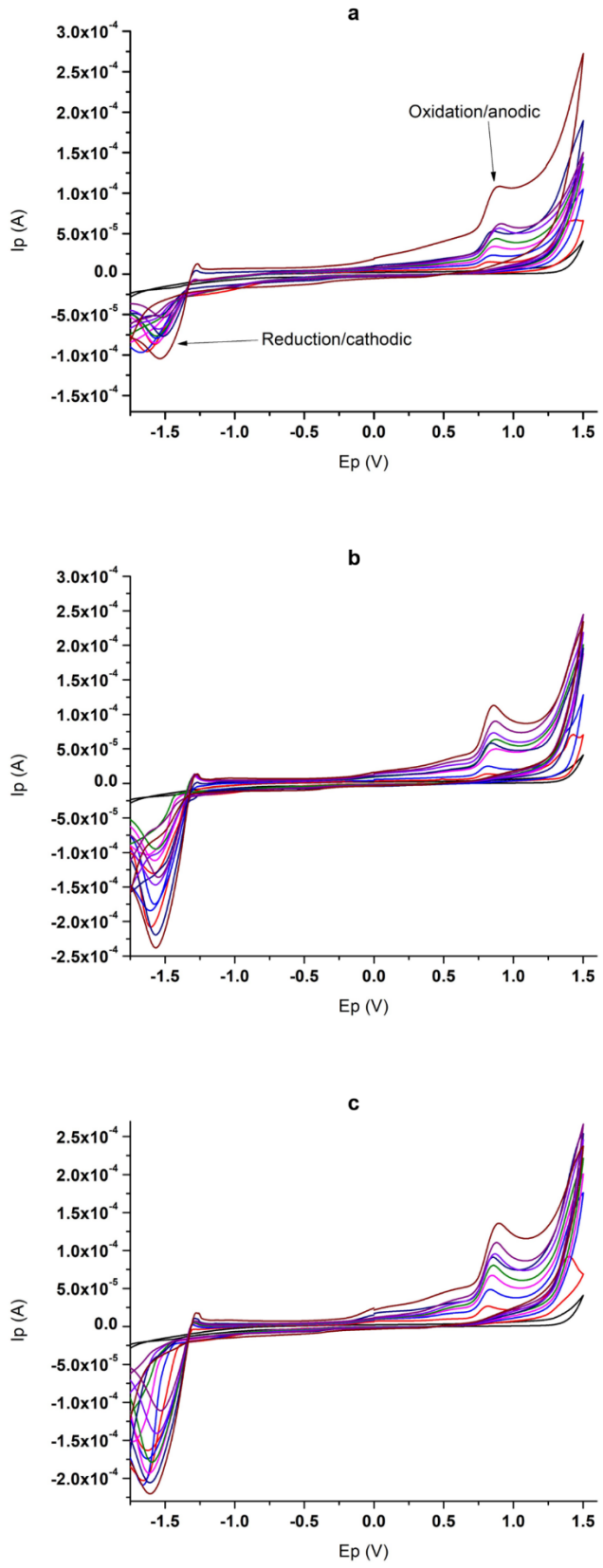

Figure 4.8: The cyclic voltammogram overlay of a) 0,5g, b) 1g and c) 1,5g PGV ZnO composite using $ZnNO_3$ as precursor at scan rates 10 to 100mV/s

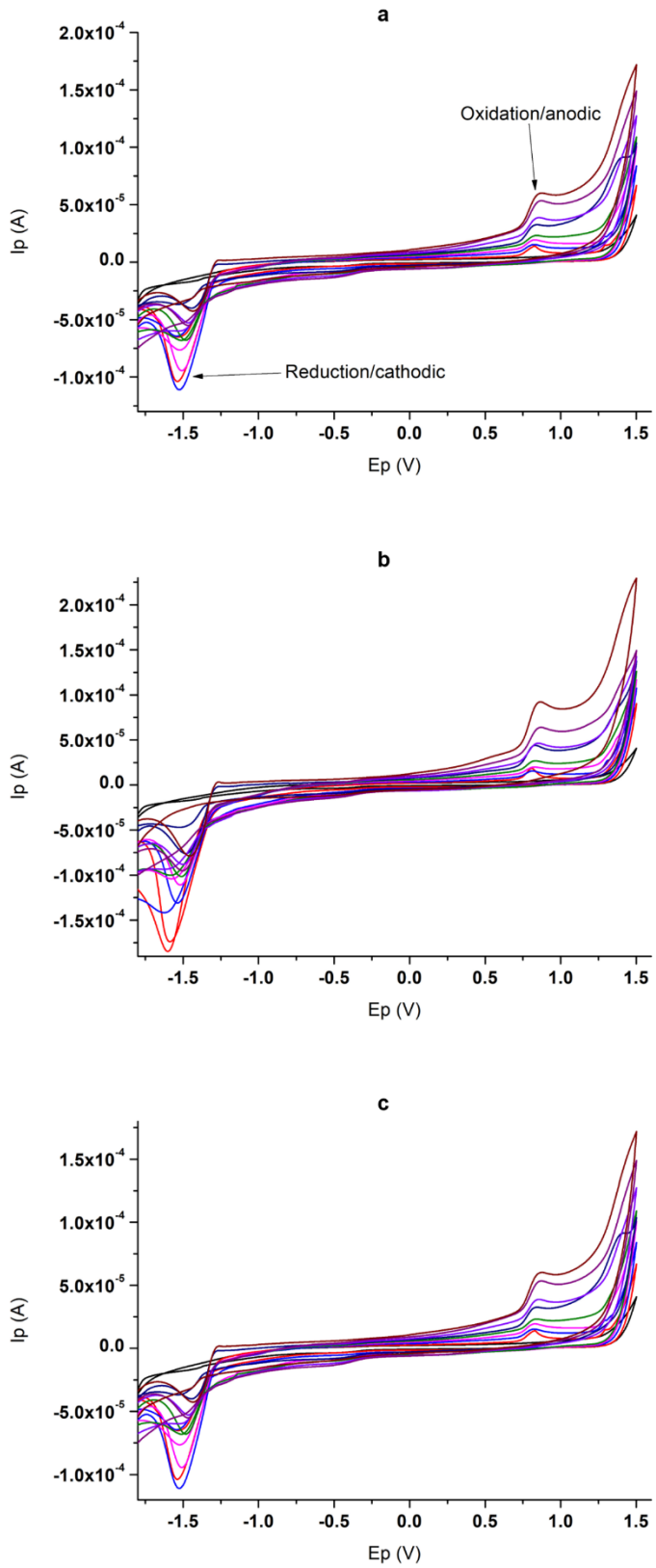

Figure 4.9: The cyclic voltammogram overlay of a) 0,5g, b) 1g and c) 1,5g 1.44P ZnO composite using $ZnNO_3$ as precursor at scan rates 10 to 100mV/

4.7.5 Electrochemical kinetics

The peak currents connected to anodic and cathodic activities at a modified electrode are essential to investigate electron transfer kinetics thoroughly. The shift of the redox potentials towards more positive values with increasing scan rate is linked to kinetic limitation at the surface of the PGV ZnO modified electrodes. Such phenomena be connected to the presence of uneven or non-equivalent sites within the PGV ZnO composites used as modifiers as well as chemical interactions between it and electrolyte ions. To further understand the electron transfer kinetics happening at the 1.44P ZnO modified electrode surface, the little shift in oxidation potentials due to 1.44P incorporation indicates well intercalation of ZnO onto nanoclay surface while a larger shift in reduction potentials to positive values due to 1.44P integration is linked to lesser free ZnO[22] affecting the transfer of electrons. Figures 4.10 and 4.11 is a summary of the type of anodic current behavior due to the nanoclay ZnO modified electrode surface reactions. For all PGV ZnO and 1.44P ZnO composites, the plots of Ipa vs v have linear correlations while those of Ipa vs $\sqrt{v}$ revealed the same pattern; this suggests that processes at the nanoclay ZnO modified electrode surface were adsorption as well as diffusion controlled. To determine the diffusion coefficients of ZnO through both PGV and 1.44P ZnO nanocomposites, regression analysis was used by considering the slope of the best-fitted line of the current against the square root of the scan rate plot. Equation 3.5 from chapter 3 was used to determine the diffusion coefficient of ZnO in nanocaly composites where the process is indeed diffusion-controlled; three nanoclay ZnO ratios were identified as such namely 1g PGV, 1,5g PGV, and 1g 1.44P while the rest were governed by adsorption. The values respectively are in order of 1g PGV and 1,5g PGV the largest followed by 1g 1.44P. This serves as an indication that with these three composites, the rate of transport of the nanoparticles through the clay[23] and hence selectivity while adsorption experienced in other composites favors the mobility of ZnO and improves migration of nanoparticles.

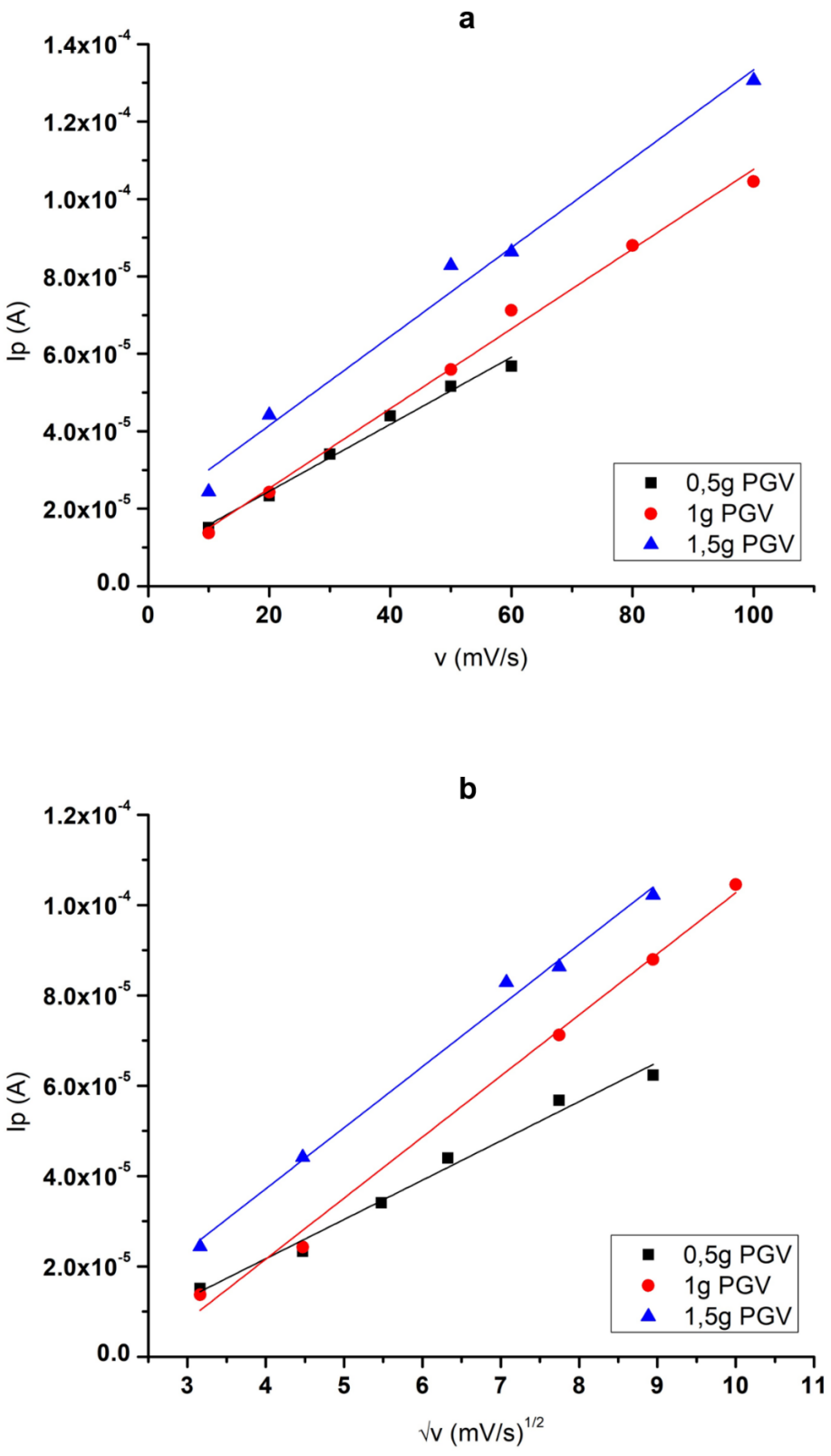

Figure 4.10: The plot of the Ipa vs a) v and b) √v of PGV ZnO composites using $ZnNO_3$ as the precursor

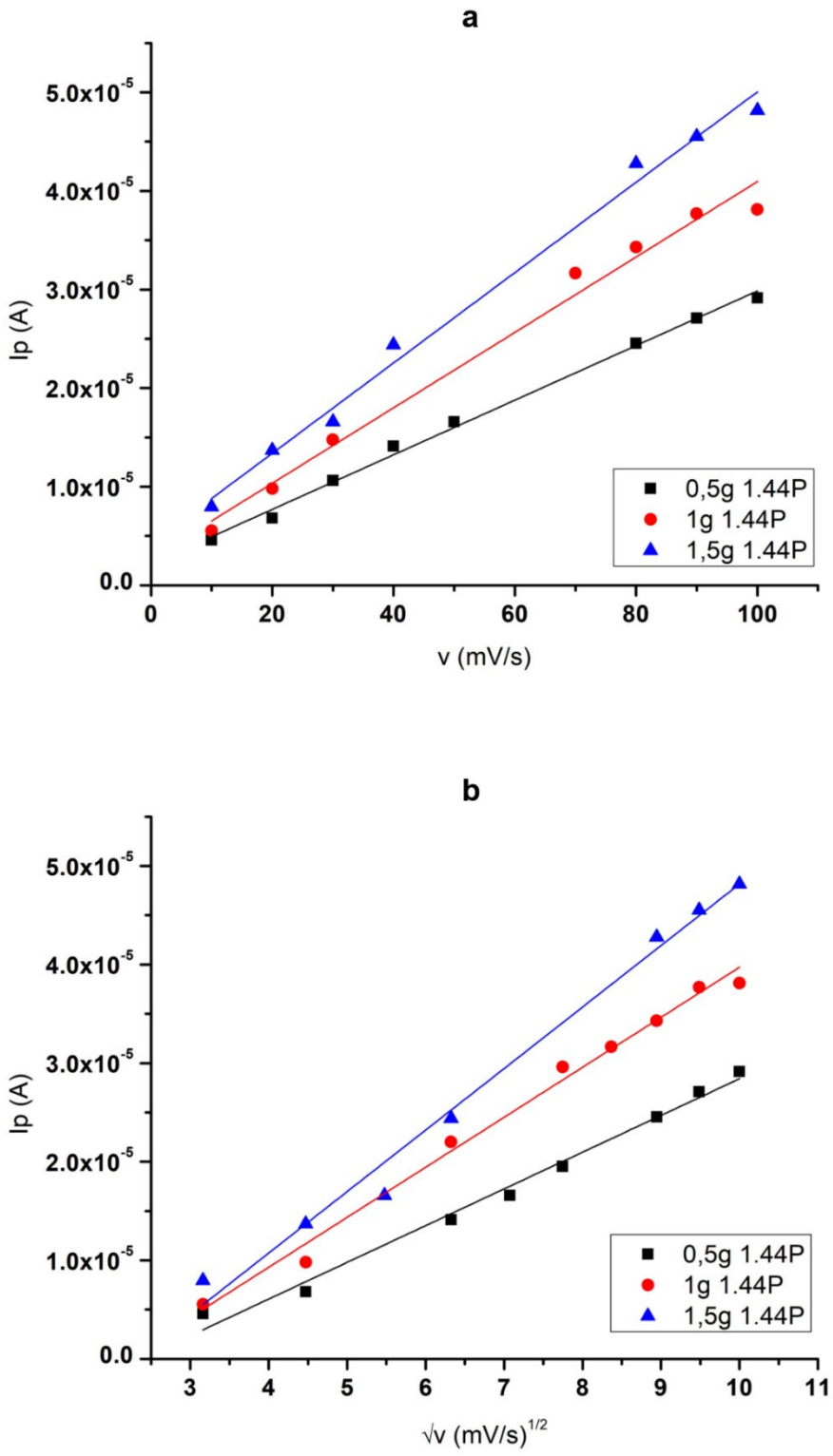

Figure 4.11: The plot of Ipa vs a) v and b) √v of 1.44P ZnO composites using $ZnNO_3$ as the precursor

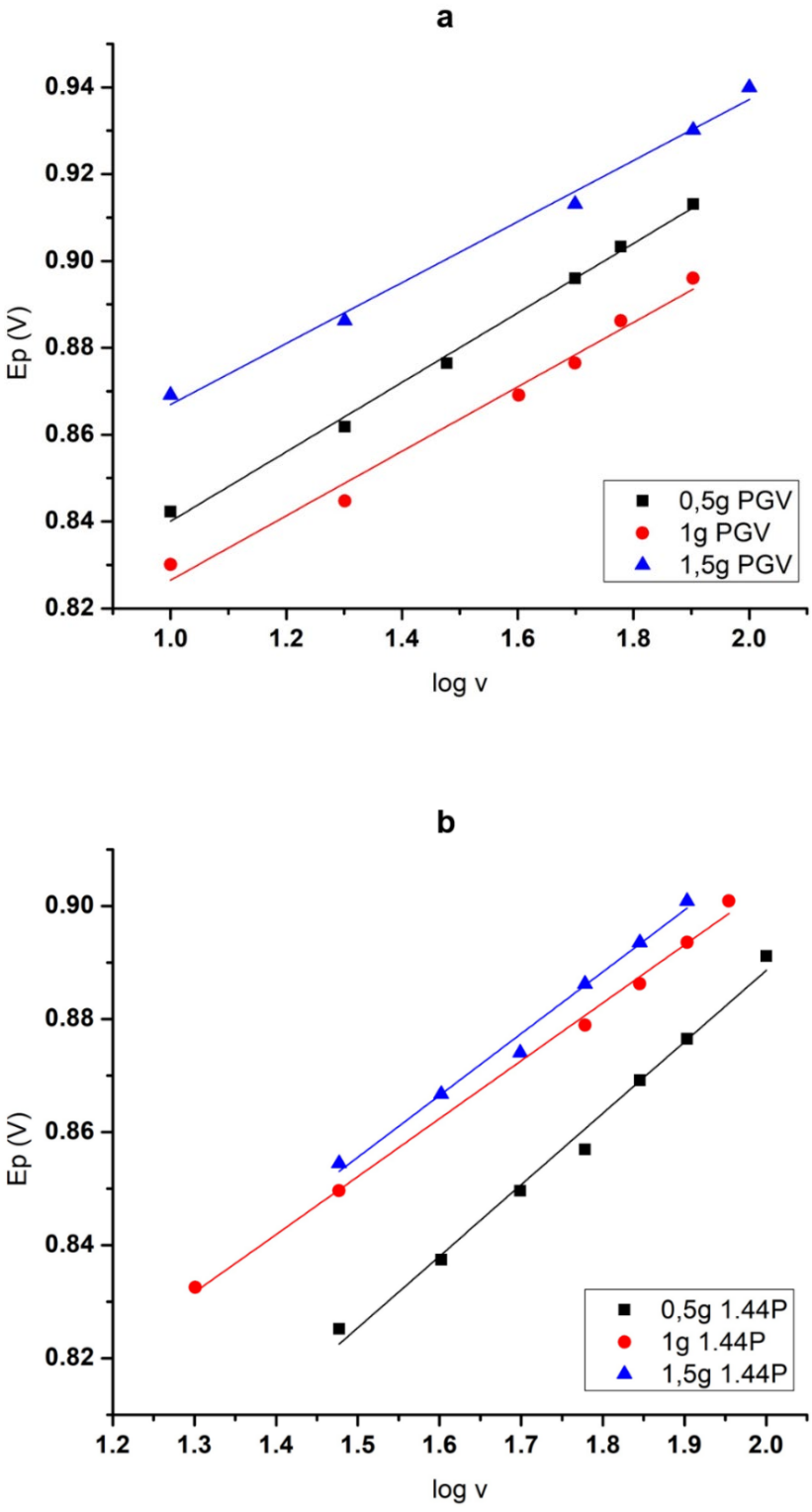

Figure 4.12: The variation of E_p anodic vs logarithm of v plot for a) PGV and b) 1.44P ZnO composites using $ZnNO_3$ as the precursor

Electrode potentials and scan rate offered useful parameters from the cyclic voltammetry experiment to indicate a measure of reversibility[24] of electrochemical reactions as well as using a variation of the plot of potential against the log of scan rate as in figure.4.12, to obtain the slope of the straight-line relationship and substituted in equation 3.6 from the previous chapter. For the anodic peaks, the slope was used to determine the electron transfer coefficient, α, for ZnO in the PGV and 1.44P nanocomposite products. The calculated values for α by all the PGV and 1.44P ZnO composites are in order of increasing value, 0,5g 1.44P<1g 1.44P<1,5g 1.44P<0,5g PGV<1g PGV<1,5g PGV. and it is noted that all the composites obeyed a reasonable 0.5+/-0.2 tolerance[25] for reversibility. It can thus be suggested that PGV and 1.44P equally offer electron stability to ZnO but respective values will indicate the exact extent to which this occurs. When PGV and 1.44P offer electron stability to ZnO. ZnO gets oxidized in the anodic reaction while the reluctance of ZnO in PGV and 1.44P to receive electrons for the cathodic reaction, exists. Furthermore, if α is close to 1, effective functionalization[26] within nanocomposite systems has been reported. Using equation 3.7 from chapter 3, the heterogeneous standard rate constant, k_s, PGV and 1.44P ZnO modified electrodes presented values showing the pattern of 1,5g 1.44P>0,5g 1.44P>1g 1.44P>1,5g PGV>0,5g PGV>1g PGV. 1.44P ZnO composites have the fastest electron transfer process and reversibility[26] followed then by PGV ZnO ratios. Overall, it can be deduced that PGV and 1.44P ratios affect rates and hence the performance of the platform due to clay particles incorporated; PGV restricts electron flow while 1.44P promotes it. This observation supports the validity of ZnO's semiconductor properties.[27] The electron transfer process is retained, and the anodic and cathodic reactions are therefore reversible. The electrochemical features of PGV and 1.44P ZnO ratios, as the amount of nanoclay is varied, present evidence that electron transfer is either being affected by the hydrophilicity (PGV) or due to hydrophobicity (1.44P) which becomes the future nature of the nanoclay ZnO products. Table 4.3 lists the important electrochemical parameters relevant to the nanoclay ZnO composites.

Table 4.3: The electrochemical parameters of PGV and 1.44P ZnO composites synthesized from $ZnNO_3$ and different nanoclay masses

Electrochemical parameter	Mass (g) PGV used			Mass (g) 1.44P used		
	0,5	1	1,5	0,5	1	1,5
Epa (V)	0.82	0.75	0.84	0.81	0.83	0.84
Epc (V)	-1.48	-1.44	-1.40	-1.41	-1.40	-1.38
E_o (V)	0.33	0.35	0.28	0.30	0.29	0.27
ΔEp (V)	0.66	0.69	0.56	0.60	0.57	0.54
Slope fig. 4.11a & 4.12a $x10^{-7}$	8.66	10.30	11.48	2.77	3.82	4.58
R^2 fig. 4.11a & 4.12a	0.995	0.997	0.993	0.998	0.993	0.996
Slope fig. 4.11b & 4.12b $x10^{-6}$ (Slope fig 4.13)	8.70 (0.08)	13.52 (0.07)	13.51 (0.07)	3.72 (0.13)	5.07 (0.10)	6.24 (0.11)
R^2 fig. 4.11b & 4.12b (R^2 fig. 4.13)	0.993 (0.998)	0.998 (0.992)	0.997 (0.997)	0.994 (0.995)	0.996 (0.999)	0.994 (0.995)
α	0.37	0.40	0.42	0.23	0.29	0.27
k_s (s^{-1})	0.0044	0.0019	0.018	0.11	0.064	0.14
Ip_{red}/Ip_{ox}	1.91	3.18	2.01	1.97	2.86	2.59

4.8 Conclusion

HR TEM images and SAED patterns obtained showed surface magnification of pristine 1.44P, synthesized ZnO from zinc nitrate, and a 1.44P ZnO composite. Laminated clay layers and high crystallinity were confirmed in the pristine 1.44P sample while observing partial agglomeration and spherical nanoparticles representing crystal growth of synthesized ZnO. The resulting 1.44P ZnO composite revealed exfoliation by the clay particles and an amorphous solid. FTIR results collectively show the chemical composition and structural identification of pristine PGV and 1.44P, as well as 0,5, 1, and 1,5g composites with all the zinc salt precursors. XRD revealed the changes in morphology which 0,5, 1, and 1,5g 1.44P respectively, underwent when functionalized with ZnO. Electrochemical characterization of PGV and 1.44P ZnO product composites with cyclic voltammetry revealed that 1,5g PGV ZnO and 1g 1.44P

ZnO show the best redox symmetry, but it is 0,5g 1.44P ZnO then 0,5g PGV ZnO that has significantly fast electron transfer process rates based on the heterogenous standard rate constant. The probability of oxidation is more with 0,5g PGV ZnO followed by 0,5g 1.44P ZnO. Overall is it 1.44P ZnO composite films that are retained for longer to the glassy carbon electrode surface after modification compared to PGV ZnO thus would be more favourable for use in the fabrication of the analyte sensor in the next chapter; more especially 0.5g 1.44P ZnO.

4.9 References

1. Deba Kumar Tripathy Bibhu Prasad Sahoo. Properties and Applications of Polymer Nanocomposites. Springer-Verlag GmbH Germany 2017
2. ZengweiGuo, Bengt Hagstrom Preparation of Polypropylene/Nanoclay Composite Fibres. Polymer engineering and science-2013
3. Chern Chiet Eng, Nor Azowa Ibrahim, Norhazlin Zainuddin, Hidayah Ariffin, Wan Md. Zin Wan Yunus, Yoon Yee Then, and Cher CheanTeh. Enhancement of Mechanical and Thermal Properties of Polylactic Acid/Polycaprolactone Blends by Hydrophilic Nanoclay. Indian Journal of Materials Science Volume 2013, Article ID 816503
4. Jimoh K. Adewole, Usamah A. Al-Mubaiyedh, Anwar Ul-Hamid, Abdulhadi A. Al-Juhani and Ibnelwaleed A. Hussein. Bulk and Surface Mechanical Properties of Clay Modified HDPE used in Liner Applications. Can. J. Chem. Eng. 90:1066-1078, 2012
5. Tipu Sultan, Rezaur Rahman, Sinin Hamdan, Faruk Hossen, and Amaliah Binti Mazlan. Improved interfacial interaction between wood and styrene with the help of organically modified nanoclay. BioResources 13(4), 8100-8112
6. N. Garshasbi, M. Ghorbanpour, A. Nouri, and S. Lotfiman. Preparation of zinc oxide-nanoclay hybrids by alkaline ion-exchange method. Brazilian Journal of Chemical Engineering Vol. 34, No. 04, pp. 1055-1063, October-December 2017
7. Biplab K. Deka, Tarun K. Maji. Effect of Nanoclay and ZnO on the Physical and Chemical Properties of Wood Polymer Nanocomposite. Journal of Applied Polymer Science, Vol. 124, 2919–2929 (2012)

8. Suchithra Padmajan Sasikala, T. A. Nibila, Kunnathuparambil Babu Babitha, Abdul Azeez Peer Mohamed and Ananthakumar Solaiappan. Competitive photo-degradation performance of ZnO modified bentonite clay in water containing both organic and inorganic contaminants. Sustainable Environment Research (2019) 29:1
9. S. Manocha, Nikesh Patel, and L.M. Manocha. Development and Characterisation of Nanoclays from Indian Clays. Defense Science Journal, Vol. 58, No. 4, July 2008, pp. 517-524
10. Valery Hambate Gomdje, Abdoul Ntieche Rahman, Abdoul Wahabou, Benoît Loura and Abdelilah Chtaini. Synthesis of Organoclay and its Applications in Electrochemical Detection of Paracetamol. Der Chemica Sinica, 2017, 8(1):206-217
11. Tugrul Yumak, Filiz Kuralay, Mihrican Muti, Ali Sinag, Arzum Erdem, Serdar Abaci. Preparation and characterization of zinc oxide nanoparticles and their sensor applications for electrochemical monitoring of nucleic acid hybridization. Colloids and Surfaces B: Biointerfaces 86 (2011) 397-403
12. Jalal Rouhi, Mohamad Hafiz Mamat, C. H. Raymond Ooi, Shahrom Mahmud, Mohamad Rusop Mahmood. High-Performance Dye-Sensitized Solar Cells Based on Morphology-Controllable Synthesis of ZnO-ZnS Heterostructure Nanocone Photoanodes. PLoS ONE 10(4): e0123433
13. Veeradasan Perumal, Uda Hashim, Subash C. B. Gopinath, Haarindraprasad Rajintra Prasad, Liu Wei-Wen, S. R. Balakrishnan, Thivina Vijayakumar and Ruslinda Abdul Rahim. Characterization of Gold-Sputtered Zinc Oxide Nanorods-a Potential Hybrid Material. Nanoscale Research Letters (2016) 11:31
14. Victoria V. Krupskaya, Sergey V. Zakusin, Ekaterina A. Tyupina, Olga V. Dorzhieva, Anatoliy P. Zhukhlistov, Petr E. Belousov and Maria N. Timofeeva. Experimental Study of Montmorillonite Structure and Transformation of Its Properties under Treatment with Inorganic Acid Solutions. Minerals 2017, 7, 49
15. A Khorsand Zak, R Razali, WH Abd Majid, Majid Darroudi. Synthesis and characterization of narrow size distribution of zinc oxide nanoparticles. International Journal of Nanomedicine 2011:6 1399-1403

16. Shambhu Sharan Kumar. Chemical synthesis of Zinc oxide nanoparticles by precipitation method. International Journal of Engineering and Technical Research (IJETR). Volume-2012, January-June 2012
17. E. O. Dare, O. W. Makinde, K. T. Ogundele, G. A. Osinkolu, Y. A. Fasasi, I. Sonde, J. T. Bamgbose, M. Maaza, J. Sithole, F. Ezema, and O. O. Adewoye. Zinc salt mediated synthesis, and growth kinetic, and shaped the evolution of silver nanoparticles. ISRN Nanomaterials Volume 2012, Article ID 376940
18. Yu Ya, Cuiwen Jiang, Tao Li, Jie Liao, Yegeng Fan, Yuning Wei, Feiyan Yan and Liping Xie. A Zinc Oxide Nanoflower-Based Electrochemical Sensor for Trace Detection of Sunset Yellow. Sensors 2017, 17, 545
19. Maikap, K. Mukherjee, B. Mondal and N. Mandal. Zinc oxide thin film-based nonenzymatic electrochemical sensor for the detection of trace-level catechol. RSC Adv., 2016, 6, 64611-64616
20. Abu R Abi-Stankovic, A. Milutinovic-Nikolic, N. Jovic-Jovic IC, P Bankovic, M.Z. Unic, Z. Mojovic and D. Jovanovic. p-Nitrophenol electro-oxidation on a $BTMA^{+}$ bentonite modified electrode. Clays and Clay Minerals, Vol. 60, No. 3, 291–299, 2012
21. S.Surendra, H.P. Nagaswarupa, K.S. Anantharaju, M.R. Anil Kumar, H. Nagabhushana, Krushitha Shettya. Acid Activation of Bentonite Clay under Microwave Irradiation: Characterization, Cyclic Voltammetry, and Photocatalytic activity. Materials Today: Proceedings 5 (2018) 22643–22651
22. Ravangave L. S. and Shaikh R. S. Influence of pH on Structure, Morphology and UV-Visible Spectra of ZnO nanorods. International Journal of Engineering Science Invention Volume 6 Issues 11, November 2017, PP. 76-79
23. K. Prabakaran & S. Mohanty & S. K. Nayak Influence of surface-modified nanoclay on electrochemical properties of PVDF-HFP composite electrolytes. Int J Plast Technol (December 2014) 18(3): 349-361
24. E. Laviron. The general expression of the linear potential sweep voltammogram in the case of diffusionless electrochemical systems. Electroanal. Chem., 101 (1979) 19-28
25. Blessing Tatenda Shekede, MC Matoetoe. Bactericidal efficacy of wound gauze treated with chitosan nanomaterial hybrids of zinc, silver, and copper on common wound bacteria. Cape Peninsula University of Technology, Cape Town 2018

26. Fredrick O. Okumu, Bongiwe Silwana and Mangaka C. Matoetoe. Application of MWCNT/Ag-Pt nanocomposite modified GCE for the detection of Nevirapine in pharmaceutical formulation and biological samples. Electroanalysis 2020, 32, 3000-3008
27. Omolola E. Fayemi, Abolanle S. Adekunle, Eno E. Ebenso. Electrochemical determination of serotonin in urine samples based on metal oxide nanoparticles/MWCNT on the modified glassy carbon electrode. Sensing and Bio-Sensing Research 13 (2017) 17-27

CHAPTER FIVE: Development of an electrochemical biosensor for Nevirapine

5.1 Summary

This chapter starts with an introduction to glassy carbon electrodes and the opportunities to modify such analytical platforms for specific sensing reasons by making mention of nanoclay, ZnO, and human serum albumin. The electrochemical behavior of the analyte was considered and the effect of human serum albumin was. Choice of supporting electrolyte, starting potential and, modulation amplitude were used to establish some optimal experimental conditions for the detection of Nevirapine. Scan rate studies were performed as well as calibration protocol helped to confirm a linear range for current as a function of analyte concentration. Repeatability and stability of the modified glassy carbon electrode were looked at including its responsiveness to interferants in the presence of Nevirapine. Hence the fundamental conclusions are at the end of the chapter.

5.2 Introduction

5.2.1 Glassy carbon electrodes

Surface features such as nanostructure, neatness, and molecular arrangement presented by the working electrode are essential since they are determining factors of how electron transfer will proceed. An adsorption isotherm is defined as when a bulk concentration of molecules attaches to the surface of an electrode other than water but ionic species from supporting electrolyte, adhering competitively with water. Extremely monolayer overload or exposure is the result of quantitatively adsorbed particles. High-temperature pyrolysis of carbon polymer conditions at 2000^{o}C is ideal to prepare glass carbon which is the widely used carbon-based material for electrodes in analytical determinations. Consequential properties such as chemical inertness, firmness, and elevated conductivity together with an interlinking configuration follow that affects electrochemistry of the surface due to carbon-oxygen behavior as well as the absence of impurities.[1] The boundary of electroactive molecules and the working electrode facilitates the transfer of electrons which is the major course of action when molecules are dissolved or trapped at the electrode surface. The nature of functional groups like oxides that could be present on the electrode surface as well as obstruction

of available spaces by adsorbed species will affect its physical condition such as roughness including porosity and hence the kinetics of the electron transfer behavior. For an electrode surface to produce reproducible results, absorbed species must be removed by suitable laboratory protocol. The immediate working state of the working electrode surface can be improved by mechanical polishing as part of measuring surface preparation. An alternative to this is electrochemical pretreatment[2] which is done by exposing the electrode surface to conditioning potentials before measurements in cases where it is impossible to polish electrodes thoroughly. The working electrode surface roughness and microstructure get altered[3] through the removal of adsorbed species using polishing or electrochemical pretreatment while the expected performance[4] will be influenced by its intended use. Just as metals, heavily boron-doped diamond contains sp^3 carbon atoms while polycrystalline graphite as well as glassy carbon has disordered sp^2 carbon atoms and can facilitate electron transfer quantitatively due to expectational electronic properties adequate for purposes in electrochemistry.[5] Lower electronic density of states (DOS) of carbon materials causes reduced conductivity compared to metals due to carbon not exhibiting significant gaps at particular energy levels for electrons to occupy. Noticeable impact on electron transfer behavior however has been observed at the surface of ordered graphite, carbon nanotubes, and lightly doped diamond because of their lower as well as energy-dependent DOS. The surface chemistry[6,7] of carbon materials and metals vary vastly even though many carbon materials are considered in electrochemical applications due to them being electronically active with no gaps in DOS. Despite the black color of bulk carbon, thin-film versions of graphitic carbon are partially transparent in the visible region of the electromagnetic spectrum while glassy carbon can absorb light over a broad energy span, ranging from deep UV to radio frequencies. Functional carbon electrode materials that are optically transparent have been produced by depositing carbon with an electron beam[8], through the pyrolysis of an anhydride regaent[9] from the gas phase and a thin film of the pyrolyzed polymer was obtained on quartz.[10] Careful monitoring of electrochemical parameters like redox potential, surface coverage, and the heterogenous electron transfer rate indicate the electrode's suitability for use including the choice of surface preparation method. The nature of carbon for electrode material is essential due to the ability of carbon-based surfaces to bond with many functional groups related to the type of carbon

microstructure which is much more complex than metals. Unless for special pretreatment procedures of carbon electrodes, reactions with oxygen-containing functional groups[11,12], water, and oxygen are expected compounds; amongst the oxygen-containing functional groups are carbonyls, phenolic hydroxide, lactones ethers, and carboxylates. The goal behind the use of the carbon electrode will determine if the adsorption of species is an asset or indeed problem, based on the forces that regulate adsorption to the carbon surface of the adsorbate. The history and preparation of the carbon type use as well as is related to covalent and electrostatic bonds, hydrophobic effects, and induced diploes including dipole-dipole intercations[13] which control adsorption between the electrode surface and adsorbate. Surface modifaction[14] of carbon has been explored extensively due to its ability to bond strongly covalently with several materials, permanent dipoles being encouraged by association with adsorbates, and a high microscopic surface area. In most cases, strong surface/adsorbate bonds are a result and possible too with sp^2 hybridized carbon material. The thermal and hydrolytic stability of the C-C bond[16,17] in boron-doped diamond and glassy carbon electrodes causes overall stability after modification by covalent monolayers. The nature of a modifying film[18] also affects the performance of the electrode in terms of binding to adsorbing species.

5.2.2 Glassy carbon electrode modifications

In electroanalytical applications to accurately measure analytes there is wide use of carbon-based electrodes such as glassy carbon (GC), carbon past including graphite pencil, and which makes their utilization even more appealing is the fact their surfaces can be modified for versality[19] with several chemical modifiers like polymers which conduct, nanoparticles of metals as well as the nanotube form of carbon. In this manner, the working electrode can be made selective at a low cost and with materials readily obtainable. For successful fabrication of a modified electrode, its performance needs to be optimal and enhanced catalytic activity towards the analyte when executing the suitable electrochemical method that is functional at trace levels[20] of the compound detected. The chemical environment i.e., supporting electrolytes plays an important role in optimizing testing conditions and needs to be carefully reckoned with. The flow of inert gas[21] in an electrochemical cell removes oxygen from the matrix since it can affect redox molecules of interest which are moisture sensitive and hence the

transfer of electrons. Reproducibility and specificity[22] of electrochemical detection can be obtained at certain supporting electrolyte pH levels, modification of electrode, and through the nature of the resulting modifier film on the GC electrode surface. Analytes that can be detected by electroanalytical techniques in phosphate-buffered saline (PBS) are paracetamol, acyclovir, ascorbic acid, and dopamine. Attempting to grasp the significance of biomolecules like proteins[23] such as human serum albumin (HSA) on the electrochemical detection of compounds can be considered through drop coating or adsorption fabrication modification methods of the GC electrodes. Furthermore, can composite material containing HSA be introduced as a modifier to bare GC electrode surfaces to improve binding[24] of an analyte to the electrode's surface and better stability of electrochemical detection. Modification of GC electrode surfaces with HSA or a 1-butyl-3-methylimidazolium hexafluorophosphate/HSA composite can lead to the sensing of 8-anilino-naphthalene sulfonic acid or retinol respectively.

5.3 Experimental

Reagents and materials

Distilled water was cleaned by a Milli-Q system from Merck. Zinc nitrate; $Zn(NO_3)_2$ (Merck, 98%), nanoclay surface modified, (Nanomer 1.44P, Aldrich), sodium chloride, potassium chloride, disodium hydrogen phosphate, dipotassium hydrogen phosphate, sodium hydroxide (Merck, 99%), human serum albumin (Thermo Fisher Scientific, 96%), Nevirapine anhydrous reference standard (USP, 100mg), ascorbic acid, citric acid, d-glucose, Efavirenz, Zidovudine, fresh urine sample, Nevirapine pharmaceutical tablet (local clinic, 200mg), pestle, mortar as well as microSPE 0.45µm.

5.4 Methodology

5.4.1 Electrode preparation

Preparing the glassy carbon electrodes (GCE) for electrochemical characterization involved cleaning by polishing the measuring surface with 1, 0.3, and 0.05 µm alumina slurries on separate occasions to achieve a shiny appearance followed by thorough rising with water and ultrasonication at room temperature for approximately 15 minutes. The synthesized nanoclay ZnO products were centrifuged and washed with water one time to collect the nanoparticles quantitively; about 2 drops of this resulting

solution were drop-coated on the GCE surface to prepare a reactive film and left to dry overnight. Forming the 0.5g 1.44P ZnO human serum albumin (HSA) composite included drop coating the protein but in the case of adsorption, immersing the 0.5g 1.44P ZnO modified electrode took place. Electrochemical measurements were performed with Autolab PGSTAT 101 supplied from Metrohm South Africa in the presence of PBS supporting electrolyte, the counter electrode, and reference electrode were platinum wire and Ag/AgCl in 3M KCl respectively. Various scan rates were applied to the cell.

5.4.2 Electrochemical behavior of NVP

A 525,7μM stock solution of Nevirapine (NVP) was prepared in 100ml by dissolving the pure drug in just enough in methanol and then making it up to the volume with distilled water. Working standards involved diluting specific volumes with the supporting electrolyte. The concentration of 36,68μM analyte was used as a sample to measure the electrochemical response of the 0,5g 1.44P ZnO HSA modified glass carbon electrode with cyclic voltammetry (CV) and differential pulse voltammetry (DPV).

5.4.3 Effect of HSA concentration and adsorption time on the electrooxidation of NVP

Human serum albumin (HSA) stock solution of 3.09μM was made in 25ml distilled water. Different working solutions were then used with electrolyte as a chemical environment to consider the influence of protein concentration including adsorption time on 16.55μM and 29.76μM Nevirapine respectively. Both drop-coating and adsorption fabrication was thus examined.

5.4.4 Choice of supporting electrolyte

Phosphate buffered saline (PBS) was chosen as the supporting electrolyte and the choice was between concentrations of 0.05M, 0.1M, and 1M which was prepared by diluting sodium chloride, potassium chloride, disodium hydrogen phosphate, dipotassium hydrogen phosphate with distilled water in different ratios to achieve respectively, 0.5x, 1x and 10x ionic strength of the buffer system. The signal response of a 22.64μM solution of the analyte was considered.

5.4.5 Effect of starting potential and modulation amplitude

The initial cyclic voltammetry settings to identify the electrochemical response of NVP were over a range of -0.1 to 1V at a scan rate of 20mV/s thus the same was in the case of differential pulse voltammetry. However, optimization in the DPV mode of the signal involved changing gradually the starting potential and modulation amplitude to investigate how the analytical peak is affected with a concentration of 3.91µM NVP.

5.4.6 Effect of scan rate on the electrooxidation of Nevirapine

Cyclic voltammetry of the 0,5g 1.44P ZnO HSA modified GCE in the presence of 36.68µM Nevirapine was used to measure the impact of scan rate on the analyte's oxidation. A wide range of scan rates was applied to inspect the proportionality of current density to concentration.

5.4.7 Calibration studies

Under optimized conditions, the electrochemical response of the 0,5g 1.44P ZnO HSA modified glassy carbon electrode for various concentrations of the analyte, Nevirapine, was considered using cyclic voltammetry and differential pulse voltammetry.

5.4.8 Repeatability and stability

The reproducibility of the 0,5g 1.44P ZnO HSA biosensor for NVP was evaluated by executing the same fabricating procedure at least six times to measure 17.78µM Nevirapine utilizing differential pulse voltammetry. Precision was confirmed by testing the same concentration of the analyte four times and noting the closeness of analyte peak currents. The repeatability of the method using the 0,5g 1.44P ZnO HSA modified GC electrode was confirmed in the analyte's presence with three measurements while the stability of the modified electrode was determined by fabricating and storage to see consistency in NVP oxidation current after five days.

5.4.9 Interferences studies

The effects of interfering food additives (supplements) on the biosensing ability of the 0,5g 1.44P ZnO HSA composite modified electrode were considered in the presence of approximately 6.94Mm NVP at a scan rate of 20mV/s and in 0.1M PBS. The direct

consequence of ascorbic acid (AA), citric acid (CA), d-glucose (DG), and sodium chloride (NaCl), at approximately 905.6μM levels, on the current response of the analyte was monitored. Ratios of Nevirapine to supplement, of (a) 1 to 1, (b) 1 to 5, and (c) 5 to 1 were prepared, and determining means of differential pulse voltammetry, the impact on potential and current density in each case were examined. Also, examined were drug-to-drug interactions of NVP with other drugs when using the biosensor were looked at by verifying any disturbance of 12.82μM Nevirapine by other HIV treatment drugs such as Efavirenz (EFV) and Zidovudine (ZDV) at concentrations of 1267μM and 3740μM respectively.

5.4.10 Application to spiked urine and drug tablet analysis

The optimized method was used to measure NVP concentrations in a spiked urine specimen in which known amounts of the drug were added to fresh urine. 5ml fresh urine was filtered once with a pore size 0.45μm syringe filter and 10μl was used followed by dilution with supporting electrolyte. The drug-free urine was spiked with 3.91, 7.77, 11.57, and 15.31μM respectively of Nevirapine while the actual amounts of the drug added to the urine were then concluded from the calibration curve. The appropriateness of the proposed method was again considered by using the modified electrode and suggested experimental parameters to determine the Nevirapine concentrations in a therapeutic drug tablet. One Nevirapine tablet was taken, finely grounded, and dissolved in a methanol/water mixture. This was followed by diluting the solution with Milli-Q pure water up to 1000ml and analyzed in a supporting electrolyte environment. The quantity of NVP in the tablet was calculated using the calibration curve which provided the equation of the linear relationship.

5.5 Results and discussion

5.5.1 Electrochemical behavior of NVP

To look at the specific electrochemical response of the analyte of interest, Nevirapine (NVP), on the modified glassy carbon electrode (GCE) surface, cyclic voltammetry (CV) and differential pulse voltammetry (DPV), were applied bearing in mind the goal of determining optimum conditions at 20mV/s. The proposed platform, 0,5g 1.44P ZnO HSA, had to be inspected for efficiency. CV was performed in the potential range of -0.1 to 1V while DPV was done over 0.4 to 0.9V in the presence of 0.1M phosphate-

buffered saline (PBS) vs Ag/AgCl. A concentration of 36,68µM NVP produced the voltammograms featured in figure 5.1.

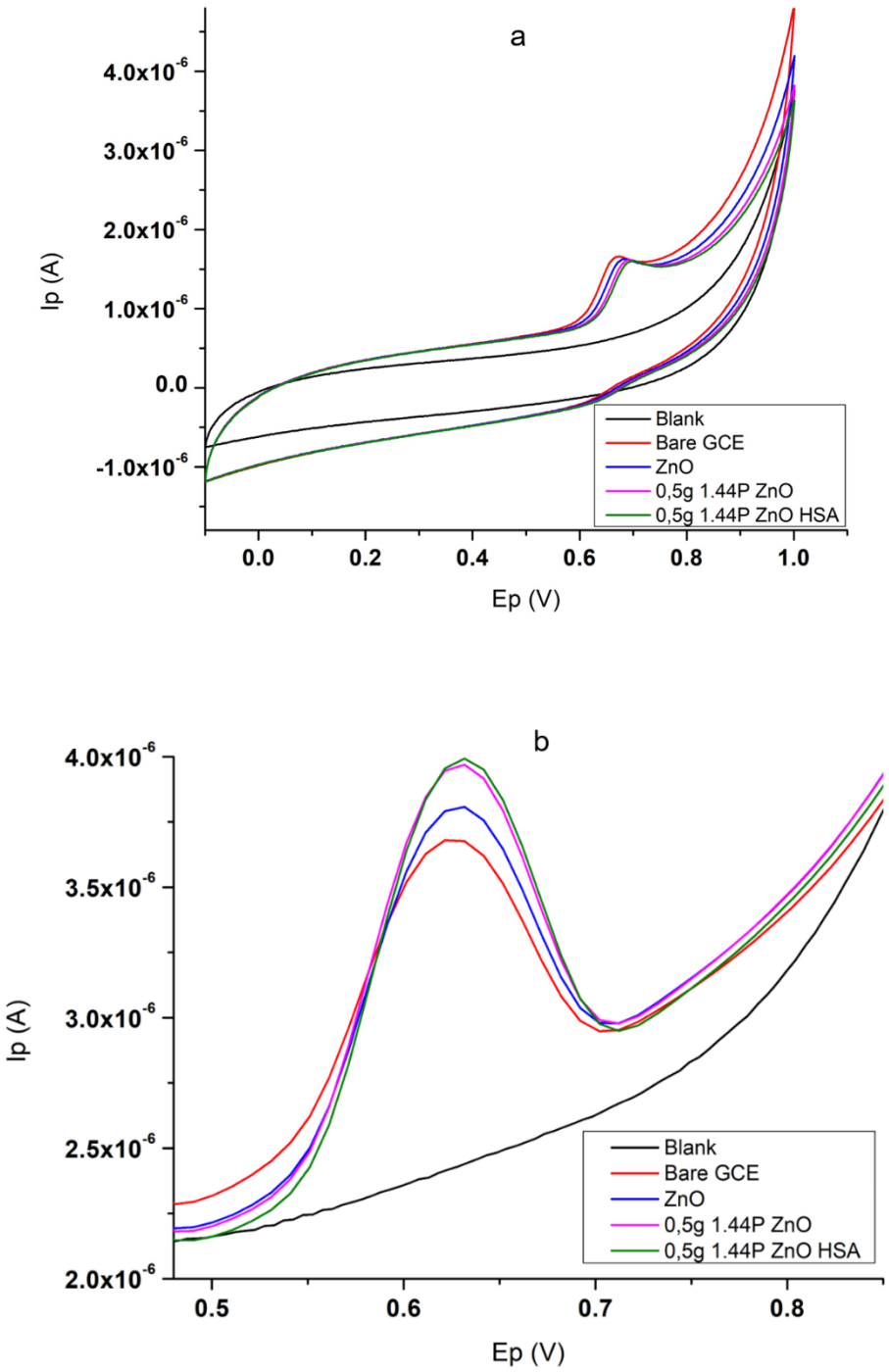

Figure 5.1: The electrochemical responses of different platforms given by a) cyclic voltammogram and b) differential pulse voltammogram in 36.68µM Nevirapine

As per the electrochemical behavior representing the analyte, CV indicated a single oxidation peak at 0.6641V with the bare GCE but as modification of the platform developed, 0,5g 1.44P ZnO HSA showed a significant shift in potential until approximately 0.6885V. Previous reports as well confirmed similar noticeable behavior with the bare GCE at 0.6700[25] and even lower to 0.5672V[26] and 0.6800V.[27] Such behavior is triggered by the immediate chemical environment i.e., electrolyte conditions in which the analyte is, and using the bare GCE only isn't novel and compromises selectivity ultimately. The shift in potential due to the 0,5g 1.44P ZnO HSA platform pointed towards the fact that this modifier increases the electrode's surface area and thus better sensitivity. DPV indicated much promise in terms of current density moving from bare GCE to 0,5g 1.44P ZnO HSA; at approximately 0.6316V; a gradual increase was observed due to oxidation of the analyte which is strongly linked to protonation of NVP[27] by the electrolyte together with synergistic action of the 0,5g 1.44P ZnO composite and HSA molecule modification film is available to absorb substantially NVP at the electrode's interface to enhance detection ability due to the analyte's negative charge.[25]

5.5.2 Effect of HSA concentration on the electrooxidation of NVP

To monitor enough i.e., the concentration of HSA required to fabricate the biosensor for Nevirapine, 5 to 35µL (0.007708 to 0.05316µM) quantities of a 3.091µM stock solution of the protein were drop coated onto the 0,5g 1.44P ZnO composite and exposed to 16.55µM NVP at 20mV/s. DPV was used to measure the electrochemical features and captured in figure 5.2.

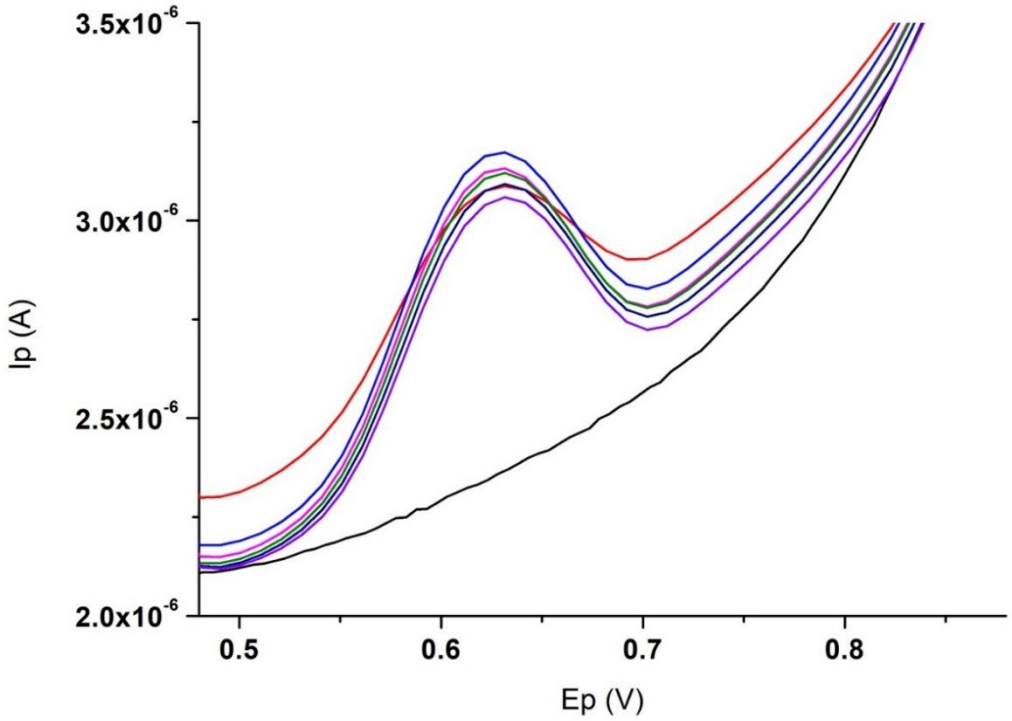

Figure 5.2: The differential pulse voltammogram response of 0,5g 1.44P ZnO HSA modified GCE in 16.55µM Nevirapine at different HSA concentrations

Based on current densities representing oxidation of the analyte, Nevirapine, in the absence of any HSA, provides a signal, and as the concentration of the protein increases until 15µL which is approximately 0.02301µM but just as more is added, no more significant increase in current is observed until a constant of current persists at about 35µL (0.05316µM). The interaction between NVP and human serum albumin could be said to be one where an electrochemically inactive complex forms that block electron transfer between the analyte and the glassy carbon electrode surface, the protein is adsorbed competitively at the GCE surface and any slight shift in potential is due to electrostatic attraction or intercalation.[28] Increases in concentration can lead to barring effects since HSA begins to act as an insulator but at lower concentrations, it is optimum.[29] The binding between Nevirapine and human serum albumin is deemed to be very specific with no appearance of new oxidation peaks[30], the electrochemical impedance due to increased levels of HSA in such an electrode modifying film would be high[31] due to the bulkiness of the protein molecules hindering electron transfer but improves selectivity towards Nevirapine regardless. It can additionally also be said that

the strong protein-0,5g 1.44P ZnO surface interaction produces surface states with different energies[32] because of NVP detection bearing in mind that the predominant form of the ε-amino groups in the protein is available in its protonated state[33] to promote charge transfer if between 15 and 20μL is used.

5.5.3 The effect of HSA adsorption time on Nevirapine detection

After establishing that approximately 20μL of a 3.091μM HSA solution can be drop coated onto the 0,5g 1.44P ZnO composite to fabricate the biosensor for sufficient NVP analysis, the next step was to look at the influence of adsorption time if it was to be considered as an option as well in developing fabrication protocol for the biosensor. This procedure involved adding the same amount of the protein solution to the electrolyte and immersion of the 0,5g 1.44P ZnO modified electrode to facilitate adsorption of HSA molecules onto the modified GCE surface. Figure 5.3 are the findings of analyte detection as a function of protein-GCE interaction time to detect a solution containing 29.76μM Nevirapine using DPV at 20mV/s.

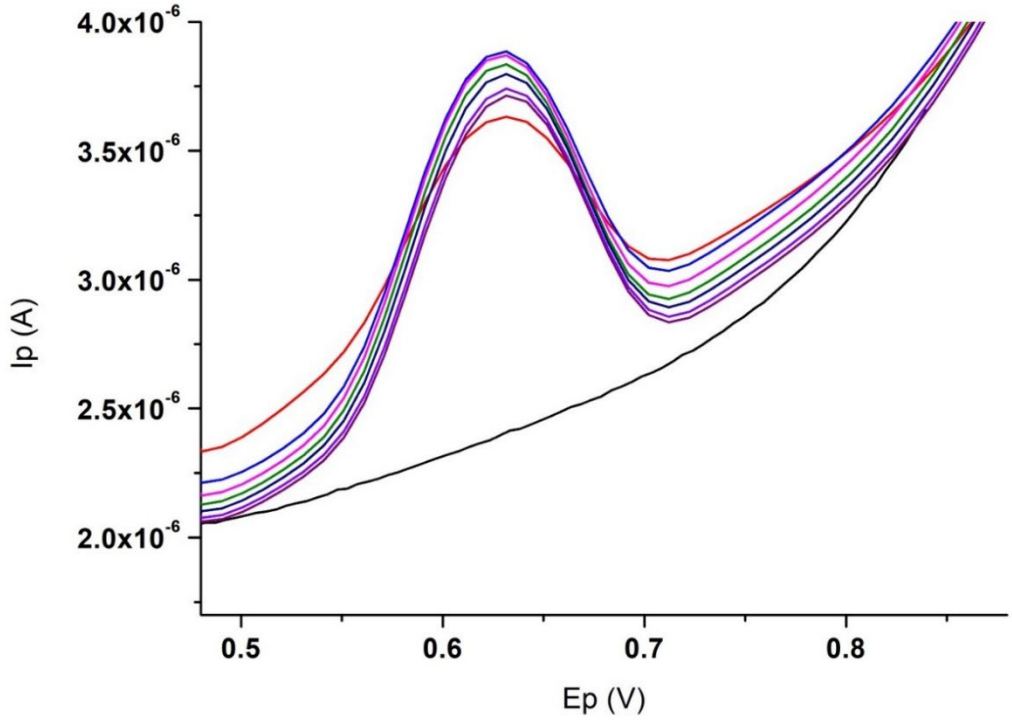

Figure 5.3: The differential pulse voltammogram response of 0,5g 1.44P ZnO HSA modified GCE in 29.76μM Nevirapine at different time intervals

It was discovered that upon exposure of HSA to the modified GCE electrode surface, current density representing NVP oxidation increases up to the 10 minutes mark but then slowly reduces as time proceeds to 30 minutes but is still consistently higher than measured at time 0 minutes which is almost immediately after immersion of the modified electrode without allowing for any real adsorption. This is promising since it has been previously known that when a modified GCE is exposed to an HSA solution the consequence was a reduction in peak current over a certain period and related to a continuous layer of the protein that forms on the GCE and hinders electron transfer between protonated species of the analyte and electrode surface.[23] In addition to this, it can also be concluded that Nevirapine's oxidation at a slightly lower current attributes to human serum albumin since the protein now acts as a mediator to facilitate electron transfer for the analyte and the 0,5g 1.44P ZnO composite offers a large surface area to stabilize HSA molecules so that the analytical signal can be discriminated at the end of the interaction of the protein and Neviparine.[34] The interaction of HSA and the analyte NVP can be said to be hydrophobic and electrostatic due to weak interactions like van der Waals and hydrogen bonding to form an analyte-protein complex because no major shift in peak potential occurs or new peaks were seen.[36] The effect of HSA adsorption time serves as justification that there is strong adsorption of the modified GCE surface and the analyte, noticed by the current signal and is a function of NVP concentration.[36]

5.5.4 Choice of supporting electrolyte

Phosphate buffered saline (PBS) is the best candidate for the specific detection of NVP at the modified electrode surface due to its composition which is adequate for biological species studies since it is isotonic, phosphoric acid has three dissociation constants[37] thus permitting adjustment to pH levels of 2, 7 and 12. PBS won't interfere with the structural and physiological integrity of NVP and can be supplemented with additives like bovine serum albumin.[38] Figure 5.4 are the voltammograms which resulted when examining options of different concentrations of PBS namely 0.5x(approximately 0.05M), 1x (approximately 0,1M) and 10x (1M).

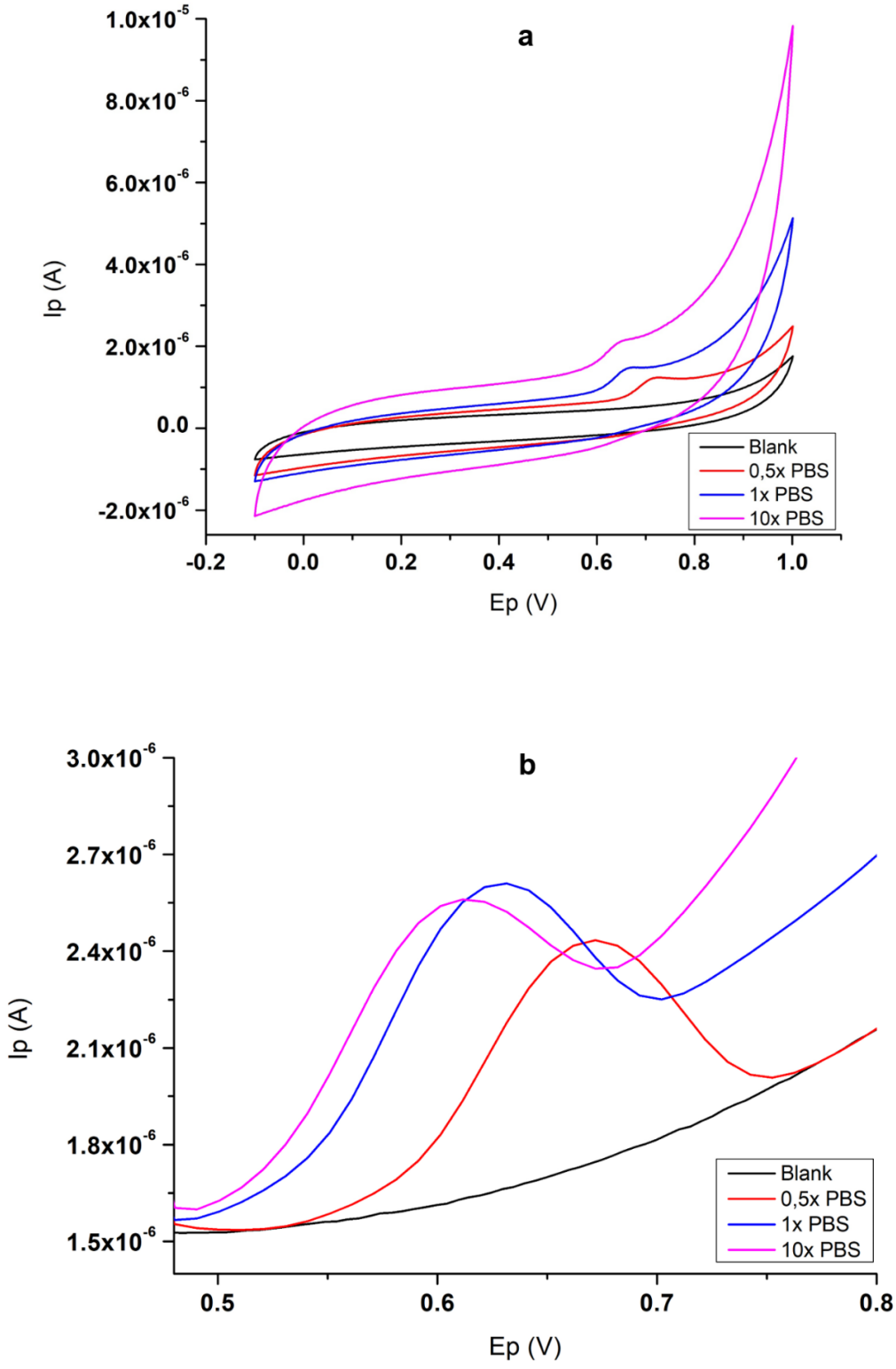

Figure 5.4: The response of 0,5g 1.44P ZnO HSA modified GCE in 22.64µM Nevirapine; a) cyclic voltammogram and b) differential pulse voltammogram in 0.5x, 1x and 10x PBS

The electrooxidation of NVP was considered in various chemical media and is depicted in figure 5.4. CV shows the shift in potential due to different concentrations i.e., ionic strengths of PBS, and resulted in 0.7080V (0.5x), 0.6787V (1x), and 0.6397V (10x); furthermore, can it also be added that a trend of increasing current is observed as concentration is increased. DPV revealed a pattern of 0.6718, 0.6316, and 0.6114V which again is promising since such shifts bring about lower overpotential. It is however 1x that provides satisfactory peak symmetry (shape) and thus its composition affects the electrooxidation of the analyte; 0.5x has the correct electrolyte composition but creates low current density as seen while the 10x does not have the adequate balance of salts for protonation ideal for NVP.

5.5.5 Effect of starting potential and modulation amplitude

Changing settings of starting potential and modulation amplitude allows for improvement of peak resolution and sensitivity of the measurement in DPV mode. 3.91μM NVP at 20mV/s was considered, and its peak current maximum was focused on as starting potential and modulation amplitude were varied. The summary of the findings is in figure 5.5. Since cyclic voltammetry happed between -0.1 and 1V, the initial range for DPV was -0.1 to 0.9V to start with. Analysis time and the electrode surface consistency nature are thus important factors also since electrochemical kinetics will suggest optimal conditions while modulation amplitude controls the pulse that is responsible for determining the final oxidation current measurement. After careful consideration, starting potential of 0.4V and modulation amplitude of 0.045V gave pleasing peak current density as well as resolution without encountering any disturbing instrument noise.

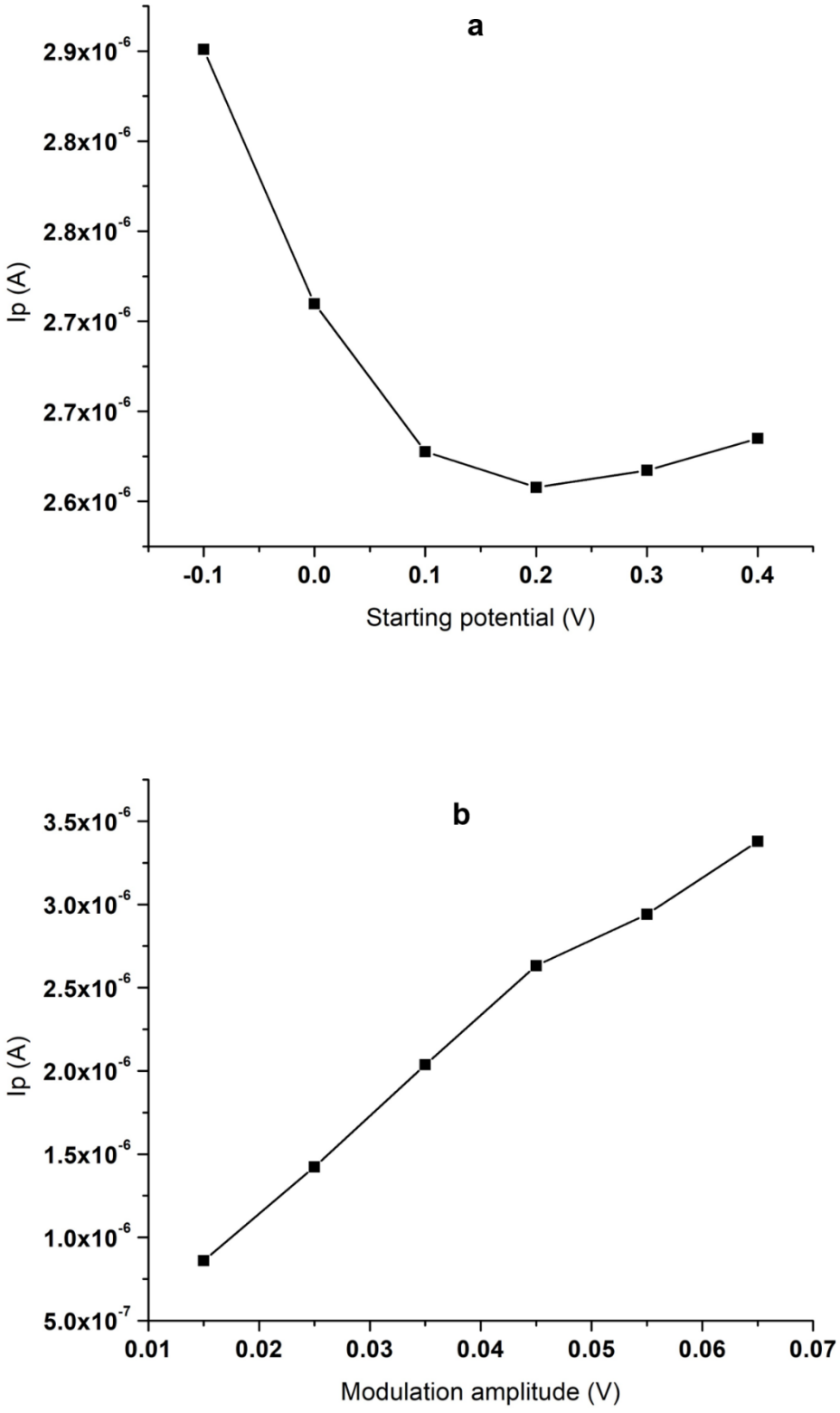

Figure 5.5: The effect of optimizing parameters, a) starting potential and b) modulation amplitude on 0,5g 1.44P ZnO HSA modified GCE response in 3.91µM Nevirapine

5.5.6 Effect of scan rate on the electrooxidation of Nevirapine

Cyclic voltammetry of the 0,5g 1.44P ZnO HSA modified GCE in the presence of 36.68µM Nevirapine (figure 5.6) was used to study the impact of scan rate on the analyte's oxidation. Scan rates between 10 and 130mV/s indicated proportionality between oxidation current and scan rate but showed as well optimal scan rates representing NVP detection.

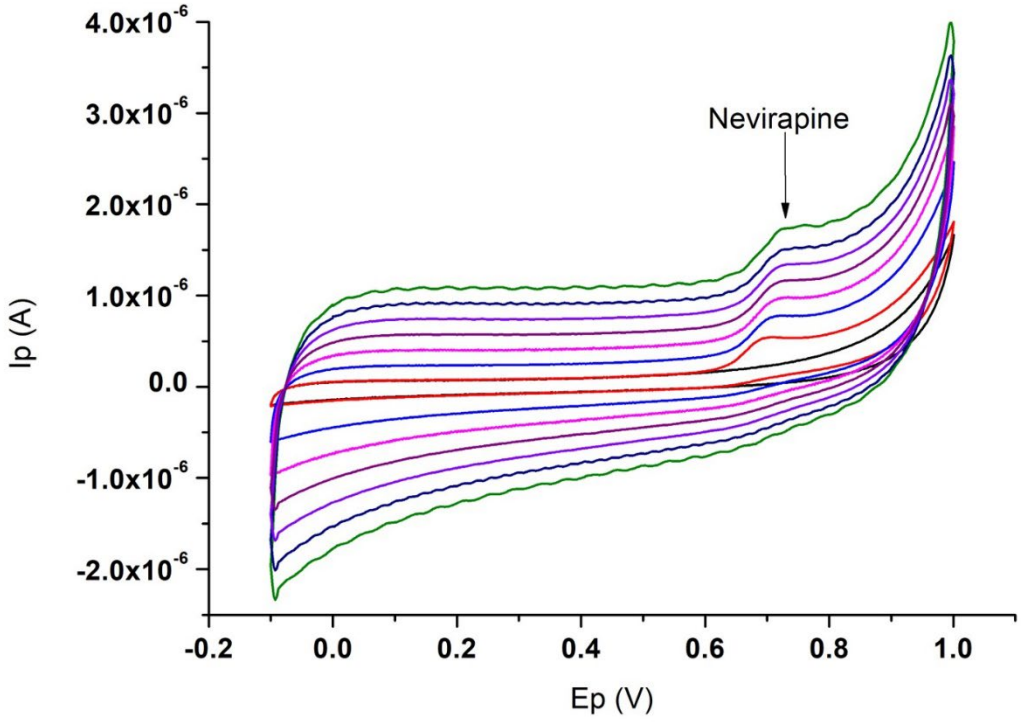

Figure 5.6: The cyclic voltammogram overlay of 0,5g 1.44P ZnO HSA modified GCE in the presence of 36.68µM NVP at different scan rates

Figure 5.7 are the plots for Ipa against v and Ipa against √v, respectively, are based on Randle-Sevick theory[39] and were used to understand the nature of the process at the modified electrode surface due to the analyte and indicated that it is diffusion-controlled because of R^2 being 0.999 for Ipa against v and 0.997 for Ipa against square root v. The diffusion coefficient was determined to 3.738×10^{-9} cm^2/s and hence the mass transport involved, 9.141×10^{-6} which are influenced by electrode modification as well as scan rate.

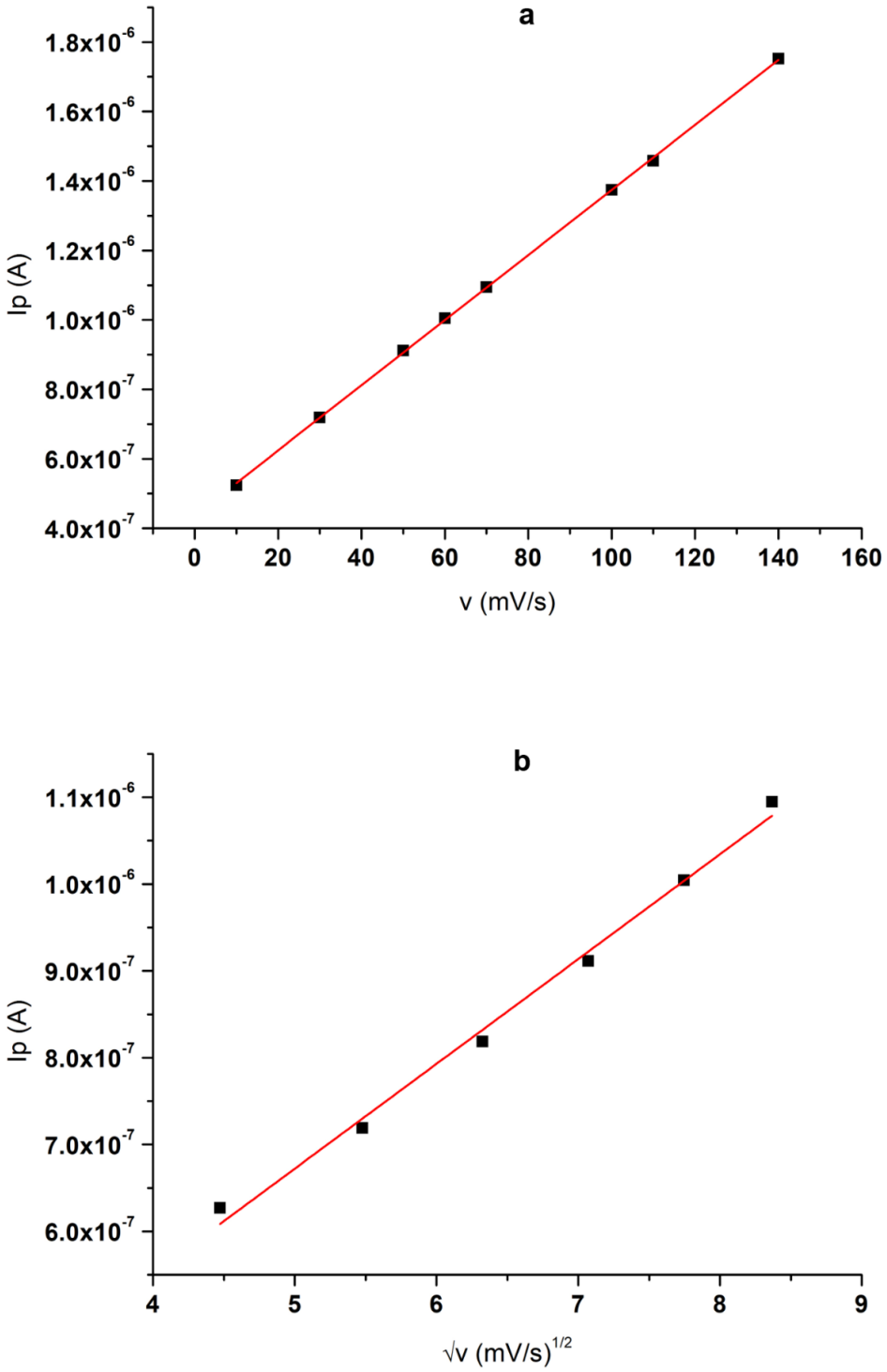

Figure 5.7: Plot of Ipa vs a) v as well as b) √v of 0,5g 1.44P ZnO HSA modified GCE in 36.68µM Nevirapine

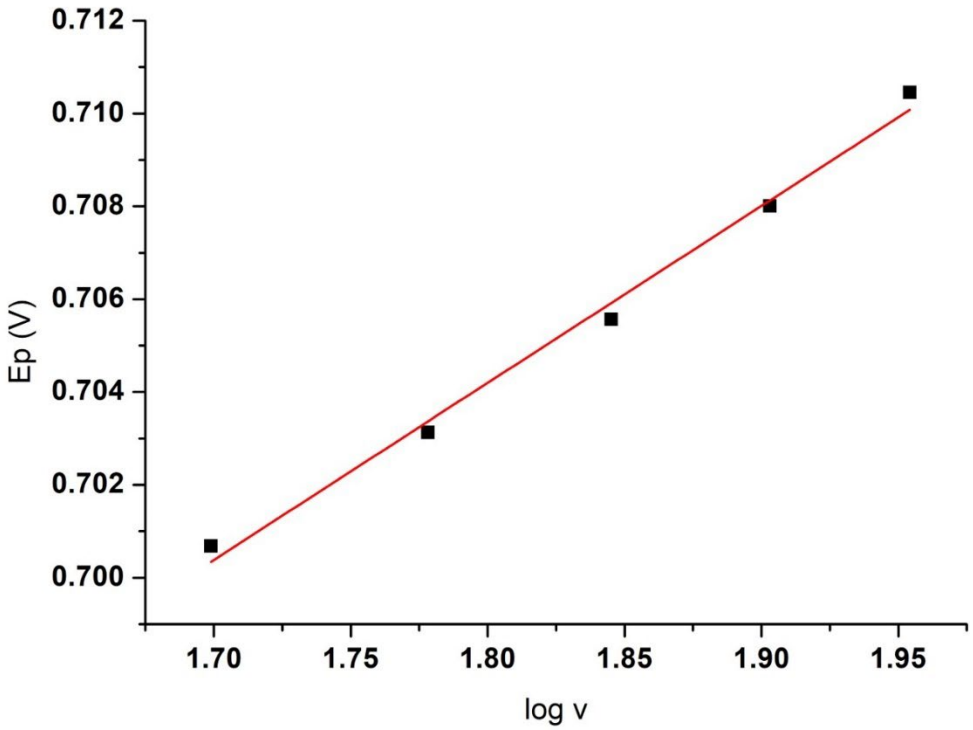

Figure 5.8: Variation of Ep vs logarithm of v plot for 0,5g 1.44P ZnO HSA modified GCE in 36.68µM Nevirapine

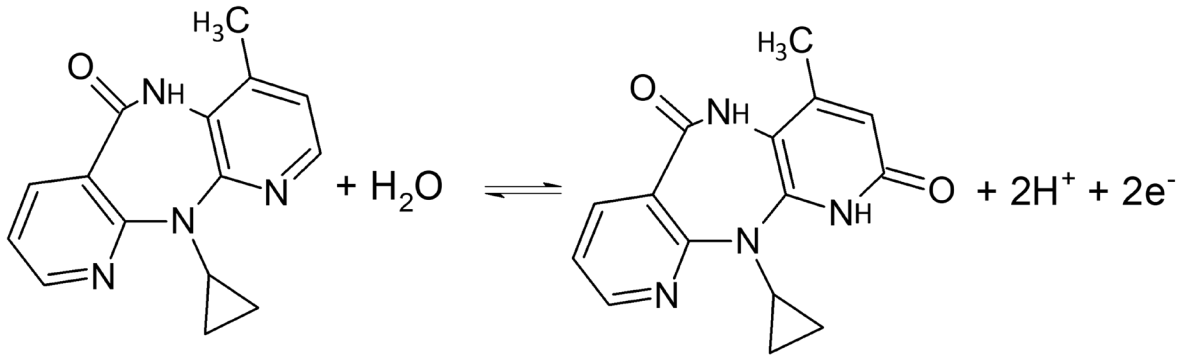

Figure 5.9: The confirmed electrochemical mechanism for NVP

The oxidation of Nevirapine is therefore irreversible and was the plot of Epa against log v, figure 5.8, derived from Laviron theory[40] used to determine the electron transfer coefficient, α, to 0.7748; the number of electrons responsible for analyte oxidation[41], n, is 2 and explained by the mechanism in figure 5.9. The relationship between potential and logarithm of scan rate further exhibits linearity as well (R^2 = 0.9963) and supports the fact that no reduction of Nevirapine could have taken place but where

adsorption of NVP has been reported was due to π–π stacking, hydrogen bonding, and covalent interactions which were related to functional groups in the electrode modifier material.[42] Table 5.1 summarises all the crucial electrochemical kinetics parameters.

Table 5.1: The electrochemical parameters of 0,5g 1.44P ZnO HSA modified GCE response in 36.68μM Nevirapine

Electrochemical kinetics parameter	0,5g 1.44P ZnO HSA
Slope fig. 5.9b x10^{-7} (Slope fig. 5.10)	1.21 (0.038)
R^2 fig. 5.9b (R^2 fig. 5.10)	0.997 (0.996)
n, number of electrons	2
D (cm^2/s), diffusion coefficient x10^{-9}	3.74
m_{trans} (s^{-1}), mass transfer x10^{-6}	9.14
α, electron transfer coefficient	0.77

5.5.7 Calibration studies

Under optimized conditions, the electrochemical response of the 0,5g 1.44P ZnO HSA modified glassy carbo electrode for various concentrations of the analyte, Nevirapine, was considered through CV and DPV at 20mV/s. The results are featured in figure 5.10 showing the oxidation peak currents increasing noticeably with the increase of NVP concentration. Linearity of the two methods is comparable as per figure 5.11, between oxidative peak current and analyte concentration and differential pulse voltammetry achieved in the range of 2.62 to 38.94μM with an equation of this relationship described as $y = 3.9961x10^{-8}x + 2.57087x10^{-6}$ ($R^2 = 0.996$).

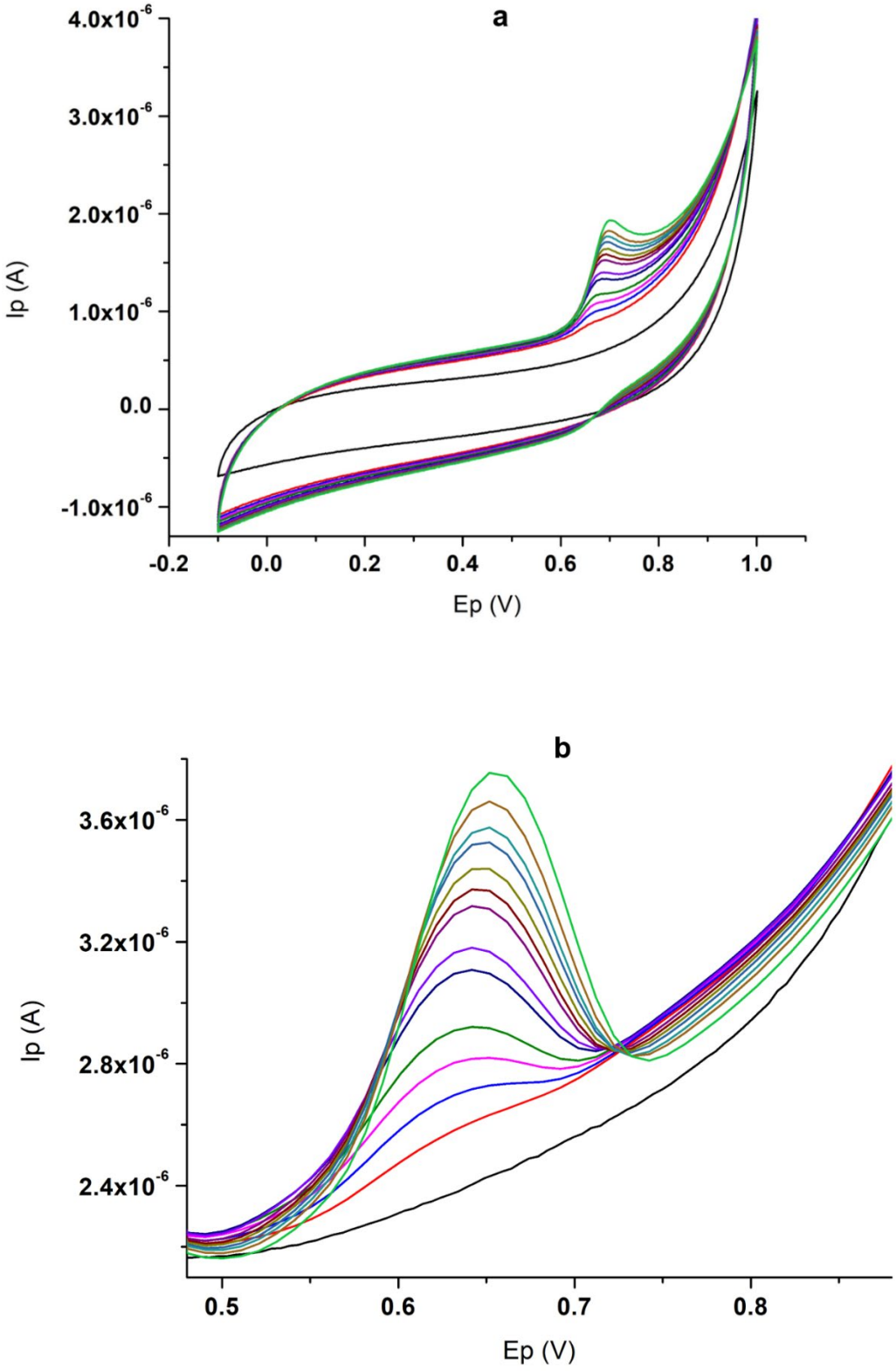

Figure 5.10: The response of 0,5g 1.44P ZnO HSA modified GCE in increasing concentration of Nevirapine; a) cyclic voltammogram and b) differential pulse voltammogram

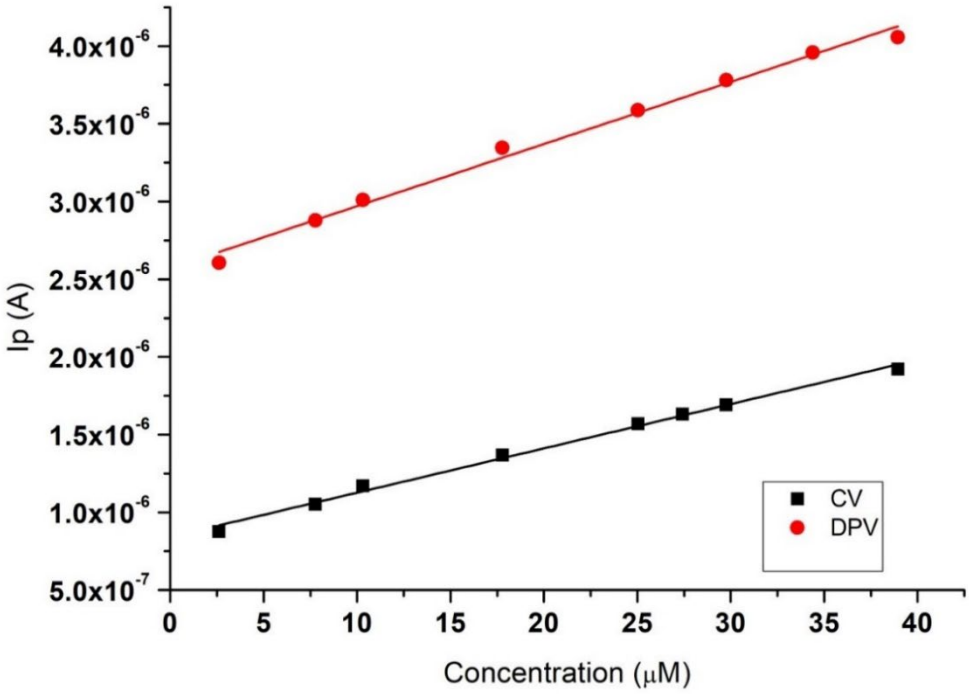

Figure 5.11: The linear regression of CV (cyclic voltammetry) and DPV (differential voltammetry) responses from the 0,5g 1.44P ZnO HSA modified GCE

$$LOD = 3\left(\frac{S}{m}\right) \quad 5.1$$

$$LOQ = 10\left(\frac{S}{m}\right) \quad 5.2$$

Table 5.2: The characteristic parameters of the differential pulse voltammetry calibration plot

Parameter	Value
Linear range (μM)	2 - 38
Equation of straight line	$y = 3.9961x10^{-8}x + 2.57087x10^{-6}$
R^2, the regression coefficient	0.996
LOD (μM), the limit of detection	0.39
LOQ (μM), limit of quantification	1.30

Table 5.3: The comparison between reported electrochemical methods and the proposed for Nevirapine

Electrode	Method	LOD (μM)	Linear range (μM)	Reference
Ura/CPE	DPV	0.050	0.10 - 70.0	43
GCE	DPV	1.026	5.0 - 350	44
Au/CB	DPV	-	1.1 - 6	45
CuO/CNP/GCE	LSV	0.06600	0.1 - 100	46
0.5g 144P ZnO HSA	DPV	0.39	2 - 38	This research

Validation of these optimized settings to quantify Nevirapine was further examined by evaluating LOD (limit of detection) and LOQ (limit of quantification) and calculated by equation 5.1 and equation 5.2 respectively.

In the expressions, s is the standard deviation of blank signals while m is the slope of the calibration curve. LOD was determined to be 0.3905μM and LOQ was established at 1.302μM. Table 5.2 summarises the important calibration parameters while table 5.3 highlights previously fabricated sensors for the analyte of interest.

5.5.8 Repeatability and stability

The reproducibility of the 0,5g 1.44P ZnO HSA biosensor for NVP was evaluated by executing the same fabricating procedure at least six times to measure 17.78μM Nevirapine consecutively using differential pulse voltammetry and achieved % relative standard deviation (RSD) of 1.17%. The precision of the method in the presence of the same concentration of the analyte was established by about four replicate measurements which resulted in a %RSD of 1.35% while the repeatability for three determinations gave a %RSD of 0.99%. Establishing the stability of the modified electrode involved storage for five days at room temperature before measurements to notice if the oxidation current response representing NVP was maintained; an accuracy of 98.65% was achieved.

5.5.9 Interferences

5.5.9.1 Food additives

The effects of interfering compounds on the biosensing ability of the 0,5g 1.44P ZnO HSA composite modified electrode were considered in the presence of approximately 6.94μM NVP at a scan rate of 20mV/s and in 0.1M PBS. Figure 5.12 shows the direct consequence of food additives at the concentration level of 905.6μM such as ascorbic acid (AA), citric acid (CA), d-glucose (DG), and sodium chloride (NaCl) on the current response of the analyte; these compounds are said to be point sources as food supplements that are consumed tighter with the NVP drug. Three ratios of Nevirapine to supplement, of (a) 1 to 1, (b) 1 to 5, and (c) 5 to 1 were prepared and using differential pulse voltammetry, the impact on potential and current density in each case were examined. At equal amounts of analyte and food supplement, no real shift in potential is observed and little interference to fundamental peak current, as seen in figure 5.12a except for the food supplements now sharing the chemical environment with NVP which affects the shape ultimately of the voltammogram slightly. When five times more interferent is introduced, the impact is pronounced in figure 5.12b as expected with a slight shift of potential to positive potentials due to pH levels of interferents and an indication of Nevirapine binding sufficiently to interferents but restricting analyte detection because of their abundance leading to a reduction in current density without quenching the analytical response completely. The 5 to 1 effect of analyte to interferant in figure 5.12c resulted in major bonding of NVP to interfere since there are now more free drug molecules to be quantified, the influence of interferent is small of the crucial current response is unhindered but with the reduced presence of interferent, the fundamental peak shows little more shouldering due to accommodation of interferent by Nevirapine which is oxidized noticeably.

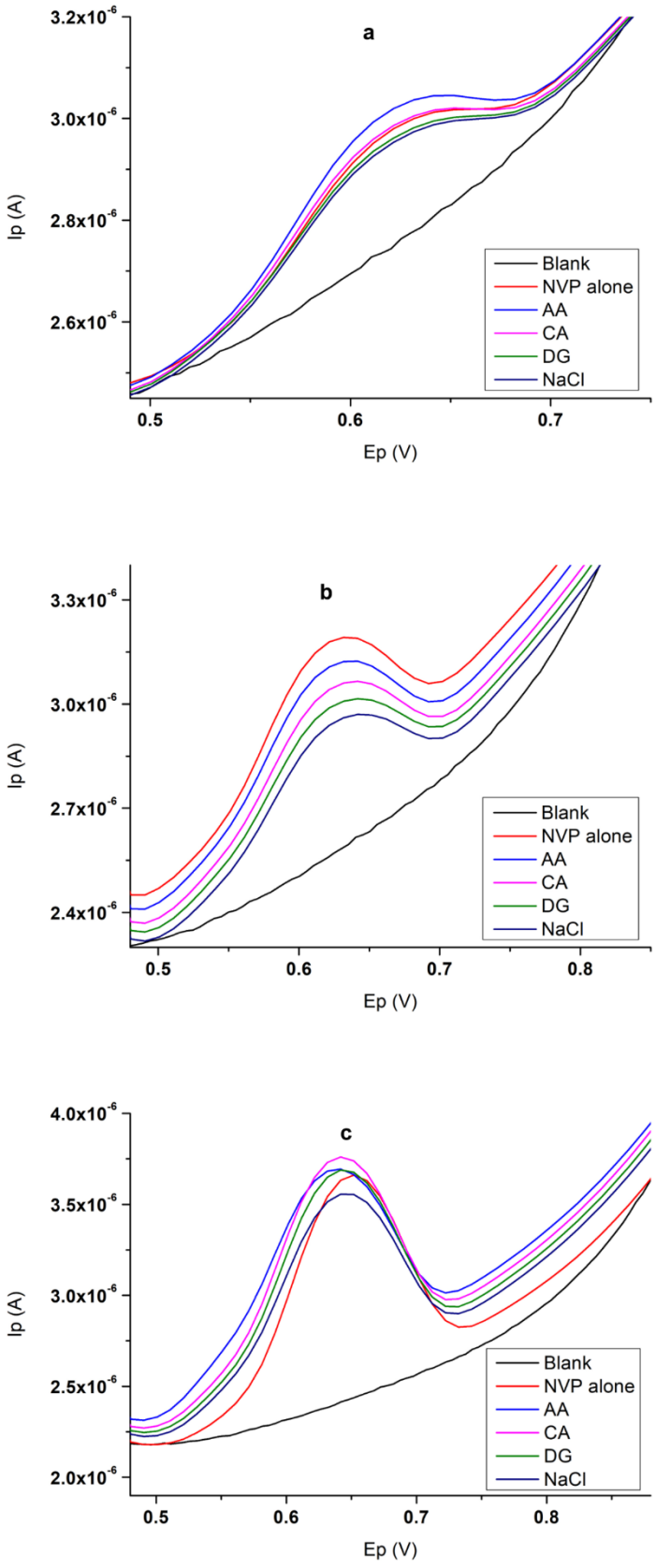

Figure 5.12: The DPV response of 0,5g 1.44P ZnO HSA modified GCE in presence of AA, CA, DG, and NaCl at 20mV/s in 0.1M PBS

5.5.9.2 Drug-to-drug

To further look at the selectivity of the 0,5g 1.44P ZnO HSA biosensor towards Nevirapine, resistance to interfering species such as even other HIV treatment drugs like Efavirenz (EFV) and Zidovudine (ZDV) at concentrations of 1267µM and 3740µM respectively against 12.82µM NVP, was examined under standard conditions with differential pulse voltammetry. Figure 5.13 is depicting the results of the drug-to-drug interaction in the case of so-called combination therapy.

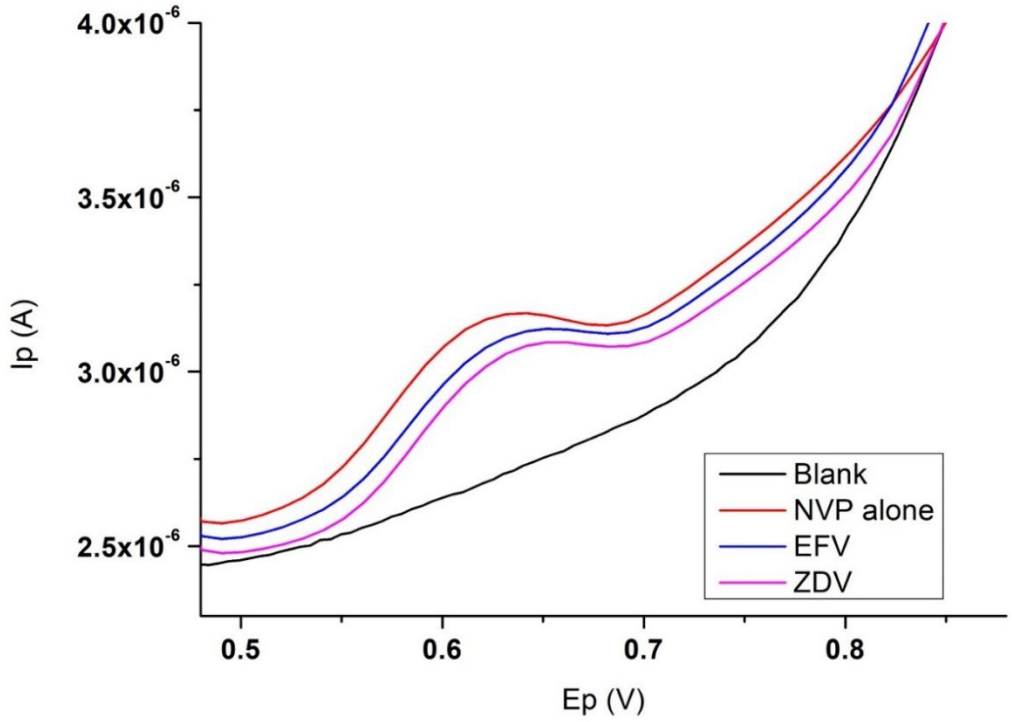

Figure 5.13: The differential pulse voltammogram of the interaction of 12.82µM NVP with other HIV drugs namely EFV and ZDV at 20mV/s in 0.1M PBS

The drugs used to monitor any impact of current response due to the analyte does not have any voltammetric signal in the experimental conditions for NVP detection and hence its potential window there the sensor is comfortably drug interference-free from EFV and ZDV. The minimal shift in potential and lowered peak current observed is attributed to Nevirapine facilitating EFV and ZDV molecules but experiencing yet enough protonation to provide quantitatively an electrochemical signal response.

5.5.10 Application

5.5.10.1 Spiked urine sample

The optimized method was used to measure known Nevirapine concentrations in a spiked urine specimen.

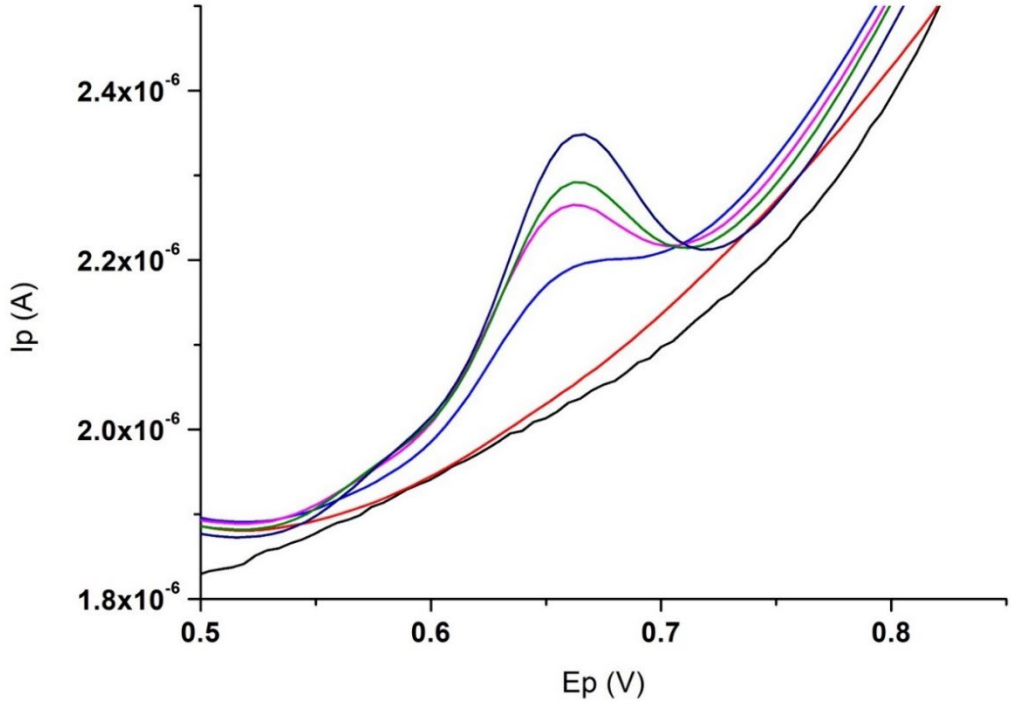

Figure 5.14: The differential pulse voltammogram of the spiking of a fresh urine sample with Nevirapine at 20mV/s in 0.1M PBS

Table 5.4: The results of Nevirapine analysis in spiked urine (n=3)

NVP added (µM)	Amount measured (µM)	Accuracy (%)	Standard deviation	RSD (%)
3.91	3.89	99.29	4.40	4.44
7.77	7.53	96.89	4.26	4.40
11.57	11.73	101.43	4.90	4.83
15.31	14.75	96.33	4.04	4.19

5.5.10.2 Nevirapine tablet

The feasibility of the proposed method was considered by using the modified electrode and experimental parameters to determine Nevirapine in a therapeutic drug tablet; the label specification is 200mg and measurements were performed five times (n = 5); figure 5.15 are the different analytical peak responses. The response current of the analyte was divided by the slope of the calibration curve followed by division with the molar mass. After the dilution was factored in, the average result is 210.93mg, standard deviation of 5.566 while the percentage RSD is 2.64% that confirming the selectivity and specificity of the electrochemical mode as well as electrode modifier to Nevirapine.

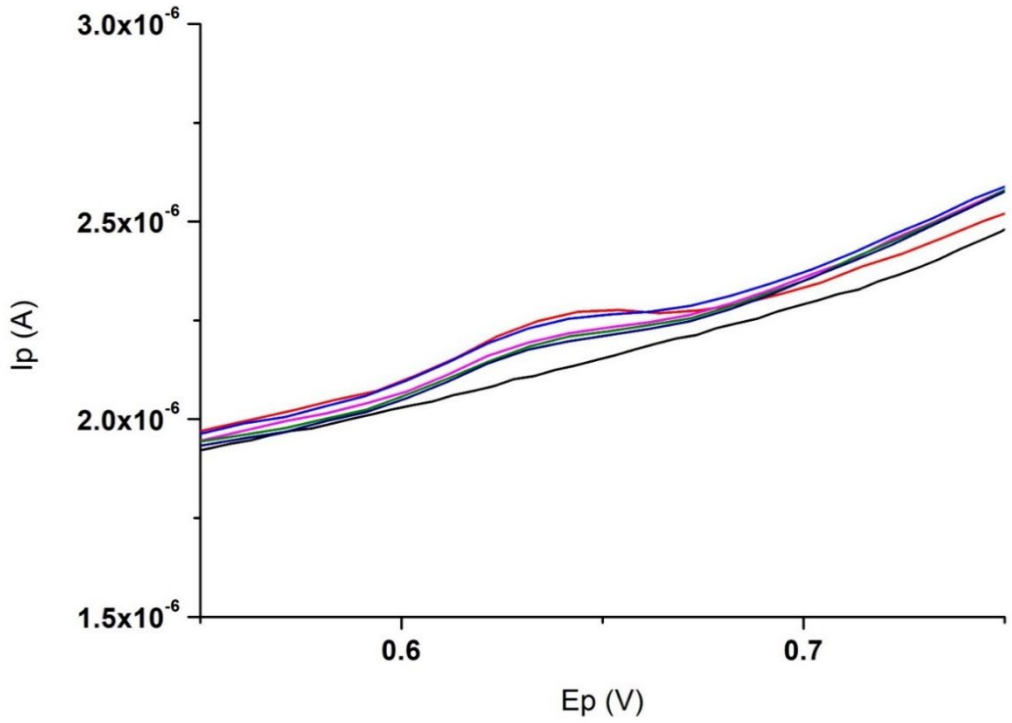

Figure 5.15: The differential pulse voltammogram of Nevirapine tablet analysis at 20mV/s in 0.1M PBS (n = 5)

5.6 Conclusion

The electrochemical response of the modified glassy carbon electrode modified with 0,5g 1.44P ZnO human serum albumin (HSA) towards Nevirapine electrooxidation has been examined and proven to exhibit electron transfer for the electrooxidation of the analyte because of its high surface area as well as realistic catalytic activity. The effect of the protein (HSA) concentration when drop coated or involved in adsorption has been monitored for the best conditions for optimal peak potential at 0.63V vs Ag/AgCl with acceptable current density to approve selectivity to NVP. The impact of supporting electrolyte 1x (0.1M) PBS showed that certain chemical environments will have a pronounced influence on Nevirapine detection that is proportional to peak potential and current including an overview revealing how starting potential and modulation amplitude can be optimized to improve analyte determination. Scan rate and calibration studies assisted to confirm that NVP electrooxidation is diffusion-controlled while differential pulse voltammetry is the most appropriate voltammetric method to test the analyte over a broad linear concentration range which was 2 to 38μM. A low limit of detection of 0.39μM and limit of quantification at 1.30μM indicates improved sensitivity and hence preferred reproducibility for the 0,5g 1.44P ZnO HSA platform towards Nevirapine and comparable to other reported sensors. Reproducibility of the modified glassy carbon electrode fabrication protocol resulted in a RSD of 1.17% while the precision was 1.35% for measurements at a single analyte concentration. Repeatability of the modified glassy carbon electrode for consecutive measurements was RSD of 0.99% whereas the percentage of accuracy to evaluate stability was 98.65%. The 0,5g 1.44P ZnO HSA biosensor was furthermore used in samples of spiked urine and pharmaceutical tablet leading to RSD values of 4.47% and 2.64% respectively for determinations of the analyte.

5.7 References

1. David J. Weiss. The Care and Feeding of Electrodes. Experiments in Analytical Electrochemistry. The University of Colorado, Colorado Springs
2. László Kiss, Sándor Kunsági-Máté. Effect of Anodic Pretreatment on the Performance of Glassy Carbon Electrode in Acetonitrile and Electrooxidation of Para-substituted Phenols in Acetonitrile on Platinum and Glassy Carbon Electrode. Periodica Polytechnica Chemical Engineering, 28 November 2019

3. Adrian W. Bott. Practical Problems in Voltammetry: Preparation of Working Electrodes. Bioanalytical Systems, Inc. West Lafayette, IN. 2000
4. Instruction manual for Basi Epsilon for electrochemistry. Version 2.10.73, 2000-2009 Bioanalytical Systems
5. Kinoshita, K. Carbon, Electrochemical and Physicochemical Properties; John Wiley and Sons: New York, 1988.
6. Kokko, K.; Ojala, E.; Mansikka, K. Phys. Status Solidi B 1989, 153,
7. Dresselhaus, M. S. Graphite Fibers and Filaments; Springer-Verlag: New York, 1988.
8. Mattson, J. S.; Smith, C. A. Anal. Chem. 1975, 47, 1122-1125.
9. Anjo, D. M.; Brown, S.; Wang, L. Anal. Chem. 1993, 65, 317–319.
10. Donner, S.; Li, H. W.; Yeung, E. S.; Porter, M. D. Anal. Chem. 2006, 78, 2816–2822.
11. Kinoshita, K. Carbon, Electrochemical and Physicochemical Properties; John Wiley and Sons: New York, 1988.
12. McCreery, R. L. In Electroanalytical Chemistry; Bard, A. J., Ed.; Dekker, New York, 1991; Vol 17.
13. McDermott, C. A.; McCreery, R. L. Langmuir 1994, 10, 4307
14. Jaegfeldt, H.; Kuwana, T.; Johansson, G. J. Am. Chem. Soc. 1983, 105, 1805–1814.
15. Barbier, B.; Pinson, J.; Desarmot, G.; Sanchez, M. J. Electrochem. Soc. 1990, 137, 1757.
16. Yang, W.; Auciello, O.; Butler, J. E.; Cai, W.; Carlisle, J.; Gerbi, J, Gruen, D.; Knickerbocker, T.; Lasseter, T.; John, N.; Russell, J.; Smith, L. M.; Hamers, R. J. Nat. Mater. 2002, 1, 253-257.
17. Lasseter, T.; Clare, B.; Abbott, N.; Hamers, R. J. J. Am. Chem. Soc. 2004, 126, 10220-10221.
18. Richard L. McCreery. Advanced Carbon Electrode Materials for Molecular Electrochemistry. National Institute for Nanotechnology, University of Alberta, Edmonton, Alberta. Chem. Rev. 2008, 108, 2646-2687
19. Žaklina Z.Tasić, Marija B.Petrović, Mihajlović Ana T. Simonović, Milan B. Radovanović, Milan M.Antonijević. Review of applied surface modifications of

pencil graphite electrodes for paracetamol sensing. Results in Physics. Volume 22, March 2021, 103911

20. Nagaraj P.Shetti, Deepti S.Nayak, Shweta J.Malode, Raviraj M.Kulkarni. Nanomolar detection of acyclovir, an antiviral drug at nanoclay modified carbon paste electrode. Sensing and Biosensing research. Volume 14. June 2017, 39-46
21. Nadia Ait Ahmed, Houa Hammachè, Marielle Eyraud, Carine Chassigneux, Floence Vacandio, Philippe Knauth, Laid Makhloufi, Nour-eddine Gabouze. Voltammetric determination of ascorbic acid with zinc oxide modified glassy carbon electrode. Journal of the Iranian chemical society. Volume 16, 1957-1963 (2019)
22. K.Pandiselvi, S.Thambidurai. Chitosan-ZnO/polyaniline nanocomposite modified glassy carbon electrode for selective detection of dopamine. International Journal of biological macromolecules. Volume 67, June 2014, Pages 270-278
23. H. Helia, N. Sattarahmady, A. Jabbari, A.A. Moosavi-Movahedi, G.H. Hakimelahi, Fu-Yuan Tsai. Adsorption of human serum albumin onto glassy carbon surface-Applied to albumin-modified electrode: Mode of protein-ligand interactions. Journal of Electroanalytical Chemistry 610 (2007) 67-74
24. Deia Abd El-Hady and Hassan M Albishri. Green Ionic Liquid Albumin Glassy Carbon Biosensor (ILAGC) for On-line Binding Studies of Human Serum Albumin with Retinol. Journal of Analytical & Bioanalytical Techniques 2013, S7
25. Mohammad Bagher Gholivand, Elahe Ahmadi, Mozhdeh Haseli. A novel voltammetric sensor for nevirapine, based on modified graphite electrode by MWCNs/poly(methylene blue)/gold nanoparticle Analytical Biochemistry 527 (2017) 4-12
26. Fredrick O. Okumu, Bongiwe Silwana and Mangaka C. Matoetoe. Application of MWCNT/Ag-Pt Nanocomposite Modified GCE for the Detection of Nevirapine in Pharmaceutical Formulation and Biological Samples Electroanalysis 2020, 32, 3000-3008
27. Elahe Ahmadi, Mohamad Reza Eyvani, Vahid Riahifar, Hossein Momeneh, Changiz Karami. Amperometric determination of nevirapine by GCE modified with c-MWCNTs and synthesized 11-mercaptoundecanoyl hydrazine

carbothioamide coated silver nanoparticles. Microchemical Journal 146 (2019) 1218-122

28. Jules-Blaise Mabou Leuna, Sergeot Kungo Sop, Suzanne Makota, Evangeline Njanja, Thiery Christophe Ebelle, Anatole Guy Azebaze, Emmanuel Ngameni, Achille Nassi. Voltammetric behavior of Mammeisin (MA) at a glassy carbon electrode and its interaction with Bovine Serum Albumin (BSA). Bioelectrochemistry 119 (2018) 20-25
29. Hadi Afsharan, Mohammad Hasanzadeh, Nasrin Shadjou, Abolghasem Jouyban. Interaction of some cardiovascular drugs with bovine serum albumin at physiological conditions using glassy carbon electrode: A new approach. Materials Science and Engineering C 65 (2016) 97–108
30. Jing Zhao, Xiaofeng Zheng, Wei Xing, Junyi Huang, and Genxi Li. Electrochemical Studies of Camptothecin and Its Interaction with Human Serum Albumin. Int. J. Mol. Sci. 2007, 8, 42-50
31. Aisha M. Attar, Mark B. Richardson, Gaetano Speciale, Sudipta Majumdar, Rebekah P. Dyer, Emily C. Sanders, Reginald M. Penner, and Gregory A. Weiss. Electrochemical quantification of glycated and non-glycated human serum albumin in synthetic urine. ACS Appl Mater Interfaces. 2019 February 06; 11(5): 4757-4765
32. Fabiana Y. Oliva, Lucı´a B. Avalle, Osvaldo R. Ca´mara. Electrochemical behavior of human serum albumin/TiO_2 nanocrystalline electrodes studied as a function of pH, part 1: voltammetric response. Journal of Electroanalytical Chemistry 534 (2002) 19/29
33. Lucia B. Avalle, Osvaldo R. Ca´mara, Fabiana Y. Oliva. Electrochemical behavior of human serum albumin-TiO_2 nanocrystalline electrodes studied as a function of pH, part 2: Presence of $[Fe(CN)_6]^{3-/4-}$ redox couple in solution. Journal of Electroanalytical Chemistry 585 (2005) 281–289
34. Erhan Zor, Imren Hatay Patir, Haluk Bingol, Mustafa Ersoz. An electrochemical biosensor based on human serum albumin/ graphene oxide/3-aminopropyltriethoxysilane modified ITO electrode for the enantioselective discrimination of D- and L-tryptophan. Biosensors and Bioelectronics 42 (2013) 321-325

35. Jichun Yang, Danfeng Zhang, Lingling Wang, Na Long, Minhui Zhang & Lei Zhang. An Electrochemical Method for High Sensitive Detection of Thiabendazole and Its Interaction with Human Serum Albumin. Food Anal. Methods (2015) 8:507-514
36. Emil Palecek, Jan Tkać, Martin Bartosĭk, Tomaš Bertok, Veronika Ostatna and Jan Paleceǩ. Electrochemistry of Nonconjugated Proteins and Glycoproteins. Toward Sensors for Biomedicine and Glycomics. Chem. Rev. 2015, 115, 2045-2108
37. Universal buffers for use in biochemistry and biophysical experiments Dewey Brooke, Navid Movahed, and Brian Bothner AIMS Biophysics Volume 2, Issue 3, 336-342.
38. Jorge Alfredo Uquillas, Vipuil Kishore, and Ozan Akkus. Effects of Phosphate Buffered Saline Concentration and Incubation Time on the Mechanical and Structural Properties of Electrochemically Aligned Collagen Threads. Biomed Mater. 2011 June; 6(3): 035008
39. N. Aristov, and A. Habekost, Cyclic Voltammetry-A Versatile Electrochemical Method Investigating Electron Transfer Processes. World Journal of Chemical Education, Vol. 3, no. 5 (2015): 115-119
40. Amanda L. Eckermann, Daniel J. Feld, Justine A. Shaw, Thomas J. Meade. Electrochemistry of redox-active self-assembled monolayers. Coordination Chemistry Reviews 254 (2010) 1769-1802
41. Saeed Shahrokhian, Razieh Kohansal, Masoumeh Ghalkhani, and Mohammad K. Amini. Electrodeposition of Copper Oxide Nanoparticles on Precasted Carbon Nanoparticles Film for Electrochemical Investigation of anti-HIV Drug Nevirapine. Electroanalysis 2015, 27, 1989-1997
42. Daniel Apath, Mambo Moyo and Munyaradzi Shumba. TiO_2 Nanoparticles Decorated Graphene Nanoribbons for Voltammetric Determination of an Anti-HIV Drug Nevirapine. Hindawi Journal of Chemistry Volume 2020, Article ID 3932715
43. Fenfen Zhang, Li Li, Liqiang Luo, Yaping Ding, Xiao Liu. Electrochemical oxidation and determination of antiretroviral drug nevirapine based on uracil-modified carbon paste electrode. J Appl Electrochem (2013) 43:263-269

44. Nagappa Laxman Teradal, Shankar Narayan Prashanth, Jaldappagari Seetharamappa J. Electrochemical studies of nevirapine, an anti-HIV drug, and its assay in tablets and biological samples. J. Electrochem. Sci. Eng. 2(2) (2012) 67-75
45. Ana M. Esteva, Elias Blanco, Juan J. Pina, Abel I. Balbin, Carmen Quintana, Pedro Hernandez. Determination of nevirapine in the presence of cucurbit(7)uril with a gold electrode. J. Electrochem. Sci. Eng. 4(1) (2014) 37-44
46. Saeed Shahrokhian, Razieh Kohansal, Masoumeh Ghalkhani, and Mohammad K. Amini. Electrodeposition of Copper Oxide Nanoparticles on Precasted Carbon Nanoparticles Film for Electrochemical Investigation of anti-HIV Drug Nevirapine Electroanalysis 2015, 27, 1989-1997

CHAPTER SIX: Conclusion and recommendation

6.1 Objectives

The main objectives of the study were:

- Synthesis of ZnONPs using three different precursors and the functionalization of two nanoclays with this ZnO
- Characterization of the synthesized nanoparticles (ZnO and nanoclay ZnO composites) with spectrometry and electrochemistry
- Fabrication of the sensor for Nevirapine through glassy carbon electrode modified with the nanoparticles and human serum albumin (HSA)
- Optimization of measuring for NVP through an electrolyte, fabrication procedure, and electrochemical detection mode.
- Method validation using optimum conditions to determine analytical parameters, electrode stability, and repeatability
- Application to spiked biological sample and pharmaceutical tablet.

6.2 Conclusion

The optical and electrochemical characterization of the ZnO synthesized samples confirmed successful synthesis and the morphological examination supports the presence of diagnostic functional groups like the Zn-O bond. Furthermore, was a significant trend observed in the features of ZnO using various precursor salts (zinc nitrate, acetate, and chloride). Dispersity characteristics were measured, and aggregation of nanoparticles, size distribution, and stability were established which would as well influence conductivity. The crystallinity of ZnO crystals was inspected and the results showed how the precursor salts impacted preferred growth planes while essential electrochemical parameters indicated reversibility of the electrochemical behaviour of synthesized ZnO. Under the specific electrolyte conditions, the rate of electron transfer was a direct measure of current density, and electrical resistance and indicated that the nitrate precursor produced a pleasing ZnO product.

Preparing nanoclay (PGV and 1.44P) ZnO composites included the synthesis of a few ratios to establish the most acceptable nanoclay and fraction based on optical and electrochemical qualities. HR TEM images and SAED patterns showed laminated clay layers and high crystallinity were confirmed in pristine 1.44P, including partial agglomeration and spherical nanoparticles in ZnO and exfoliation and amorphous nature of the 1.44P ZnO composite. FTIR and XRD confirmed the chemical identity of PGV and 1.44P ZnO composites while cyclic voltammetry suggested the most acceptable electron transfer and hence the suitable nanoclay ZnO composite which was 0.5g 1.44P ZnO.

The application of the 0.5g 1.44P ZnO composite with HSA modified glassy carbon electrode platform for electrooxidation of Nevirapine resulted in a confirmation in terms of electrode potential at 0.63V vs Ag/AgCl as previously reported. Choosing supporting electrolyte 1x (0.1M) PBS and optimization of the differential pulse voltammetry methodology led to acceptable current densities as well as selectivity over a linear range. The platform responded specifically in the presence of interferants and during the analysis of samples containing the analyte. Reproducibility of the modified glassy carbon electrode fabrication protocol resulted in RSD figures of 1.17% while the precision was 1.35% for measurements at a single analyte concentration. Repeatability of the modified glassy carbon electrode for consecutive measurements was RSD of 0.99% whereas the percentage of accuracy to evaluate stability was 98.65%. The 0,5g 1.44P ZnO HSA biosensor was furthermore used in samples of spiked urine and pharmaceutical tablet producing RSD values of 4.47% and 2.64% respectively for determinations of the analyte.

The relationship of this study to literature is one in which the results address the issues with reported biosensors. A more sensitive platform, better electron transfer, increased current response, catalytic activity, synergistically enhanced electrooxidation response towards the analyte, simple and environmentally friendly.

SUPPORTING INFORMATION

S.1 Electrochemical parameter calculations

The anodic peak slope of ZnO from all three precursors was determined and the diffusion coefficient was calculated below.

$$\text{ZnNO}_3\text{: } D = \left(\frac{6\times10^{-7}}{0.4463\times2\times96485.33212\times0.0706858347\times0.0002}\right)^2\left(\frac{8.314\times298.15}{2\times96485.33212}\right)$$

$$= 2.428518245 \times 10^{-13} \times 1.284557 \times 10^{-2}$$

$$= 3.120 \times 10^{-15} cm^2/s$$

$$\text{ZnAC: } D = 3.120 \times 10^{-15} cm^2/s$$

$$\text{ZnCl: } D = 1.386 \times 10^{-15} cm^2/s$$

For the anodic peaks, the slope was used to determine the electron transfer coefficient, α, for ZnO from ZN, ZA, and ZC:

$$\text{ZnNO}_3\text{: } 0.07077 = \frac{2.3(8.314)(298.15)}{\alpha(2\times96485.33212)}$$

$$0.07077 = -\frac{5701.28393}{\alpha \times 192970.6642}$$

$$\alpha = \frac{5701.28393}{13656.53391} = 0.4175$$

$$\text{ZnAC: } \alpha = 0.3671$$

$$\text{ZnCl: } \alpha = 0.5097$$

To determine the heterogenous standard rate constant, k_s.

$$\text{ZnNO}_3\text{: } Log\ k_s = 0.4175 \log(1-0.4175) + (1-0.4175) log 0.4175 -$$

$$\log\left(\frac{8.314\times298.15}{2\times96485.33212\times40}\right) - 0.4175(1-0.4175)\frac{2\times96485.33212\times0.5957}{2.3\times8.314\times298.15}$$

$$Log\ k_s = -0.09799 + (-0.2210) - (-3.493) - 4.903$$

$$Log\ k_s = -1.72899$$

$$k_s = 10^{-1.72899} = 0.01866 s^{-1}$$

$$\text{ZnAC: } k_s = 2.510 s^{-1}$$

$$\text{ZnCl: } k_s = 5.685 s^{-1}$$

To determine the electrochemical behavioural process in terms of mass transport and how it is affected by each precursor.

$$\text{ZnNO}_3\text{: } m_{trans} = \left[\frac{(\pi nFDv)}{(RT)}\right]^{\frac{1}{2}} = \left[\frac{3.141592654\times2\times96485.33212\times3.120\times10^{-15}\times40}{8.314\times298.15}\right]^{\frac{1}{2}} = 5.507\times10^{-6}s^{-1}$$

$$\text{ZnAC: } \left[\frac{3.141592654\times2\times96485.33212\times3.120\times10^{-15}\times40}{8.314\times298.15}\right]^{\frac{1}{2}} = 5.507\times10^{-6}s^{-1}$$

$$\text{ZnCl: } \left[\frac{3.141592654\times2\times96485.33212\times1.386\times10^{-15}\times40}{8.314\times298.15}\right]^{\frac{1}{2}} = 3.688\times10^{-6}s^{-1}$$

The maximum amount of current, Ip_{max}, is directly proportional to temperature, T, concentration, C, the electrode area, A, number of electrons transferred, n, diffusion coefficient, and scan rate, *v*. Thereafter, the most favoured activity, reduction, or oxidation, will give an indication which process will proceed with ease.

$$\text{ZnNO}_3\text{: } Ip_{max} = 0.4463nFAC\left(\frac{nFvD}{RT}\right)^{1/2} = 0.4463\times2\times96485.33212\times0.07069\times0.0002\left(\frac{2\times96485.33212\times40\times3.120\times10^{-15}}{8.314\times298.15}\right)^{\frac{1}{2}} = 3.783\times10^{-6}A$$

$$\frac{Ip_{red}}{Ip_{ox}} = \frac{2.75055\times10^{-5}}{3.01605\times10^{-5}} = 0.9120$$

$$\text{ZnAC: } = 3.783\times10^{-6}A$$

$$\frac{Ip_{red}}{Ip_{ox}} = 0.8950$$

$$\text{ZnCl: } Ip_{max} = 8.010\times10^{-7}A$$

$$\frac{Ip_{red}}{Ip_{ox}} = 0.9182$$

The Nickelson parameter was calculated for the electron transfer mechanism.

$$\text{ZnNO}_3\text{: } \Lambda = \frac{k_s}{m_{trans}} = \frac{0.01866}{5.507\times10^{-6}} = 3388.41$$

$$\text{ZnAC: } 455783.55$$

$$\text{ZnCl: } 1541485.90$$